Luigi Marini

Consultant in Applied Geochemistry

via Fratti, 253

55049 Viareggio (LU)

e-mail: luigimarini@rocketmail.com

Tel/fax: 0039-584-945230

# Geochemical techniques for the exploration and exploitation of geothermal energy

Viareggio, October 2004

## 1. Introduction

Before discussing the geochemical techniques applied in the exploration and exploitation of geothermal resources, it is convenient to recall few general concepts.

Geothermal energy is the natural heat of the earth, which is transferred towards the surface through conductive and convective processes. Because of these processes, the temperature within the earth crust generally increases with depth of ~30 °C/km. Assuming that the yearly average temperature at the earth surface is 15°C, a temperature close to 105°C should be found at ~3 km depth. However, in the present economic and technologic framework, it is generally not convenient to extract these relatively low-temperature fluids from these comparatively great depths. From this simple consideration, it is clear that geothermal energy can be economically exploited in geologically favorable contexts, where a natural thermal engine, which is generally represented by the heat released from magma batches situated at depths of few kilometers, is present. This natural thermal engine triggers the convective circulation of the waters contained in the overlaying rocks. Thus, these fluids ascend towards the earth surface and are stored in relatively shallow reservoirs. These geothermal reservoirs are separated from cold waters, which are generally present at shallow depths, by either primarily impervious layers or by rocks whose poor permeability is due to self-sealing phenomena.

Since the energy contained in geothermal fluids is much smaller than that contained in the same amount of oil, a further requirement for the economic exploitation of geothermal energy is the storage of geothermal fluids into reservoirs of comparatively high permeability.

Exploitable geothermal systems can be divided in the two following groups, based on their geological setting:

(1) systems situated in areas of either active volcanism or recent magmatism;
(2) systems located in other geological frameworks.

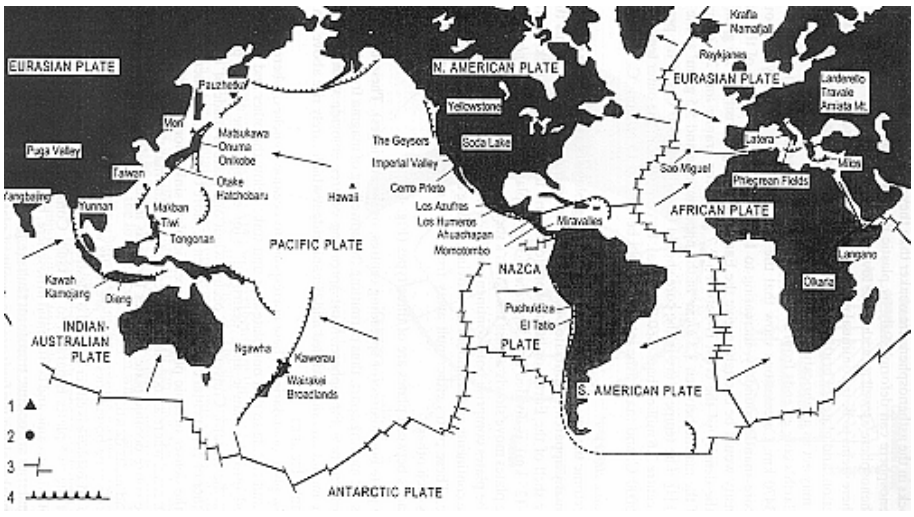


Fig. 1.1. Geographical distribution of high-temperature geothermal systems, compared with lithospheric plate boundaries. 1= fields exploited for electrical production; 2=identified high-temperature fields; 3=mid-ocean ridges and transform faults; 4=convergent plate boundaries (from Barbier, 1997).

The high-temperature (> ~180°C) geothermal systems, which are under exploitation for conventional generation of electric energy, mostly belong to the first

group, whereas the geothermal systems exploited for direct uses belong to both groups. Since most active volcanoes are situated along the margins of crustal and oceanic plates, high-temperature geothermal systems are also found close to these plate margins (Fig. 1.1).

However, geochemical techniques are very important also in investigating low-temperature geothermal systems, such as those of the Alps, where I had the opportunity to work some years ago (e.g., Martinotti et al., 1999; Pastorelli et al., 1999; Marini et al., 2000; Pastorelli et al., 2001; Perello et al., 2001).

## 2. The origin and evolution of volcanic and geothermal fluids: a review

The study of the origin and evolution of volcanic and geothermal fluids is one of the main concerns of geoscientists since many years. Possible sources contributing major and trace elements to these discharges include the magma, the host rocks, and the fluids circulating in the subsurface.

Craig (1963) found that the $D/^{1}H$ isotope ratio of thermal waters was always close to that of local groundwaters (Fig. 2.1). On the basis of these isotopic measurements he suggested that by far the major proportions of water in hydrothermal discharges are of local meteoric origin. About then, Ellis and Mahon (1964) showed that most of the chemical constituents of geothermal waters could simply be leached from crustal rocks. Based on these findings, the formation of hydrothermal solutions was explained largely in terms of the interaction of meteoric waters with crustal rocks at elevated temperatures, with magmatic contributions limited to the supply of heat.

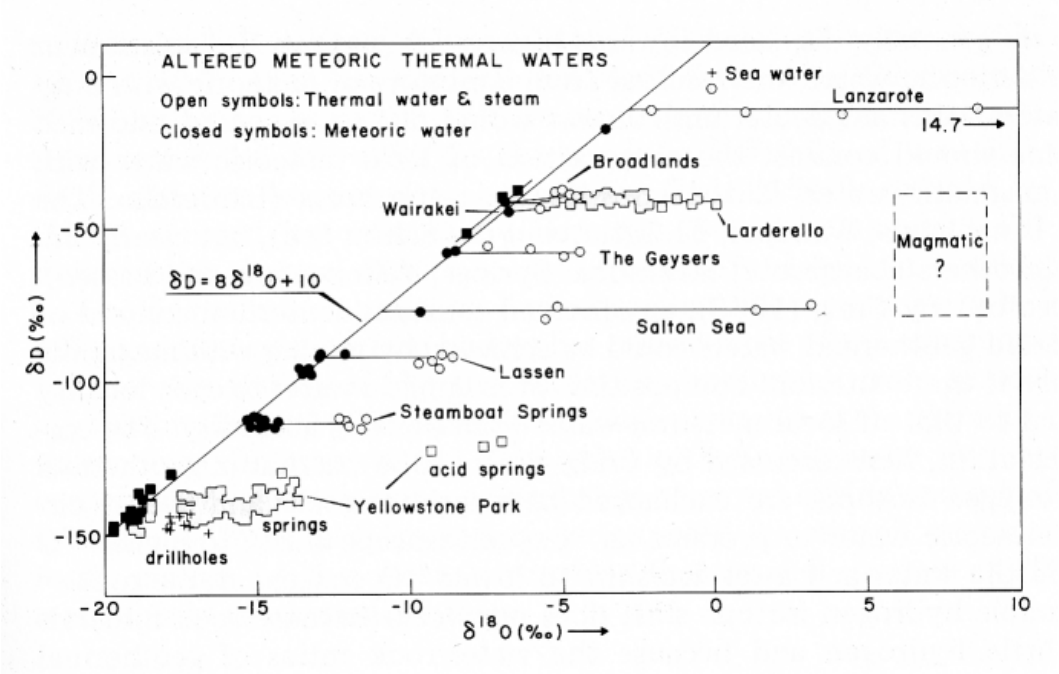


Fig. 2.1 Oxygen isotope shifts of geothermal fluids relative to local meteoric waters. Frome Truesdell and Hulston (1980).

Giggenbach (1987), by studying White Island volcano over a long time period and its changes from typically volcanic discharges to "geothermal" discharges got convinced that magmatic contributions to "geothermal" discharges may be much more important than generally assumed. In the meantime, this idea was pronounced by exploration geologists (Bonham, 1986; Hedenquist, 1987; White and Hedenquist, 1990), who found increasingly convincing evidence of a magmatic connection to ore deposition. Giggenbach (1992a), studied a big number of geothermal systems in volcanic island arcs at different latitudes and stated that the "horizontal" $^{18}O$ shifts, interpreted by Craig as due to water-rock interaction, are rather the exception than the rule. In fact, he found that significant hydrogen shifts from local meteoric water values are common in fluid discharges from island arc volcanoes and proposed a common magmatic endmember for these systems (Fig. 2.2). He termed this latter "andesitic" water and suggested that it originated as seawater that was altered during diagenesis and subduction. As shown in Fig. 2.2, volcanic condensates plot close to the andesitic end

member indicating high contributions of this latter, whereas the geothermal discharges are in general characterized by much higher proportions of local groundwater.

Besides $H_2O$, excess amounts of $CO_2$ and $N_2$ are also a characteristic of many vapor discharges along convergent plate boundaries (Marty et al. 1989; Varekamp et al. 1992; Kita et al, 1993; Giggenbach and Poreda, 1993; Sano et Marty, 1995; Giggenbach, 1997a). They are generally explained as being derived from the subducted slab. This same origin was proposed for a considerable part of the S and Cl in vapor discharges (Giggenbach, 1996).

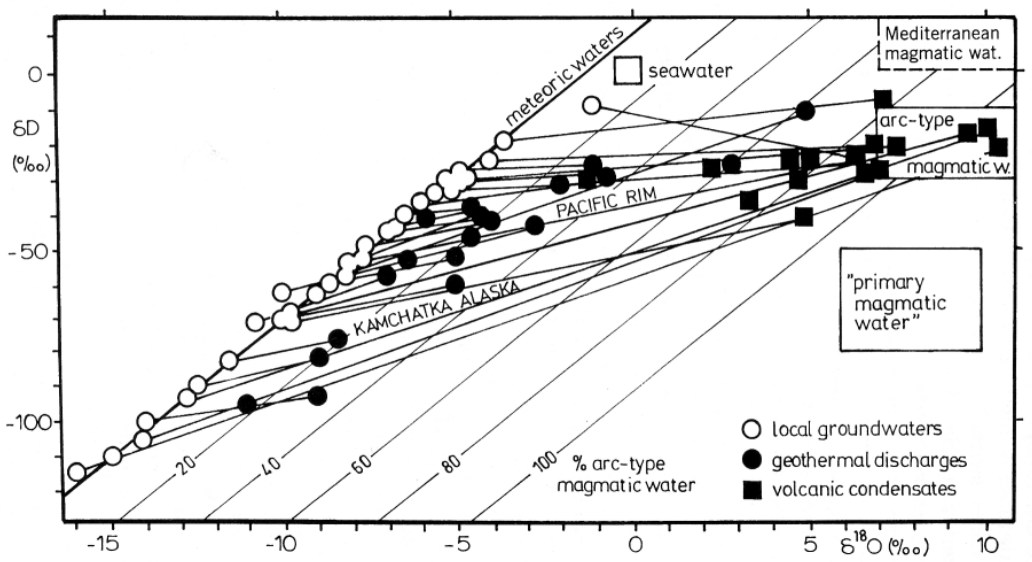


Fig. 2.2 Isotopic composition of geothermal and volcanic water discharges and associated local groundwaters (from Giggenbach, 1992a).

In summary, the origin of hydrothermal fluids in volcanic island arcs is depicted in the generally proposed cross-section of Fig. 2.3. The generation of a $H_2O$-rich fluid phase (Stolper and Newman, 1994) initiates partial melting of the mantle wedge in the vicinity of the subduction slab. Dehydration of the sediments that accompany the subducting slab and melting of the slab add components to the melt. The melt thus formed rises through the crust, which may act as another potential source for adding components to the magma.

Fluids produced through the degassing of a magma consist mainly of water vapor, $CO_2$, $SO_2$ and/or $H_2S$ and HCl (Giggenbach, 1987). Variations in their relative concentrations depend mainly on differences in magmatic volatile solubility and degree of degassing of the magma (Giggenbach, 1996). Absorption of these gases into deep circulating groundwater and cooling leads to the formation of acid, relatively oxidized, and highly reactive solutions. These are reduced and neutralized through the interaction with wall rocks in a zone of primary neutralization, whereby major cations are leached and added to the fluid (Giggenbach, 1988, 1997a; Reed, 1997). Boiling of the geothermal liquid thus formed liberates the dissolved gases, which fractionate into the vapor phase that ascends to the surface, discharging at 100ºC fumaroles. Condensation of these vapors into groundwaters may generate steam-heated acid-sulfate waters from atmospheric oxidation of $H_2S$. The residual deep geothermal liquid is likely to flow out laterally where it can mix with external waters and discharge as neutral-pH chloride springs.

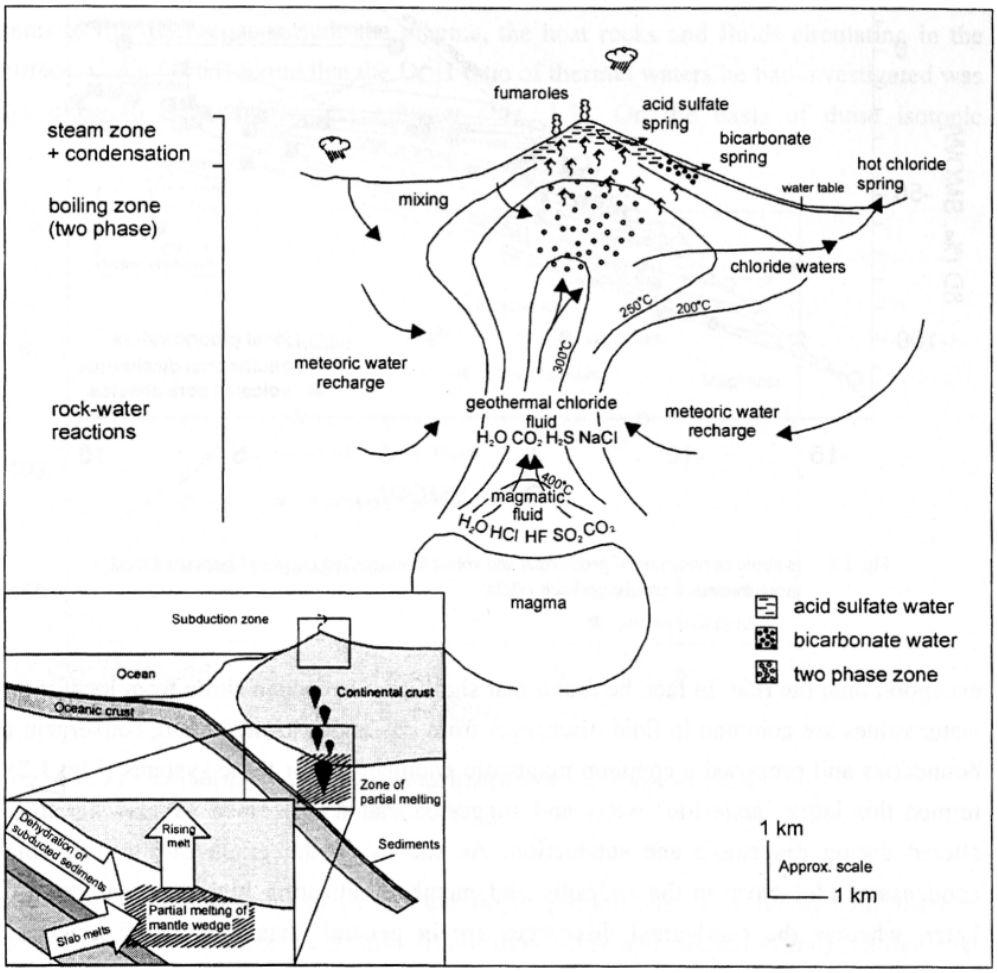


Fig. 2.3 Schematic cross section of a typical hydrothermal-volcanic system in active island-arc andesite volcanoes. Modified, after Hedenquist (1986) and Hedenquist and Lowenstein (1994).

## 3. Sampling and analysis of geothermal fluids

### *3.1. Geothermal liquids*

The strategies of sampling and analysis of the natural waters circulating in the geothermal area to be investigated (i.e., the number of samples to be collected and the analytical routine) chiefly depend on the scale and state of advancement of each specific project, the available funds, and logistic constraints. In general, it is not advisable either to analyze a large number of chemical and isotopic parameters in a small number of samples nor to determine a small number of chemical parameters in a huge number of samples. Besides, oversampling is not possible because water samples are stable for limited periods of time.

The best strategy is to collect samples from a reasonable number of thermal and non thermal waters, distributed all over the investigated area, to be analyzed, as soon as possible, for the following constituents: Li, Na, K, Mg, Ca, alkalinity, $SO_4$, Cl, F, B, $SiO_2$ and $NH_3$. Additional constituents useful to investigate specific problems are Al (total and monomeric), $H_2S$, Rb, Cs, Br, As, and Hg.

If possible, the hydrogeochemical survey should be carried out at the end of the dry season, to get water samples least affected by mixing with surface (rain) water.

#### *3.1.1. Field work*

In order to simplify logistics, field operations must be minimized. However, because some species are unstable, they must either be analyzed in the field or preserved by means of simple treatments, such as filtration, acidification, and dilution.

Filtration must be carried out to prevent algal growth, which may bring about removal of dissolved chemical constituents, such as $NH_3$ and $SO_4$, and clogging of laboratory instruments during water analysis. Filtration is usually carried out through a 0.45 μm membrane filter, although use of this size does not assure complete removal of suspended solids; in fact, finely dispersed Al-oxyhydroxides may pass through the 0.45 μm membrane filters (Kennedy and Zellweger, 1974; Laxen and Chandler, 1982).

Acidification is needed to preserve cation contents of high-temperature waters, which become supersaturated upon cooling, and to prevent precipitation of trace metals from both high-temperature and low-temperature waters. Acidification is usually done by the addition of either HCl (e.g., 1 ml HCl 1:1 [~6 N] to 50 ml of sample) or $HNO_3$ (e.g., 0.5 ml $HNO_3$ 1:3 [~4 N] to 50 ml of sample). In order to avoid dissolution of suspended solids, never acidify unfiltered water !

Since precipitation of $SiO_2$ from supersaturated waters, accompanied by co-precipitation of trace elements (e.g., Al), takes place even at pH as low as 1.5, dilution of filtered or filtered-acidified samples is advisable for silica determination.

Based on previous observations, the following sample aliquots are usually collected:

- a filtered aliquot for the analysis of anions, $D/^1H$ and $^{18}O/^{16}O$ isotopic ratios, and $^3H$ activity;
- a filtered-acidified aliquot for the determination of cations;
- a filtered-diluted (1:10) aliquot for the determination of silica.

Other sample aliquots have to be collected for specific purposes, e.g., complexing with 8-hydroxy-quinoline and extraction in methyl-isobutyl-ketone is needed for the determination of monomeric Al (Srinivasan et al., 1999). Sample size depends on the number of constituents to be determined and on laboratory requirements. Large water amounts are generally needed for tritium determination and when trace elements are analyzed after a pre-concentration step. Polyethylene bottles are generally preferred to

fragile glass bottles, but acid-cleaned glass bottles are sometimes needed, e.g., for Hg determination.

The field measurements to be carried out are:

- temperature, which is generally measured by means of a digital thermometer; however, normal- and maximum-glass thermometers are also needed for calibration and measurement of hot, unapproachable springs;
- pH by means of a portable, digital mV-pH-meter equipped with a glass electrode;
- Eh by means of a portable, digital mV-pH-meter equipped with a Pt electrode;
- conductivity by means of a portable, digitable conductivity-meter equipped with a suitable cell (range 0.1-100,000 μS/cm);
- alkalinity by acidimetric titration using HCl 0.1 or 0.01 N and methyl orange as indicator; utilization of a microdosimeter (minimum added HCl volume 0.5 μL) allows to work with 200-1000 μL of water. It must be noted that the parameter measured in this way is total alkalinity, $Alk_t$, although in most non-thermal waters this is practically equal to carbonate alkalinity, $Alk_c$, i.e., the sum of bicarbonate + carbonate contents (in equivalents). In most geothermal waters and high-pH, high-salinity waters, $Alk_t$ is greater than $Alk_c$, since other species, mainly $H_2BO_3^-$, $H_3SiO_4^-$, and $NH_3$, are also titrated. The effects of these species may be corrected carrying out an alkalinity titration followed by $CO_2$ removal and by a back titration in the laboratory, or by means of speciation calculations. Determination of $Alk_t$ in the field is needed to calculate reliable $P_{CO2}$ values, which are of upmost importance in geothermal prospecting.
- $H_2S$ by addition of a known amount of iodine and titration of excess iodine with sodium thiosulfate; addition of a few drops of starch indicator just before the end point is needed; alternatively, $H_2S$ can be measured by means of the methylene blue colorimetric method; the analysis of $H_2S$ is generally performed for environmental purposes and is not part of the standard analytical routine.

Flowrate of springs can be roughly evaluated by measuring the time needed by a leaf or some other floating object to travel a known distance along the flow channel. The distance/time ratio represents the average water velocity. The flowrate is then obtained by multiplying the average water velocity times the average cross-section of the channel. Consistent units have to be used.

Sample number and other details have to be written on bottles by using indelible marker pen. Results of field analyses and other sampling details have to be written in a field note book.

*3.1.2. Geothermal wells*

The geothermal wells, which tap a single liquid phase at temperatures > 100°C under reservoir conditions, obviously discharge two-phase liquid + vapor mixtures, which are generated through boiling of the original single liquid phase Incidentally, it must be noted that the term "vapor" is commonly used in the geothermal slang, due to the prevalence of water vapor, instead of the proper term "gas".

Sampling and analysis of both liquid and vapor phases, separated at known P,T conditions, are required to recalculate the composition of the original single liquid phase. The two phases can be separated by means of either a wellhead pressure separator, if available, or a small-scale sampling line, comprising a small Webre-type separator, a cooler for the separated liquid, a cooler-condenser for the separated vapor, and a gas/condendate separator (e.g., Fig. 3.1).

A similar equipment (Fig. 3.2) was earlier described by Ellis and Mahon (1977) and Giggenbach and Goguel (1989) and references therein, where operating procedures are also found.

The composition of the single liquid phase under reservoir conditions is then calculated by means of the simple mass balance:

$$C_O = C_L (1 - y) + y C_V \qquad (3.1)$$

Indices O, L, V refer to the single liquid phase initially present in the geothermal reservoir, the liquid phase at separation conditions, and the vapor phase (see below) at separation conditions, respectively, and y is the steam fraction.

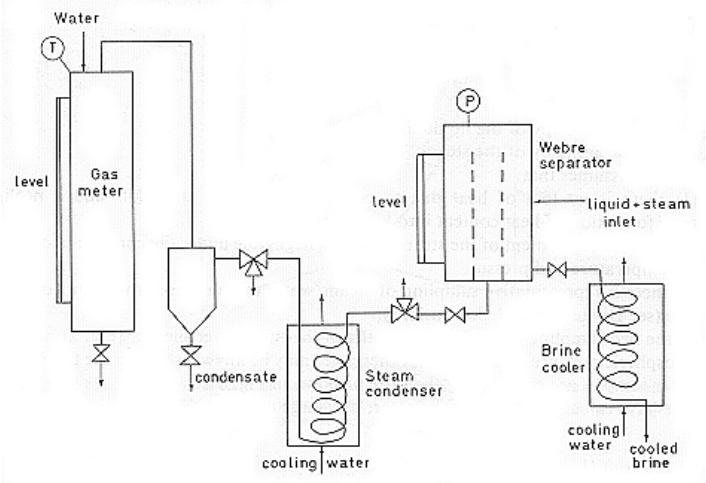


Fig. 3.1. Small-scale sampling line for geothermal well discharges (Marini and Cioni, 1985).

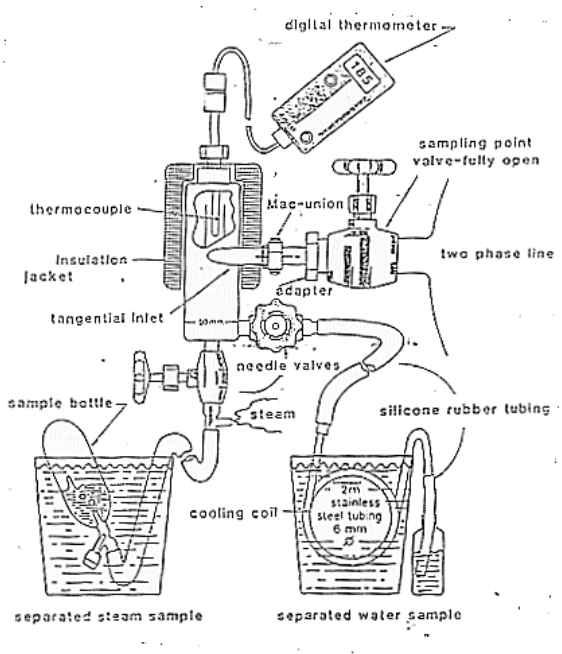


Fig. 3.2. Sampling line for two-phase geothermal discharges (from Giggenbach and Goguel, 1989).

From the previous discussion it is clear that when samples of separated liquid and vapor phases are collected from a geothermal well, it is necessary to know:

- separation temperature and/or pressure (specifying if bar-g or bar-a);

- well-bottom temperature and/or pressure and total discharge enthalpy.

Above it was hypothesized the presence of a single liquid phase in the geothermal reservoir. Although this is the most frequent situation, it is not the only one, since either a biphase liquid + vapor mixture or a single vapor phase can also be present in the reservoir. These possibilities can be ascertained by accurate enthalpy data or by gas geochemistry (Giggenbach, 1980; Bertrami et al., 1985).

*3.1.3. Laboratory analyses*

The standard instruments required in the analysis of geothermal samples includes:

- double-beam or modern single-beam atomic absorption spectrophotometer for the determination of cations, as well as boron (> 10 mg/kg) and silica;
- ionic chromatograph for the analysis of most anions, except fluoride and bicarbonate;
- visible-UV spectrophotometer for the colorimetric determination of boron (curcumine method) and silica (ammonium molybdate method);
- automatic titrator for the determination of alkalinity;
- pH-mV-meter which allows one to read 0.001 pH-unit and 0.1 mV, equipped with glass-electrodes for pH determination, and fluoride- and ammonia- specific electrodes.

Giggenbach and Goguel (1989) give a detailed description of the instruments and methods, which are usually used for the analysis of geothermal liquids.

In order to reduce errors in laboratory analyses, it is advisable to prepare concentrated standards from commercial solutions, to prepare diluted standards daily, to introduce frequently diluted standards in the analytical routine (to get rid of instrumental drifts), to repeat the analysis of a given sample (stored in sufficient amount in the lab), although the concentration of some solutes may change with time.

The quality of water analysis is usually checked computing the ionic balance; however, possible errors for minor constituents (e.g., Li, F, etc., but also Mg and $SO_4$ in high-temperature geothermal liquids) or neutral species (e.g., $SiO_2$, $H_3BO_3$, $NH_3$) cannot be detected in this way. At best, ionic balance gives an indication on the analytical accuracy of major constituents.

***3.2. Geothermal gases***

Gothermal gas samples are usually analysed for $H_2O$, $CO_2$, $H_2S$, $NH_3$, He, Ar, $O_2$, $N_2$, $H_2$, $CH_4$, and CO; in addition to these constituents, HCl, HF and oxidized S species (mainly $SO_2$, and subordinately $S_2$ and $SO_3$) have to be taken into account too in high-temperature volcanic gases.

*3.2.1 Sampling of geothermal gases*

Geothermal and volcanic gases are commonly sampled into ~250 ml bottles equipped with one or two Torion or Rotaflo valves (Giggenbach, 1975a; Giggenbach and Goguel, 1989). In the laboratory, ~50 ml of a 4N NaOH solution are fed into these partly evacuated bottles, which are then evacuated by means of a rotary oil pump, and weighted. The low pressure inside the bottle is indicated by the characteristic clicking sound upon shaking. Since the NaOH solution has to be carbonate free, it is advisable to quickly wash the NaOH pellets with distilled water. Besides one bottle have to be stored to determine the analytical blank.

For fumarole sampling a glass tube or a glass funnel is inserted into the vent; the discharge end of the apparatus is equipped with a short rubber pipe, where the bottle will be connected, after a given time, which must be sufficient to heat the sampling train and purge it from air (Fig. 3.3).

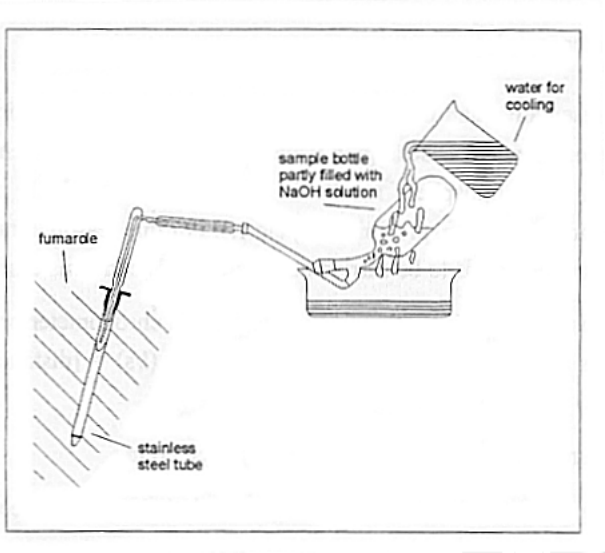


Fig. 3.3. Sampling of fumarolic gases by use of a NaOH charged bottle (from Brombach, 2000).

The fumarolic gas is allowed to enter the bottle by slowly opening the valve. Then, the valve must be regulated to have a high gas flow entering the bottle, to minimize water loss due to condensation. Condensation cannot be avoided, but the drops of steam condensate, which form in the pipes, have to be transferred to the bottle. The bottle must be held with the entrance down, in order to allow interaction between the gas and the alkaline solution.

This interaction brings about condensation of water vapor (the process has to be favored by cooling the bottle with cold water) while the acidic gases ($CO_2$ and $H_2S$ in geothermal gases, plus $SO_2$, HCl, and HF in volcanic gases) are absorbed in the alkaline solution, according to the following reactions:

$$CO_{2(g)} + 2\ OH^- = CO_3^{2-} + H_2O \quad (3.2)$$

$$H_2S_{(g)} + OH^- = HS^- + H_2O \quad (3.3)$$

$$4\ SO_{2(g)} + 7\ OH^- = 3\ SO_4^{2-} + HS^- + 3\ H_2O \quad (3.4)$$

$$HCl_{(g)} + OH^- = Cl^- + H_2O \quad (3.5)$$

$$HF_{(g)} + OH^- = F^- + H_2O \quad (3.6)$$

The non-absorbed gases ($N_2$, $O_2$, $H_2$, $CH_4$, He, Ar, ...) dissolve subordinately in the alkaline solution liquid phase and are chiefly collected in the head space above it. Therefore the flowrate of fumarolic gases entering the bottle will slow due to increasing pressure of the gases accumulating in the head space (the gas flow is obviously driven by the pressure difference between the vent and the bottle itself). If the bottle is not properly cooled also water participates significantly to gas pressure. When the flowrate slows the valve must be closed. The amount of gases that can be sampled is limited by either: (1) exhaustion of NaOH, for fluids rich in acid gases ; (2) exhaustion of vacuum, for fluids rich in non-absorbed gases; (3) exhaustion of the liquid space, for fluids rich

in water. If the chemical characteristics of the discharged fluids are known, the amount of NaOH can be adjusted accordingly.

Steam or gas discharges from a pool are collected following the same procedure of fumarole sampling. In this case a glass or plastic funnel is attached to the sampling line (Fig. 3.4). Metals should be avoided, to prevent $H_2$ production through reaction with acidic solutions, which are common in steam-heated pools. The funnel must be placed near the point where gas or steam enters the pool to prevent air contamination (pool water is aerated), which brings about addition of atmospheric gases, e.g., $N_2$, $O_2$ and Ar and consequent removal of $H_2S$ and other reduced species through reaction with $O_2$.

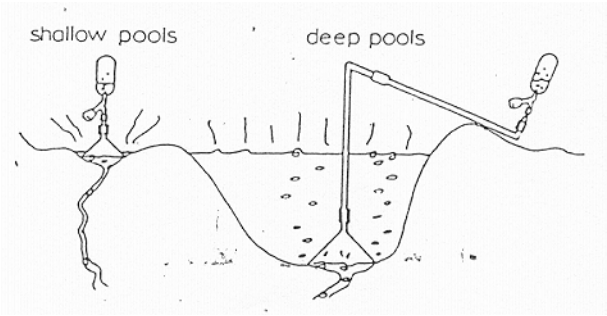


Fig. 3.4. Sampling of geothermal gases from pools (from Giggenbach and Goguel, 1989).

The same NaOH charged bottles can be used also to collect steam samples from geothermal well discharges, either from a steam line downstream of the wellhead pressure separator (in this case a T-piece should be used for safety reason) or by means of a small-scale sampling line (see above).

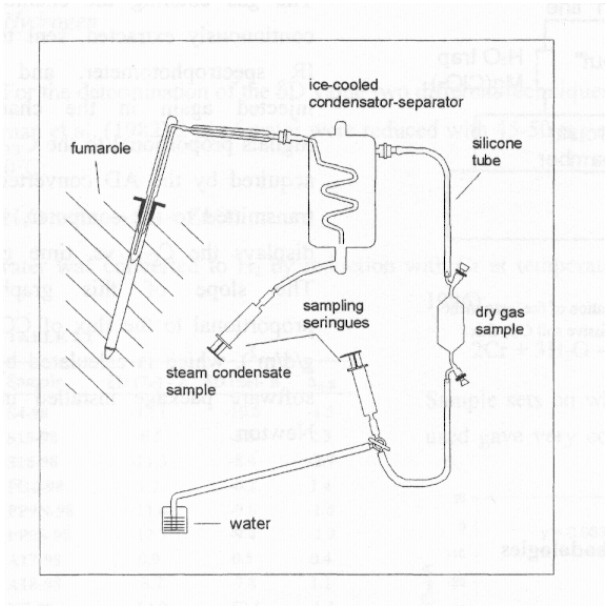


Fig. 3.5 Sampling of fumarolic gases by use of a condenser-separator (from Brombach, 2000).

Use of NaOH charged bottles allows representative sampling of both geothermal and volcanic gases. The only disadvantage of this procedure is the reaction of excess

NaOH with CO to produce sodium formate, whose kinetics is described by Giggenbach and Matsuo (1991). For CO determination, separate samples have to be collected, downstream of a condenser-separator (Fig. 3.5), which is cooled with either boiling diethyl ether or ice + liquid water or just water. Use of ether or ice maintains condensation temperature constant at 38°C or 0°C, respectively, whereas if water is used, condensation temperature must be checked and kept constant by regulating the water flow. Use of this equipment allows one to collect also samples of steam condensates (for the determination of the $D/^{1}H$ and $^{18}O/^{16}O$ ratios of $H_2O$). Uncondensable gases can also be used for isotopic analyses, e.g., the $^{13}C/^{12}C$ and $^{18}O/^{16}O$ ratios of $CO_2$.

*3.2.2 Laboratory analysis of geothermal gases*

As indicated by Giggenbach and Goguel (1989), in the laboratory, NaOH charged bottles are weighted again to determine the total amount of collected gases, $A_c$.

Then the first analytical step is the chemical (and eventually isotopic) analysis of non-absorbed gases, to avoid air contamination. Chemical analysis of non-absorbed gases, including $CH_4$ but excluding higher hydrocarbons, is performed by gas chromatography, for instance by employing the two gas chromatographs sketched in Fig. 3.6 (Giggenbach and Goguel, 1989).

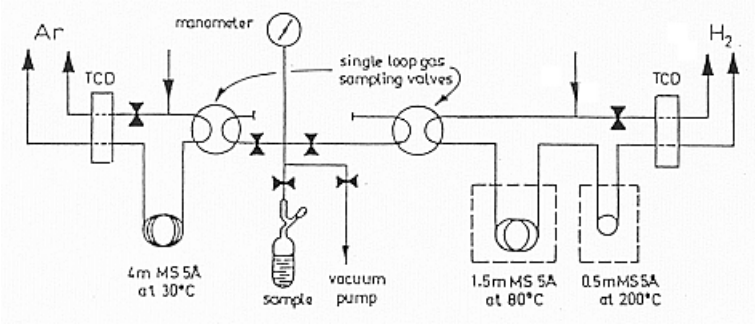


Fig. 3.6 Plumbing of the two gas-chromatograph used for chemical analysis of non-absorbed gases (from Giggenbach and Goguel, 1989)

High sensitivity determinations of He and $H_2$, and lower sensitivity analyses of $O_2$, $N_2$ and $CH_4$ are carried out by using a gas chromatograph equipped with a thermal conductivity detector (TCD). Gases are separated on a column packed with 5 Å molecular sieves, at 30°C, employing Ar as gas carrier.

High sensitivity determinations of Ar, $N_2$, and $CH_4$ are performed by using an other GC equipped with TCD, after separation on a first column packed with 5 Å molecular sieves, at 80°C, and combustion of $O_2$ in a second column also packed with 5 Å molecular sieves, but kept at 220°C, employing $H_2$ as gas carrier.

For calibration, a series of gas mixtures are introduced in the gas chromatographs at known pressure (sample injection pressure must be noted too). The partial pressure of the gases refers to the volume constituted by the head space in the bottle and the gas inlet system, which is equal to $V_f - V_c + V_g$, where $V_c$ is the condensate volume in the bottle, $V_g$ the volume of the gas inlet system, and $V_f$ the volume of the empty bottle, which was previously determined by difference between the weight of the bottle filled with water and the weight of the empty bottle.

Upon completion of chemical (and eventually isotopic) analysis of non-absorbed gases, the condensate is collected into a cylinder and its volume $V_c$ (in ml) is measured. Different portions of the condensate are then analyzed for:

(1) ammonia, as soon as possible, by means of a gas sensing ammonia electrode;
(2) hydrogen sulfide, as soon as possible, by addition of a known amount of iodine and titration of excess iodine by using sodium thiosulfate; alternatively, $H_2S$ can be analyzed by ionic chromatography, after peroxide oxidation of sulfide to sulfate;
(3) carbon dioxide, through acidimetric titration; first $H_2S$ must be removed, either through peroxide oxidation of sulfide to sulfate or precipitation of sulfide with $AgNO_3$; then a glass pH electrode is inserted in the solution and the pH is brought to 8.3, through careful addition of 0.1 N HCl, in order to convert carbonate to bicarbonate; finally the true titration is carried out from pH 8.3 to pH 3.8, where the bicarbonate is totally converted to carbonic acid.

The amount $W_i$ (in mg) and $M_i$ (in mmol) of each component is then calculated on the basis of the concentrations $C_i$ (in mg/L) obtained by wet chemistry analyses, by means of the relationships:

$$W_i = \frac{C_i \cdot V_c}{1000}, \tag{3.7}$$

$$M_i = \frac{W_i}{MW_i}, \tag{3.8}$$

where MWi is the molecular weight of the i-th component.

Following Giggenbach and Goguel (1989), the amounts of "nonabsorbed " gases $M_i$, in mmol, are calculated taking into account the dissolution of each component in the alkaline solution:

$$M_i = P_i \cdot \left( \frac{V_f - V_c + V_g}{22400} + \frac{V_c}{18 \cdot K_i} \right), \tag{3.9}$$

where $P_i$ is the gas pressure in mbar measured by gas chromatography (see above) and $K_i$ is the Henry's Law constant at 20°C, in bars (mole fraction)$^{-1}$:

| | |
|---|---|
| $K_{He}$ = 142,900 | $K_{O2}$ = 39,840 |
| $K_{N2}$ = 78,740 | $K_{Ar}$ = 36,400 |
| $K_{H2}$ = 65,500 | $K_{CH4}$= 36,100 |

The moles of water collected are then obtained as follows (Eqn. 3.10):

$$M_{H_2O} = \frac{W_c - W_{CO_2} - W_{H_2S} - W_{NH_3} - 4M_{He} - 2M_{H_2} - 40M_{Ar} - 32M_{O_2} - 28M_{N_2} - 16M_{CH_4}}{18000}$$

where $W_c$ is the amount of sample collected in mg.
The individual gas fractions of all components except $H_2O$, $X_i$, in mmol/mol dry gas are computed by means of:

$$X_i = 1000 \frac{M_i}{\sum_i M_i} \tag{3.11}$$

Finally the gas fraction, in mmol/mol total vapor is computed as follows:

$$X_g = 1000 \frac{\sum_i M_i}{M_{H_2O} + \sum_i M_i} \qquad (3.12)$$

Carbon monoxide and hydrogen are analyzed, by means of a gaschromatograph fitted with a Reduced Gas Detector (HgO), in the separated sample of dry gas. Hydrogen is used as reference component to calculate the CO fraction in total vapor.

## 4. Types of waters generally present in high-enthalpy geothermal areas

The waters circulating in high-enthalpy geothermal areas are generally ascribable to the four types described below (e.g., Ellis and Mahon, 1977; Henley et al., 1984; Giggenbach, 1988). It must be underscored, however, that each of these waters may mix with each other giving rise to hybrid water types. The usual location of the different types of waters is sketched in Fig. 4.1.

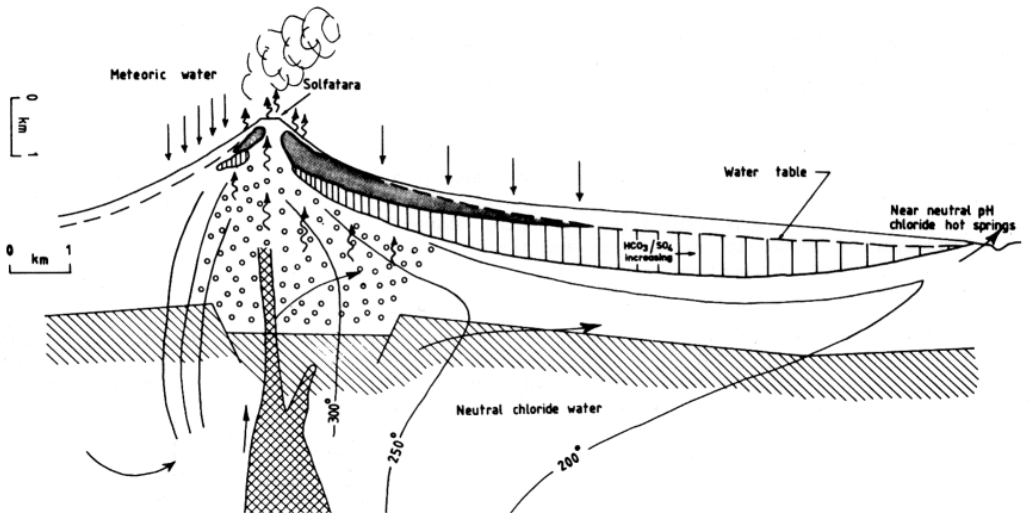


Fig. 4.1. Sketch of a geothermal system typical of active island-arc andesite volcanoes, showing the usual location of the different types of waters (from Henley and Ellis, 1983).

### *4.1. Sodium-chloride waters*

Waters circulating in deep, high-enthalpy geothermal reservoirs usually have sodium-chloride composition and chloride contents ranging up to ten thousand mg/kg, although in some systems (e.g., Salton Sea, California) chloride may be as high as 155,000 mg/kg.

The pH of these waters is close (± 1 or 2 units) to the neutral pH for the temperatures of the waters (e.g., 5.5-5.6 at 200-300 °C). Silica, potassium, lithium, boron, fluoride are much higher than in cold waters. The high chloride waters also contain appreciable calcium. Magnesium is instead much lower than in cold waters. The main dissolved gases are $CO_2$ and $H_2S$.

In general, the waters circulating in deep, high-enthalpy geothermal reservoirs are mainly of meteoric origin, but in some systems connate or other saline waters may be present. In geothermal systems with close volcanic-magmatic association and located along convergent plate boundaries, the deep, magmatic heat source may add acid gases like HCl, HF, $SO_2$, $H_2S$ and $CO_2$ as well as some 'andesitic' water (Giggenbach, 1992a, see above). Conversion of the initially acid aqueous solutions to neutral sodium-chloride waters requires extensive rock-water interaction and virtually complete removal of magmatic sulfur species in the form of sulfates and sulfides.

The deep sodium-chloride waters may flow directly to the surface and discharge from boiling, high chloride springs, whose pH ranges from near neutral to alkaline; alternatively they may mix with shallow, low-salinity waters to give relatively diluted chloride waters.

Because of the morphologic-hydrologic structure of the volcanoes distributed along convergent plate boundaries, in these areas sodium-chloride waters frequently

discharge from springs located several kilometers away from the upflow part of the geothermal systems (Fig. 4.1).

### *4.2. Acid-sulfate waters*

Acid-sulfate waters are typically found above the upflow part of the geothermal systems, where steam separation takes place. Boiling results in the transfer of gas species, mainly $CO_2$ and $H_2S$, into the vapor phase. This vapor phase can reach the surface without any interaction with shallow or surface waters, in the form of fumaroles and steam jets. Alternatively, separated vapor may condense, at least partly, in shallow groundwaters or surface waters to form steam-heated waters. In this environment, atmospheric oxygen oxidizes $H_2S$ to sulfuric acid producing acid-sulfate waters. These are characterized by low chloride contents and low pH values (0 to 3) and react quickly with host rocks to give advanced argillic alteration parageneses, which are dominated by kaolinite and alunite. Dissolved cations and silica are mainly leached from the surrounding rocks, whose compositions may be approached by these acid waters.

Shallow steam-heated waters may themselves boil, separating secondary steam, which reaches the surface in the form of low-pressure steaming grounds.

### *4.3. Sodium-bicarbonate waters*

Bicarbonate-rich waters originate through either dissolution of $CO_2$-bearing gases or condensation of geothermal steam in relatively deep, oxygen-free groundwaters. Because the absence of oxygen prevents oxidation of $H_2S$, the acidity of these aqueous solutions is due to dissociation of $H_2CO_3$. Although it is a weak acid, it converts feldspars to clays, generating neutral aqueous solutions, which are typically rich in sodium and bicarbonate, particularly at medium-high temperature. In fact:

(1) the low solubility of calcite prevents the aqueous solution to increase in calcium concentration;
(2) potassium and magnesium are fixed in clays and chlorites, respectively;
(3) sulfate concentration is limited by either low availability or by the solubility of anhydrite.

Sodium-bicarbonate waters are generally found in the 'condensation zone' of vapor-dominated systems and in the marginal parts of liquid-dominated systems. However, sodium-bicarbonate waters are also present in deep geothermal reservoirs hosted in metamorphic and/or sedimentary rocks, such as at Kizildere, Turkey (Guidi et al., 1990a).

### *4.4. Acid chloride-sulfate waters*

This type of waters is commonly found in crater lakes such as El Chichón (Casadevall et al. 1984), Kawah Ijen (Delmelle and Bernard, 1994), Poás (Brantley et al., 1987; Rowe et al., 1992), Ruapehu (Giggenbach, 1975b; Christenson and Wood, 1993), Sirung (Poorter et al., 1989), Yugama and Yakeyama (Takano and Watanuki, 1990). The chemistry of crater lake waters, especially during periods of intense volcanic activity, is obviously dominated by inflow and absorption of magmatic gases rich in HCl and S species, mainly $SO_2$ and $H_2S$ (e.g., Aguilera et al., 2000; Delmelle and Bernard, 2000; Varekamp et al., 2000, 2001; Marini et al., 2003a), leading to the production of strongly reactive aqueous solutions. In fact, through dissolution in liquid water, $SO_2$ disproportionates as specified by the following reaction (Murray and Cubicciotti, 1983):

$$4\ SO_2 + 4\ H_2O \Rightarrow H_2S + 3\ H_2SO_4. \qquad (4.1)$$

In crater lakes these highly acid oxidized solutions are very reactive with respect to cation leaching or rock dissolution, leading to deposition of alunite, anhydrite, pyrite, and kaolinite. Nevertheless the low availability of rocks in lacustrine environments often prevents the neutralization of the acid aqueous solutions. At greater depths, magmatic gases interact with water and masses of rocks much larger than in crater lakes, and at higher temperatures and for longer periods of time, with respect to crater lakes, thus leading to higher extents of neutralization and ultimately to the formation of neutral NaCl waters (Giggenbach, 1997a; Reed, 1997).

Consistently, acid Cl-$SO_4$ to $SO_4$-Cl waters are rare in geothermal reservoirs associated with recent volcanism, as pointed out by Truesdell (1991a) who reports the best documented examples of deep geothermal wells producing acid waters, i.e., Tatun, Sumikawa and Miravalles, and discusses their origin.

In particular, at Tatun, acid Cl-$SO_4$ waters come from a geothermal reservoir which is mostly developed within a 900 m-thick sequence of orthoquartzitic sandstones (containing only quartz, kaolinite, and minor alunite, and elemental sulfur) and subordinately within highly altered andesites. The HCl introduced in the Tatun reservoir water, most probably from a volcanic source, is not neutralized through water-rock interaction because no minerals capable of neutralizing acids are present in the reservoir rocks.

Corrosive acid $SO_4$-Cl waters were also found in some geothermal fields of the Philippines, such as Tiwi, Mt. Labo, Cagua, and Mt. Pinatubo (Sussman et al., 1993) and Mahanagdong (Salonga et al., 2004). Again, these acid waters do not come from separate reservoirs, but are produced through inflow of acid magmatic gases into the deepest portions of convecting neutral-pH, NaCl systems (Delfin et al., 1992; Reyes, 1990; Reyes and Giggenbach, 1992; Sugiaman et al., 2004). In particular, at Mt. Pinatubo, the high-temperature (>350°C), corrosive fluids were encountered by three wells drilled a few years before the 1991 volcanic eruption. These data testify, once more, that the acidity and the chemistry of the aqueous solution depends on the extent of water-rock "titration", which is also a function of the amount of magmatic gases added to the water and of the availability of minerals which are able to neutralize acids.

*4.4.1. The Miravalles example*

The origin of the acid Cl-$SO_4$ liquids of the Miravalles geothermal field has been recently investigated by Marini et al. (2003b). These liquids were encountered in wells PGM-2P, PGM-6, PGM-7, and PGM-19, all of which are located in a small sector of the field (Fig. 4.2). Acid Cl-$SO_4$ liquids have sulfate concentrations higher and pH values lower than the neutral Na-Cl liquids, which are tapped by most geothermal wells of Miravalles (Fig. 4.3).

Reservoir pH values of acid liquids usually range between 3 and 4 and are significantly higher than those of the liquids separated at atmospheric pressure and cooled at 25°C, ranging between 2.4 and 3.4. To understand this decrease in pH upon cooling through iso-enthalpic boiling, it must be recalled that the acidity of these waters is controlled by the dissociation of bisulfate ion, $HSO_4^-$, which is more strongly associated at high temperatures than at low temperatures (Reed, 1997; Marini et al., 2003a). Consequently, the temperature decrease determines dissociation of $HSO_4^-$ and concurrent generation of $H^+$. Since the amounts of $H^+$ delivered by this process are larger than those removed by loss of acid gases, mainly $CO_2$, the pH value decreases.

According to Truesdell (1991a) and Giggenbach and Corrales Soto (1992), the most likely hypothesis to explain the origin of these waters is the inflow of magmatic gases in the geothermal reservoir and the incomplete neutralization of these fluids. Alternatively, interaction of neutral Na-Cl waters with highly altered rocks rich in silica,

alumina, native sulfur, and sulfate minerals, representing old solfatara areas that were buried by later volcanic deposits, was indicated by Robert O. Fournier (1993, written communication) to account for the generation of these acid liquids.

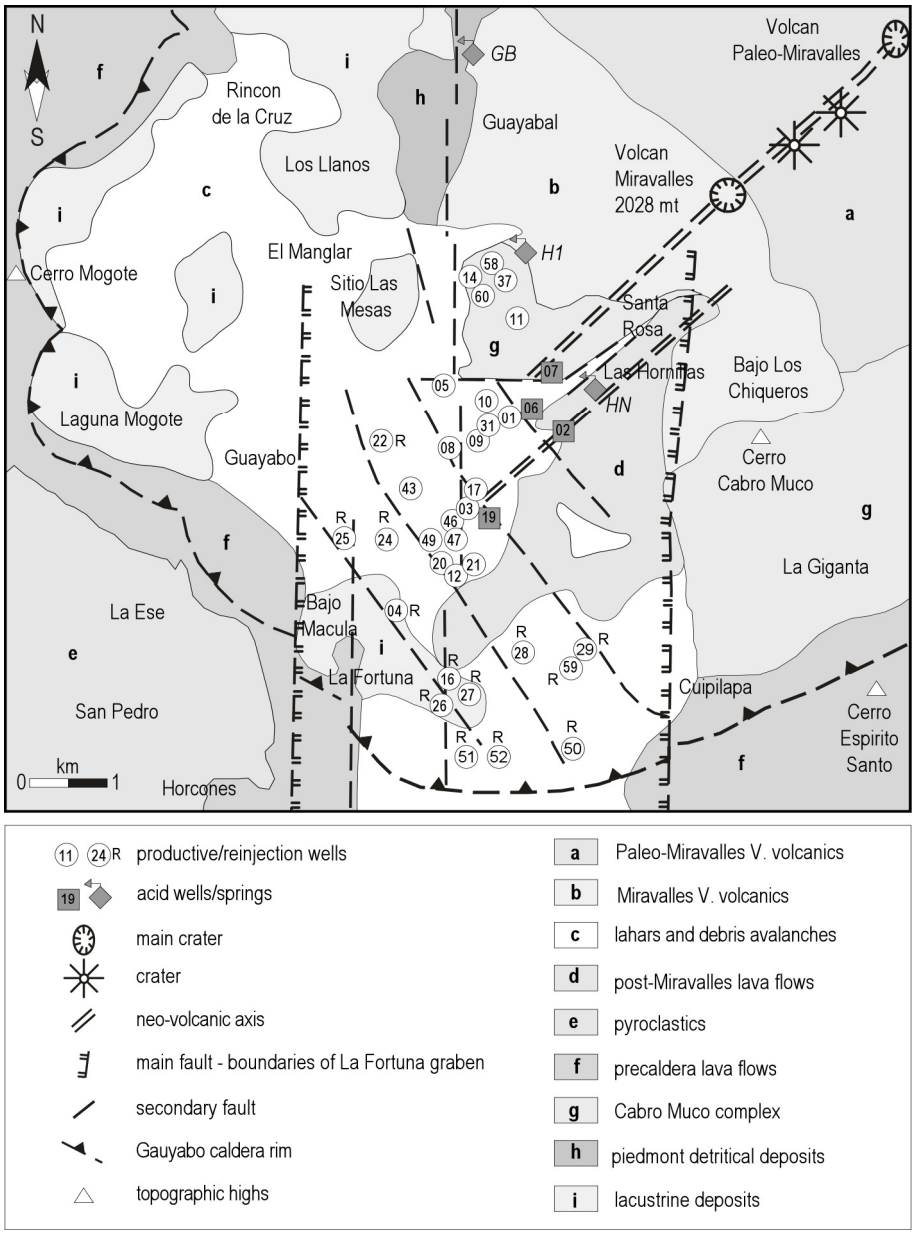


Fig. 4.2. Schematic geologic map of the Miravalles area, Costa Rica, also showing the location of relevant geothermal wells (from Gherardi et al., 2002).

To clarify this matter, Marini et al. (2003b) have investigated the irreversible water-rock mass exchanges governing the production of neutral Na-Cl and acidic Na-Cl-$SO_4$ geothermal liquids circulating at depth into the Miravalles geothermal system by means of the EQ3/6 Software Package (Wolery, 1979, 1992; Wolery and Daveler, 1992).

First, the in-situ reservoir composition, including pH, was reconstructed; the boundary conditions needed for the implementation of reaction path modeling ($P_{CO2}$, $P_{H2S}$, and/or $P_{O2}$) were evaluated; the saturation state of the reservoir liquids with

respect to relevant hydrothermal solid phases were estimated (Fig. 4.4); and the possible compositions of the initially acidic meteoric-magmatic liquids were identified.

Then, both the interaction between meteoric-magmatic fluids and calc-alkaline volcanic rocks and the interaction between neutral Na-Cl waters and highly altered volcanic rocks were modeled. Reaction path modeling was performed through a purely stoichiometric approach without considering the kinetics of irreversible mass exchanges.

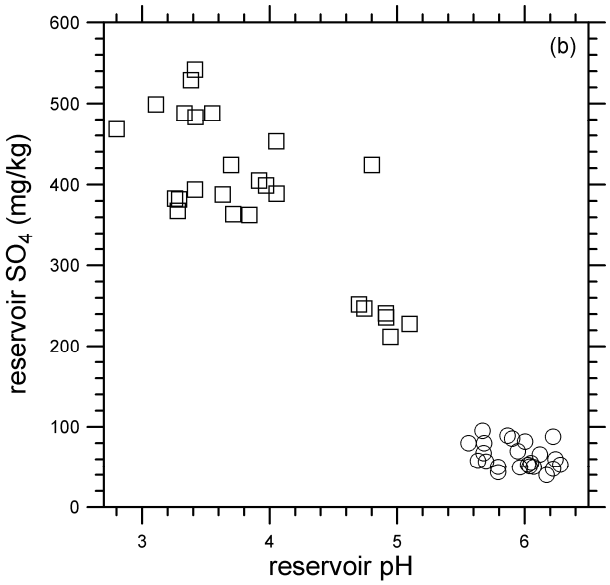


Figure 4.3. Correlation plot between sulfate concentration and pH of both neutral Na-Cl liquids (circles) and acidic Na-Cl-$SO_4$ liquids (squares) of the Miravalles geothermal field (data from Marini et al., 2003b).

Temperature was maintained at 235°C and total pressure at the corresponding saturation value, 30.6 bar, throughout the interaction with calc-alkaline volcanic rocks (an average andesite and an average dacite, in two separate runs), and progressive neutralization, of an initially acidic, meteoric-magmatic aqueous solution. Carbon dioxide partial pressure was fixed at 3 bar, and $P_{H2S}$ was kept at 0.01 bar, as these are the average value of neutral Na-Cl liquids. The possible solid product phases were selected based on the indications provided by activity plots and thermodynamic affinities to equilibrium. These minerals are part of the mineral assemblages typically found in geothermal reservoirs and epithermal ore deposits with propylitic alteration (seee section 7).

Results of reaction path modeling indicate that neutral Na-Cl liquids represent the product of the complete or almost complete neutralization of meteoric-magmatic aqueous solutions. However, the characteristics of acid Na-Cl-$SO_4$ liquids are not satisfactorily reproduced in this way.

The interaction of neutral Na-Cl waters with highly altered rocks (represented by alunite and chalcedony) as a possible mechanism to produce the acidic Na-Cl-$SO_4$ liquids was also simulated through reaction path modeling. Again, temperature, total pressure, $P_{CO2}$, and $P_{H2S}$ were fixed at 235°C, 30.6 bar, 3 bar and 0.01 bar, respectively, and precipitation of the same solid product phases of the previous simulations was allowed. In this way, the concentrations of relevant chemical components, $SO_4$, Ca, Na, K, and $SiO_2$, are satisfactorily reproduced, indicating that the acidic Na-Cl-$SO_4$ liquids of Miravalles are likely produced through interaction of neutral Na-Cl waters with volcanic rocks affected by advanced argillic alteration as suggested by Fournier (1993).

Although the general conceptual geochemical model of the hydrothermal systems with close volcanic-magmatic association (Giggenbach, 1988, 1997a; Reed, 1997) is not weakened by these new findings, they indicate that the acid sulfate-chloride waters are not exclusively produced through inflow of magmatic gases into the roots of the geothermal systems.

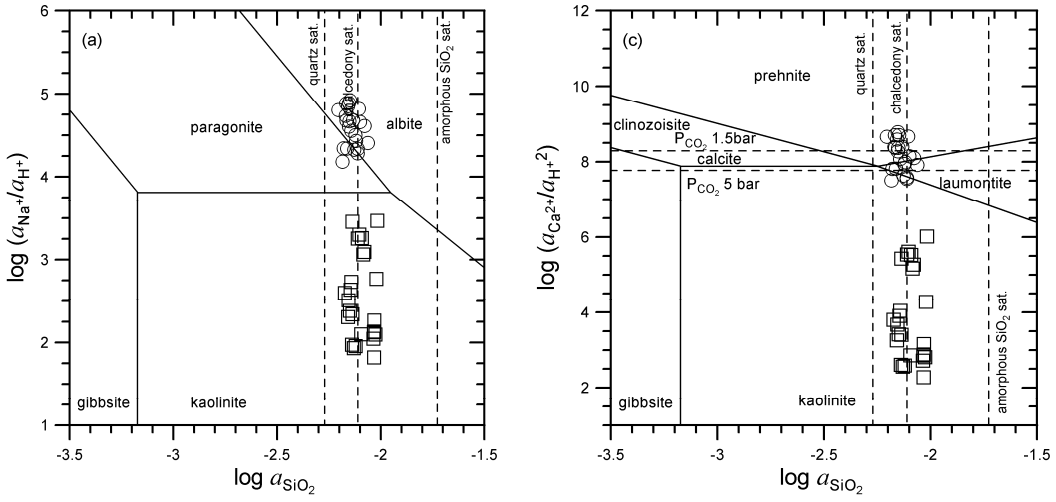


Figure 4.4. Activity plots for the systems (a) $Na_2O$-$Al_2O_3$-$SiO_2$-$H_2O$ and (c) CaO-$Al_2O_3$-$SiO_2$-$H_2O$ at 235°C and corresponding water saturation pressure also showing the neutral Na-Cl liquids (circles) and the acidic Na-Cl-$SO_4$ liquids (squares) of Miravalles.

## 5. The chemical classification of waters

The chemical classification of waters is essential for a correct utilization of geochemical techniques, which can be confidently applied only to particular kinds of fluids with limited ranges of composition, reflecting the environment of provenance.

For instance, most ionic solute geothermometers (see below) can be applied only to the samples representative of water-rock equilibrium at depth. This assumption is usually fulfilled for neutral sodium-chloride waters only. Therefore these samples have to be properly identified and selected. Furthermore, possible phenomena affecting the original characteristics of sodium-chloride waters (i.e., addition of cold, shallow groundwaters, boiling, dissolution or precipitation of mineral phases) have to be recognized and evaluated.

The chemical classification of waters can be carried out following different techniques, some of which are listed below.

### *5.1. The Schoeller plot*

It displays the log contents of several constituents for each water sample; these values are connected with a line, whose shape allows an "eyeball" comparison of the different waters plotted.

As an example, in Fig. 5.1 thermal waters exhibit higher concentrations of Li, Na, K, F, Cl, $SO_4$ and B, than cold waters, which have higher contents of Mg and Ca. Bicarbonate is similar in cold and thermal waters.

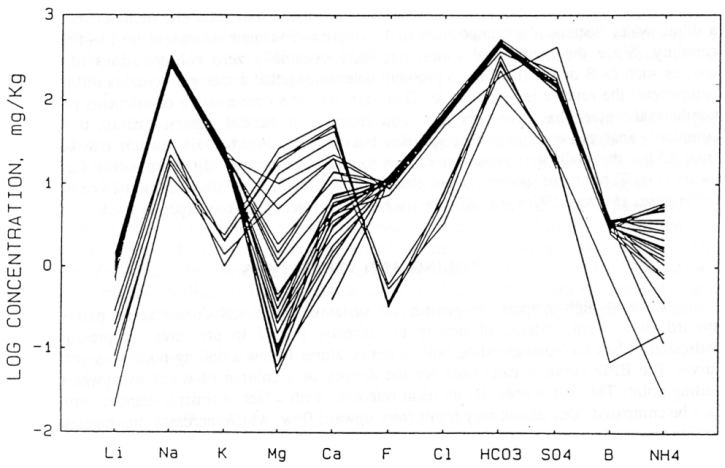


Fig. 5.1 The Schoeller plot of hot and cold waters from San Ignacio, Honduras (from Truesdell, 1991b)

Because logarithmic values are used, a wide range of contents can be arranged in this plot. The effect of mixing with dilute water, as well as gain or loss of steam, is to move the line representing a sample vertically without changing its shape.

The main disadvantage of this procedure is that when many samples are represented on the same plot, individual patterns are lost.

### *5.2. The Cl-$SO_4$-$HCO_3$ triangular plot*

The Cl-$SO_4$-$HCO_3$ triangular plot is used for an initial classification of geothermal water samples (Giggenbach, 1988; Giggenbach and Goguel, 1989). The position of a data point in this plot is obtained by first calculating the sum $\Sigma_{an}$ of the concentrations $C_i$ (in mg/kg) of all three species involved:

$$\Sigma_{an} = C_{Cl} + C_{SO4} + C_{HCO3} \quad (5.1)$$

Then the percentages of chloride, %Cl, and bicarbonate, $\%HCO_3$, are evaluated according to:

$$\%Cl = \frac{100 \cdot C_{Cl}}{\sum_{an}} \quad (5.2)$$

$$\%HCO_3 = \frac{100 \cdot C_{HCO_3}}{\sum_{an}} \quad (5.3)$$

In this plot (Fig. 5.2) are indicated the compositional ranges for the different kinds of waters typically found in geothermal areas (see chemical data in Table 1), such as:

(1) mature NaCl waters of neutral pH, which are rich in Cl and plot near the Cl vertex;
(2) Na-$HCO_3$ waters, here indicated as peripheral waters
(3) volcanic and steam-heated waters, generated through absorption into groundwater of either high-temperature, HCl-bearing volcanic gases or lower-temperature $H_2S$-bearing geothermal vapors.

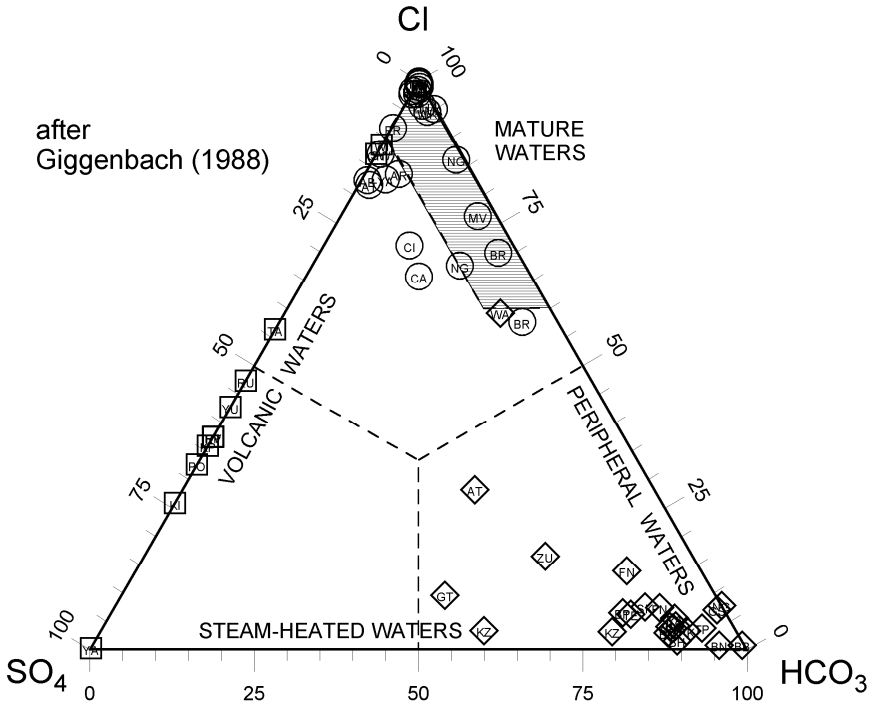


Fig. 5.2 Relative Cl, $SO_4$ and $HCO_3$ contents (on weight basis) for different kinds of waters typically found in geothermal areas (chemical data in Table 1); squares = acid sulfate waters; diamonds = bicarbonate waters; circles= neutral chloride waters.

The advantages of this diagram are:

- the three main anion are plotted separately on the three vertices of the plot;
- mixing lines are straight lines;
- all available samples can be plotted; groupings and trends can be evaluated.

Its limitations are:

- relative ratios between Cl, $SO_4$ and $HCO_3$ are displayed; the content of each species relative to water is obliterated in this plot;
- apparent correlations may be accidental; correlations have to be checked by means of additional independent data.

### *5.3. The Langelier-Ludwig square diagram*

This diagram is a sort of square version of the more popular diamond-shaped Piper plot. The position of a sample in the Langelier-Ludwig (or LL) plot is obtained by first calculating the sum of main anions, $\Sigma_{an}$, and of main cations, $\Sigma_{cat}$, by means of the following equations:

$$\Sigma_{an} = e_{Cl} + e_{SO4} + e_{HCO3} \tag{5.4}$$

$$\Sigma_{cat} = e_{Ca} + e_{Mg} + e_{Na} + e_{K}, \tag{5.5}$$

where $e_i$ refer to the concentration of the i-th component in eq/l or meq/l. Then the percentages of each cation, e.g., Na, and each anion, e.g., Cl, are evaluated according to:

$$\%\mathrm{Na} = \frac{50 \cdot e_{Na}}{\sum_{cat}} \tag{5.6}$$

$$\%\mathrm{Cl} = \frac{100 \cdot e_{Cl}}{\sum_{an}} . \tag{5.7}$$

Suitable groupings of cations and anions are selected (inspection of correlation coefficients may be useful) and plotted as percentages. Generally %Na is grouped with %K and plotted on the Y-axis, while the sum % $HCO_3$ plus %$SO_4$ is plotted on the X-axis. In such a diagram %Ca+%Mg and %Cl are also fixed by the following equations:

$$\%\mathrm{Ca}+\%\mathrm{Mg} = 50 - (\%\mathrm{Na} + \%\mathrm{K}) \tag{5.8}$$

$$\%\mathrm{Cl} = 50 - (\%\mathrm{HCO_3} + \%\ \mathrm{SO_4}) . \tag{5.9}$$

In principle, the fusion of $HCO_3$ and $SO_4$ into a unique variable does not help water classification. In practice, the different kinds of waters typically found in geothermal areas (i.e., neutral chloride waters, acid sulfate waters, and bicarbonate waters) are generally found in distinct parts of this diagram (Fig. 5.3), due to the prevalence of Na in bicarbonate waters and of alkali-earth metals in acid sulfate waters.
The identification of peculiar chemical types of waters is often improved by changing the groupings of anions and cations. For instance:

- plotting the sum %Na+%K+%Mg against % $HCO_3$ helps to identify cold, low-salinity calcium bicarbonate waters circulating in limestones;
- plotting the sum %Na+%K+%Ca against % $HCO_3$ helps to identify cold, low-salinity magnesium bicarbonate waters typically originating by interaction with mafic and ultramafic rocks;
- plotting the sum %Na+%K+%Mg against % $HCO_3$ + %Cl helps to identify cold, calcium sulfate waters produced by interaction with gypsum and/or anhydrite.

The advantages of this diagram are:

- mixing lines are straight lines;

- all available samples can be plotted; grouping and trends can be evaluated;
- the vertices display the composition of salts present in nature, e.g., calcite, anhydrite, halite, ...; dissolution or precipitation of these salts are suggested by trends mowing towards or away from the pertinent vertex.

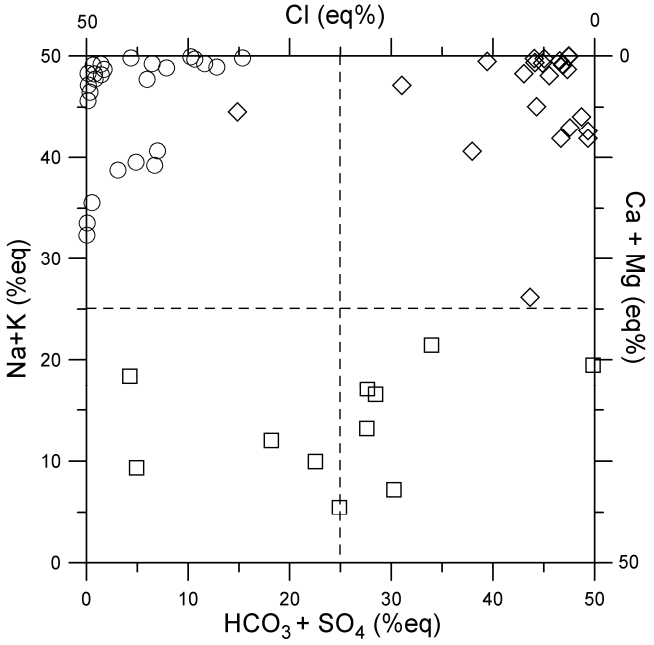


Fig. 5.3 Square Langelier-Ludwig diagram showing the different kinds of waters typically found in geothermal areas (chemical data in Table 1); squares = acid sulfate waters; diamonds = bicarbonate waters; circles= neutral chloride waters.

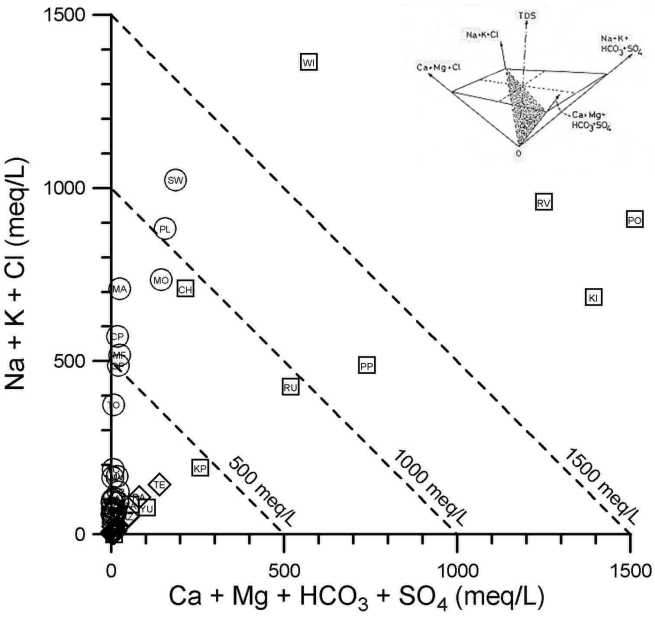


Fig. 5.4 $e_{Na} + e_K + e_{Cl}$ vs. $e_{Ca} + e_{Mg} + e_{SO4} + e_{HCO3}$ correlation plot with isosalinity lines for different kinds of waters typically found in geothermal areas (chemical data in Table 1); squares = acid sulfate waters; diamonds = bicarbonate waters; circles= neutral chloride waters.. Most waters fall in the shaded area near the origin. The diagram is equivalent to the triangular cross-section of the LL pyramid sketched on the top right.

Its limitations are:

- both anions and cations must be grouped; the use of sums of species obliterates any information carried out by individual species;
- relative ratios are displayed; the content of each species relative to water is also obliterated in this plot;
- apparent correlations may be accidental; correlations have to be checked by means of additional independent data.

According to Tonani (unpublished reports) the square LL plot represents the base of a compositional pyramid whose edges are the chemical concentrations, in eq/l or meq/l, and whose axis express the total ionic salinity (TIS, in the same unit).

The triangular cross-sections of this pyramid allow one to recover the information provided by TIS. Some of these cross-sections are equivalent to peculiar binary correlation plots. For instance, referring to the pyramid whose base is the above mentioned %Na + %K vs. % $HCO_3$ + %$SO_4$ square LL plot, it can be demonstrated that:
the cross-sections of this pyramid, whose trace is the diagonal connecting the vertex X=0, Y = 50 with the vertex X = 50, Y = 0 of the square LL plot, is equivalent to the $e_{Na} + e_K + e_{Cl}$ vs. $e_{Ca} + e_{Mg} + e_{SO4} + e_{HCO3}$ diagram;
the cross-sections of this pyramid, whose trace is the diagonal connecting the vertex X = 0, Y = 0 with the vertex X = 50, Y = 50 of the square LL plot, is equivalent to the $e_{Ca} + e_{Mg} + e_{Cl}$ vs. $e_{Na} + e_K + e_{SO4} + e_{HCO3}$ diagram;
the cross-section of this pyramid, whose trace parallels the X-axis of the square LL plot, is equivalent to the $e_{Cl}$ vs. $e_{SO4} + e_{HCO3}$ diagram;
the cross-section of this pyramid, whose trace parallels the Y-axis of the square LL plot, is equivalent to the $e_{Ca} + e_{Mg}$ vs. $e_{Na} + e_K$ diagram.
In these cross-sections the lines with slope -1 are isosalinity lines; in the latter two cross-sections isosalinity lines refer to TIS/2.

### *5.4. Principal Component Analysis (PCA)*

In general, chemical variables are intercorrelated, but these correlations are not easily discernible and raw data are therefore difficult to be interpreted. The purpose of PCA is to reduce the chemical variables to a smaller set of principal components (PC's). PC's group together correlated chemical variables and they can be, therefore, associated with sources or processes, i.e., they are interpretable.

The mathematics of PCA is beyond the scope of this brief presentation, and the reader is referred to Davis (1986) for further details.

First, chemical variables are standardized, subtracting the average and dividing by the standard deviation. The standardized variables, $Z_i$, have therefore average equal to zero and standard deviation equal to 1. They have the same "weight" in the subsequent procedure.

The PCA then expresses the ***n*** standardized variables in terms of ***n*** PC's, which are linear combination of the standardized variables, that is:

$$PC_1 = a_1 Z_1 + a_2 Z_2 + a_3 Z_3 + ... + a_n Z_n \quad (5.10)$$
$$PC_2 = b_1 Z_1 + b_2 Z_2 + b_3 Z_3 + ... + b_n Z_n$$
$$PC_3 = c_1 Z_1 + c_2 Z_2 + c_3 Z_3 + ... + c_n Z_n$$
$$.$$
$$.$$
$$PC_n = n_1 Z_1 + n_2 Z_2 + n_3 Z_3 + ... + n_n Z_n$$

the coefficients $a_1$, $a_2$, $a_3$, $a_n$... $n_1$, $n_2$, $n_3$, $n_n$ are called *loadings*. They are a measure of the extent to which each chemical variable contributes to a given PC. Loadings have

values between +1 and -1. Loadings are the key to interpret PC's. PCA is carried out in such a way that each new PC is much efficient as possible in terms of accounting for the total variance. When the ***n*** PC's have been calculated all the original variance will be accounted for.

When PCA is applied to a set of water analyses from a given area, taking into account the seven main dissolved constituents (i.e., Ca, Mg, Na, K, $HCO_3$, $SO_4$, Cl), few PC's (sometimes only two) are generally sufficient to explain a significant proportion of the total variance. The correlation plot between these PC's often looks very similar to one cross-section of the L-L compositional pyramid, substantiating the water classification carried out in a deterministic way.

## 6. Mixing and boiling

Before discussing the influence of mixing and boiling processes on geothermal liquids, it is convenient to clarify what is the meaning of mobile and compatible dissolved constituents.

### *6.1. Mobile and compatible dissolved constituents*

Dissolved constituents may be subdivided into two major groups according to their behavior:

- *mobile* or *conservative* constituents are those whose activity is not limited by saturation with respect to a solid or a gas phase; comparatively mobile constituents in geothermal waters (and in most natural waters as well) are Cl, Br, B and, to some extent, Li, Rb and Cs as well; once they have been added to a geothermal water through a complex history, their contents along the upflow path are changed only by mixing and steam loss;
- *compatible* constituents are those whose activity is controlled by saturation with respect to a solid or a gas phase; they equilibrate under reservoir conditions and may respond to termochemical changes along the upflow path of the geothermal water; Ca, Mg, Na, K, $HCO_3$, $SO_4$, F, $SiO_2$,.. usually have compatible behavior in geothermal environments.

The limits between these two groups are not absolute; for instance Cs is mobile at temperatures > 250°C, but it is taken up in hydrothermal zeolites at lower temperatures. Also the other rare alkalies are not truly mobile constituents, since Rb is incorporated in K-bearing alteration minerals (e.g., illite) already at temperatures > 300°C and Li enters authigenic quartz and chlorite (Goguel, 1983; Giggenbach and Goguel, 1989). Boric acid distributes between steam and liquid phases, especially at high temperature (Tonani, 1970).

### *6.2. Correlation plots of dissolved constituents versus chloride*

Chloride has mobile behavior in most natural waters. Saturation with respect to halite, which determines a compatible behavior of chloride, is in fact attained only in very peculiar natural environments. Therefore chloride can be confidently used as the mobile species of reference to investigate the behavior of other dissolved constituents.

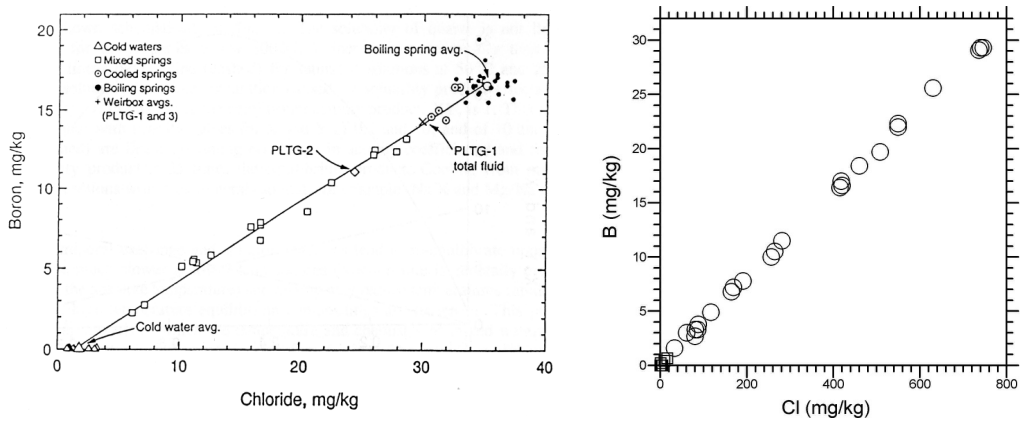


Fig. 6.1 Boron vs. chloride plots for the hot springs of Platanares, Honduras (left, from Janik et al., 1991) and those of San Marcos, Guatemala (right, from Marini et al., 1998).

Such an investigation is conveniently carried out by means of binary diagrams, where each chemical species of interest is plotted against chloride. These diagrams are

particularly useful to detect mixing and boiling processes. Water points moves away from the origin of the axis (which is representative of pure water, i.e., of separated steam) due to boiling. Binary mixing causes, instead, tight linear trends linking the geothermal endmember and the cold endmember. However, if a Cl-poor water mixes with a Cl-rich geothermal water whose chemistry is poorly constrained, the effects of mixing are very similar to and not easily discernible from boiling effects (Fig. 6.1).

The enthalpy vs. chloride plot is very useful in this respect.

### *6.3. Enthalpy vs. chloride plot*

The use of enthalpy vs. chloride plots is thoroughly discussed by Fournier (1979a) and references therein. The enthalpy vs. chloride plot is a suitable tool to distinguish the effects of boiling and mixing, since both steam and cold waters, which generally have low chloride contents, are characterized by very different enthalpy values.

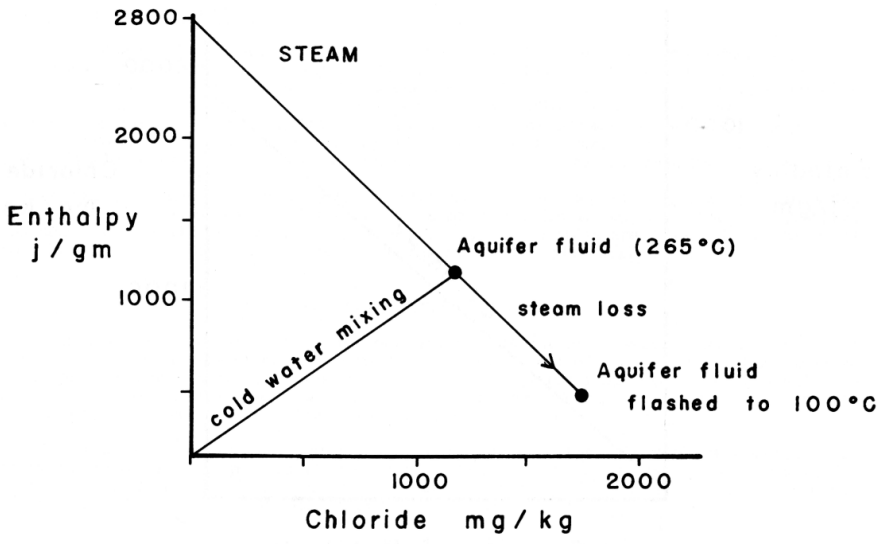


Fig. 6.2 Enthalpy vs. chloride plot showing the effects of boiling and dilution on a geothermal aquifer liquid at 265°C (from Henley et al., 1984).

The enthalpy - chloride plot of Fig. 6.2 shows that boiling (steam loss) moves the liquid from the point representative of the 265°C geothermal liquid towards higher chloride contents and lower enthalpies, whereas addition of cold, dilute waters determine a decrease in both enthalpy and chloride.

If a deep hot water is cooled mainly through conductive heat loss, its enthalpy decreases but its chloride concentration remains unchanged.

### *6.4. Two-components mixing equations for conservative constituents*

In a binary mixture the concentration, $C_M$, of any conservative constituent is given by the following equation:

$$C_M = C_A\, x + C_B\, (1 - x) \qquad (6.1)$$

where subscripts A and B refer to the two endmembers and x is the weight fraction of endmember A in the mixture. If mixing occurs without loss or gain of heat, then the following relationship holds true:

$$H_{L,M} = H_{L,A}\, x + H_{L,B}\, (1 - x) \qquad (6.2)$$

where $H_L$ stands for the specific enthalpy of liquid water.

### *6.5. Boiling equations for non-volatile constituents*

Two limiting mechanisms of boiling (steam separation) can be recognized:

(1) *single-step (or closed-system) separation*: the steam, continuously produced by decompression of the uprising liquid, remains in contact and in equilibrium with the liquid until it is separated in a unique separation event;

(2) *continuous (or open-system or Rayleigh) separation*: the steam is continuously separated from the liquid as soon as it forms.

An infinite number of intermediate mechanisms can exist; they are characterized by a finite number of separation steps (*multi-step separation*).

It is assumed that steam is separated in a single step at pressure P. The concentration, $C_L$, of any constituent, which does not enter the steam phase, at separation pressure P is fixed by the following relationship:

$$C_L = \frac{C_O}{1 - y} \tag{6.3}$$

where $C_O$ is the concentration of that constituent in the deep water and y is the steam fraction. If boiling is isoenthalpic, which is a realistic assumption for the irreversible adiabatic processes taking place in geothermal wells and high-flow rate natural geothermal manifestations, y can be obtained by means of the following isoenthalpic balance:

$$H_O = H_L (1 - y) + H_V \ y, \tag{6.4}$$

which can be rearranged to give:

$$y = \frac{H_O - H_L}{H_V - H_L} \tag{6.5}$$

where H indicates the specific enthalpy of the specified phase and subscript V stands for vapor. Since water is by far the major constituent of geothermal fluids, the specific enthalpies of pure water (tabulated by Keenan et al., 1969) are generally used in these calculations. However, if the aqueous solution has a relatively high salinity (NaCl > 5 wt%), specific enthalpies of the liquid and vapor phases differ significantly from those of pure water and should be suitably computed (e.g., Dittman, 1977).

### *6.6. Boiling equations for volatile constituents*

When steam separation takes place, the less soluble gases (e.g. $N_2$, $H_2$, $CH_4$, and CO) enter preferentially the vapor phase, while the more soluble gases ($CO_2$, $H_2S$, and $NH_3$) are retained in part in the liquid phase. Early vapors are richer in gas, especially in the low-solubility constituents, whereas late vapors are relatively gas-poor and contain preferentially high-solubility constituents.

The kind of separation mechanism, either single-step, continuous or multi-step, has a dramatic influence on the composition of the separated vapor.

The distribution of gases between liquid and vapor is conveniently expressed by the gas distribution coefficient, $B_j$, which is defined as the ratio between the

concentration of gas j in the vapor phase and the concentration of the same gas in the liquid phase:

$$B_j = \frac{\left(\frac{n_j}{n_{H_2O}}\right)_V}{\left(\frac{n_j}{n_{H_2O}}\right)_L} = \frac{C_V}{C_L} \cong \frac{X_{j,V}}{X_{j,L}} \qquad (6.6)$$

where n indicates the number of moles and X the mole fraction; the latter may be used at low gas concentration without any significant error.
Giggenbach (1980) derived the following regression equations (which are valid from 100 to 340°C) for most gas constituents of geothermal interest:

$$\log B_{NH3} = 1.4113 - .00292\ t \qquad (6.7)$$

$$\log B_{H2S} = 4.0547 - .00981\ t \qquad (6.8)$$

$$\log B_{CO2} = 4.7593 - .01092\ t \qquad (6.9)$$

$$\log B_{CH4} = 6.0783 - .01383\ t \qquad (6.10)$$

$$\log B_{H2} = 6.2283 - .01403\ t \qquad (6.11)$$

$$\log B_{N2} = 6.4426 - .01416\ t \qquad (6.12)$$

where t is the temperature in °C. Bertrami et al. (1985) obtained the following temperature dependence for CO:

$$\log B_{CO} = 6.3173 - .01388\ t. \qquad (6.13)$$

It should be noted that the logarithm of the distribution coefficient varies linearly with temperature (Fig. 6.3), while the temperature dependence of the Henry's Law constant is far from linear (Fig. 6.4). Fig. 6.4 shows also that gas solubility is a function of the salt content.

If steam is separated in a single step, the concentrations of any volatile constituent at separation pressure P, in the liquid phase, $C_L$, and in the vapor phase, $C_V$, are linked to the concentration in the initial liquid, $C_O$, by the following mass balance:

$$C_O = C_L\ (1 - y) + C_V\ y. \qquad (6.14)$$

This is equal to equation (3.1), which we used above to calculate the composition of the single liquid phase under reservoir conditions. If we are interested in calculating the concentration of gases in the vapor phase, the following expression is obtained by substituting equation (6.6) in (6.14):

$$C_V = \frac{B \cdot C_O}{1 - y + y \cdot B} \qquad (6.15)$$

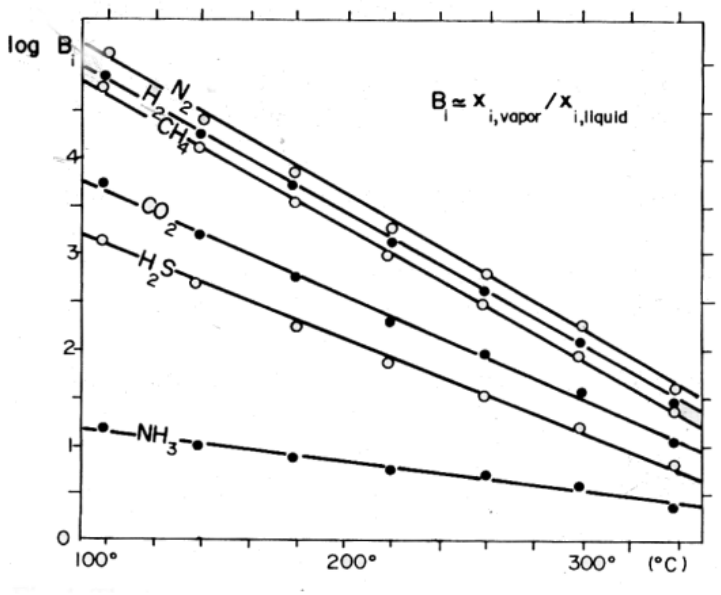


Fig. 6.3. Temperature dependence of the vapor-liquid distribution coefficient for different gases (from Giggenbach, 1980).

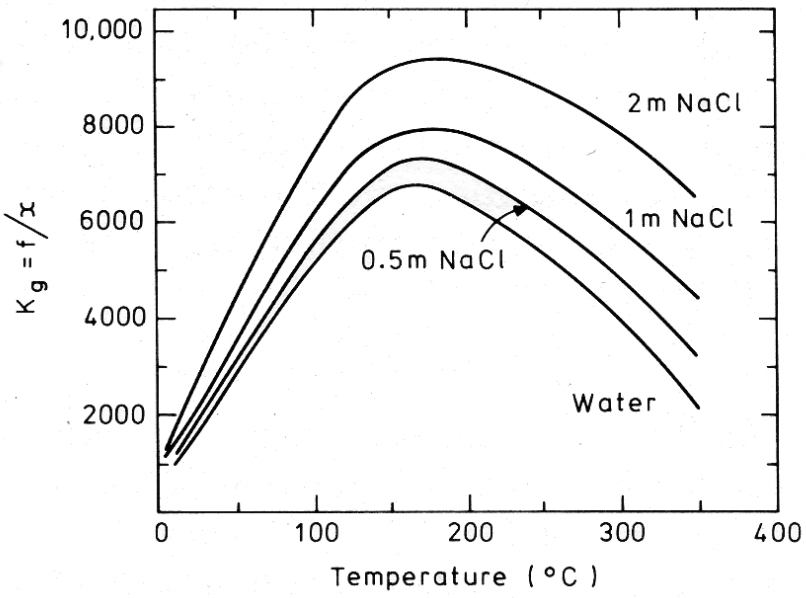


Fig. 6.4 Values of the Henry's Law constant for $CO_2$ in water and in 0.5 NaCl solution (data from Ellis and Golding, 1963).

In multi-step separation the composition of the residual liquid at any step may be taken to be representative of that of the initial liquid of the subsequent step. If a large number of steps is taken, and each step is characterized by very small, constant steam fractions, then the continuous separation mechanism is satisfactorily approached.

The influence of steam separation processes on gas composition is suitably displayed in triangular plots, such as the $H_2O$-$CO_2$-$H_2S$, $H_2O$-$CO_2$-$N_2$ and $H_2O$-$CO_2$-

$CH_4$ plots (Fig. 6.5). Let us recall that $H_2S$ is more soluble than $CO_2$ and that $CO_2$ is more soluble than both $N_2$ and $CH_4$, which have similar solubility.

In single-step separation, early vapors are close to the vertex of the least soluble gas, i.e., $CO_2$ in (a), $N_2$ in (b), and $CH_4$ in (c), while later vapors move towards the $H_2O$ vertex and get progressively close to the composition of the initial liquid (which obviously limits the process). The trend bends slightly towards the vertex of the most soluble gas, i.e., $H_2S$ in (a) and $CO_2$ in (b) and (c). Multi-step separation (not shown) is outlined by a compositional trend that moves towards the vertex of $H_2O$, bending strongly towards the vertex of of the most soluble gas.

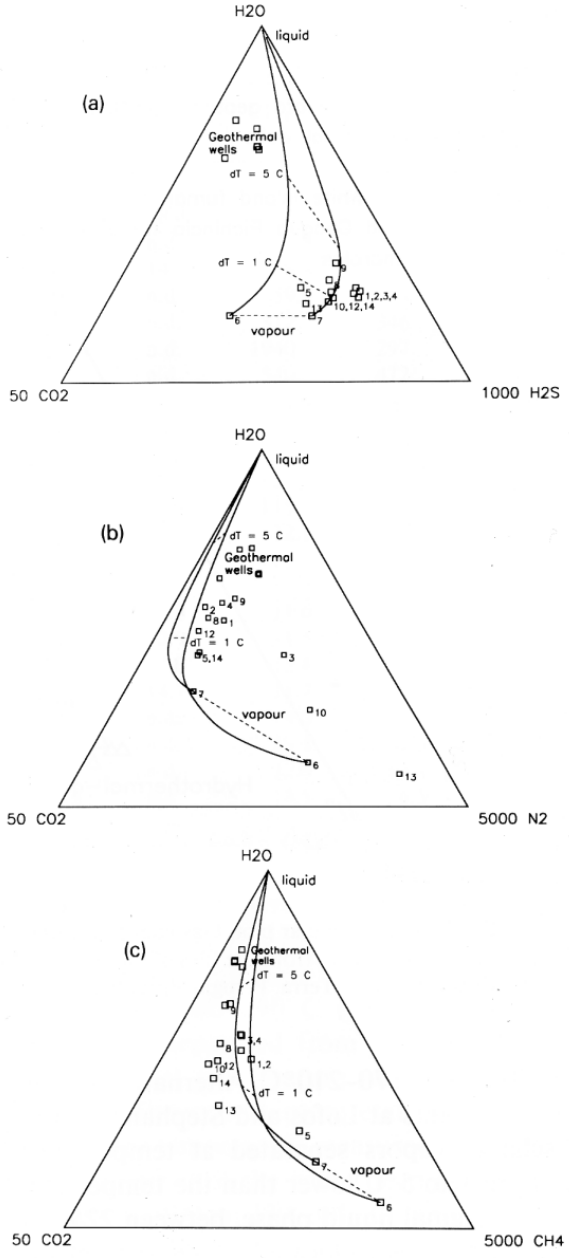


Fig. 6.5 Triangular plots (a) $H_2O$-$CO_2$-$H_2S$, (b) $H_2O$-$CO_2$-$N_2$, and (c) $H_2O$-$CO_2$-$CH_4$ for the fluids discharges by the Nisyros fumaroles, Greece, also showing the theoretical curves of single-step steam separation from the single liquid phase in equilibrium with samples 6 and 7 (from Chiodini et al., 1993a).

## 7. Hydrothermal alteration minerals in high-temperature geothermal systems

Several geochemical methods are based on the relationships between hydrothermal alteration minerals occurring in high-temperature geothermal systems and fluids circulating within these systems. These methods include not only the popular chemical geothermometers and other techniques focusing on water-rock interaction (or mineral-solution equilibrium), but also the evaluation of irreversible mass transfer taking place during water-rock interaction (Helgeson, 1968; Helgeson et al., 1969; 1970), which represents a powerful tool to reconstruct the origin of geothermal fluids (Helgeson, 1979; Reed, 1997; Marini et al., 2003b, see section 4.4.1).

Therefore, knowledge of hydrothermal alteration mineralogy developing in high-temperature geothermal systems is of upmost importance for fluid geochemistry. Luckily, hydrothermal alteration minerals, which are present within the cuttings and the less frequent cores collected during drilling, have been the subject of many investigations (e.g., Browne, 1970, 1977, 1982; Heald et al., 1987; Steiner, 1977).

Browne (1970), studying the Broadlands geothermal field, New Zealand, pointed out that some hydrothermal minerals (e.g., pyrite, calcite, and quartz) are of little use for evaluating deep temperatures and permeabilities. The reason for this is that these minerals are stable over large temperature intervals. He found that the most informative minerals are the authigenic feldspars, which are sensitive to both temperature and permeability. At Broadlands, the most common primary feldspar mineral is andesine and it is altered to quartz, clay, calcite, albite, or adularia at temperatures of 70-290°C, depending on permeability. Albite replaces andesine above 230°C. Production zones contain abundant adularia, associated with quartz and calcite.

Browne (1977) described 51 hydrothermal minerals typical of active geothermal systems, whose occurrence depends on several factors, such as temperature, pressure, fluid composition, and permeability. For instance, epidote is an indicator of high temperature, whereas adularia, again, indicates both high temperature and high permeability.

Although the sequence of alteration minerals varies from system to system, there is a general relationship between hydrothermal alteration minerals and temperature ranges, as summarized by Henley and Ellis (1983; Fig. 7.1). The same mineral parageneses were also recognized in fossil geothermal systems, i.e., in hydrothermal ore deposits.

Figure 7.1 does not report the mineral phases which forms in near-surface steam-heated zones, where acid-sulfate waters are produced through absorption of $H_2S$-bearing vapors in shallow groundwaters or surface waters, followed by oxidation, driven by atmospheric oxygen, of $H_2S$ to sulfuric acid. Interaction of these acidic solutions with rocks determines the formation of kaolinite, alunite, gypsum, opal, and hydrated iron oxides (Steiner, 1977). These are the typical phases of the so-called **advanced argillic alteration**.

Among the minerals reported in Fig. 7.1, only quartz, calcite, adularia, and albite can be considered as relatively pure phases. Several minerals (e.g., epidote and chlorites) exhibit, instead, compositional changes due to solid phase mixing. Further complications are due to the development of mixed-layer minerals, such as those involving clays and chlorites. Moreover, chlorites show a transition, with increasing temperature, from swelling chlorites through mixed swelling and non-swelling chlorites to non-swelling chlorites, as indicated in Fig. 7.1.

In spite of these complications, the geothermal systems explored through deep drilling have shown a thermal zoning of the hydrothermal alteration mineralogy, which has led to the identification of the following hydrothermal alteration zones.

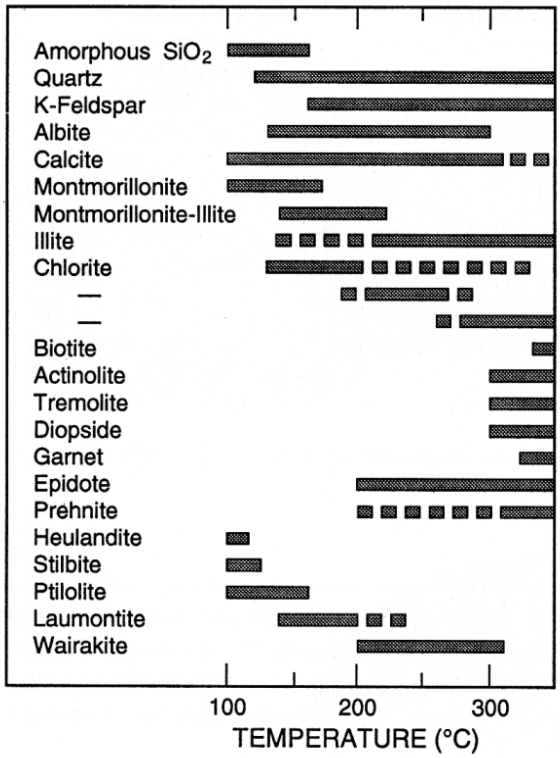


Fig. 7.1. Temperature ranges for typical hydrothermal alteration minerals. Solid and dashed bars indicate the most and less frequent temperature ranges of occurrence, respectively (from Henley and Ellis, 1983).

The shallowest zone is the **argillic** zone, which is characterized by the presence of montmorillonite, eventually accompanied by illite, chlorites and low-temperature zeolites (e.g., heulandite, stilbite). This zone develops up to temperatures of 150-160°C, above which montmorillonite becomes unstable.

The strong increase in chlorite and illite contents and the appearance of mixed-layer clays characterize the transition to the **phyllitic zone**, also termed illite-chlorite zone, which develops up to temperatures close to 200-250°C. The zeolite mineral typical of this zone is laumontite.

The following zone, called **propylitic zone** or zone of Ca-Al-silicates, is characterized by the presence of secondary minerals, which are close to equilibrium with neutral, sodium-chloride aqueous solution. This zone develops up to temperatures of 300°C. Epidote, the most typical mineral, can start to form in small amounts within the phyllitic zone, but it becomes abundant in the propylitic zone. Epidote is usually accompanied by abundant adularia, albite, and sulfide minerals (e.g., pyrite, pyrrhotite, and sphalerite). The zeolite mineral typical of this zone is wairakite. Chlorite and illite are also stable within this zone, but are less abundant than in the phyllitic zone.

The deepest zone is the **thermo-metamorphic zone**, which is characterized by remarkable textural re-organizations of the original lithotypes and by the appearance of high-temperature mineral phases, such as amphiboles (e.g., actinolite and tremolite), pyroxenes (e.g., diopside), biotite, and garnets.

It must be underscored that the rocks affected by argillic and phyllitic alterations are characterized by extremely low permeability. In fact, the minerals typical of these two zones behave plastically under mechanic stress. Therefore, these two zones constitute the cover (or cap-rock) of the geothermal system. The hydrothermal minerals

of the propylitic and thermo-metamorphic zones exhibit instead brittle behavior, permitting the development of fractures, which act as high permeability pathways for geothermal fluids. Therefore these two hydrothermal alteration zones mark the geothermal reservoirs.

On this thermal zoning of the hydrothermal alteration mineralogy are based the petrographic logs, which are generally carried out during deep geothermal drillings.

## 8. Geothermometric methods for geothermal waters

### *8.1. Introduction*

Geothermometers and $P_{CO2}$-indicators (also called geobarometers) are relatively simple functions in which one plugs in the chemical data of hydrothermal fluid samples to compute the equilibrium temperature and $P_{CO2}$, respectively, that are presumably present in the zones where these hydrothermal fluid samples are thought to have attained chemical equilibrium.

Water partial pressure is usually assumed to be constrained by coexistence of liquid and vapor phases (saturation). Total fluid pressure is then obtained by summing $P_{CO2}$ and $P_{H2O}$, as $H_2O$ and $CO_2$ are generally the two major constituents of hydrothermal fluids.

The basic assumptions of geothermometry and geobarometry are:
(1) chemical equilibrium is attained in the reservoir multiphase system, which is generally constituted by hydrothermal (secondary) minerals, the aqueous solution, and eventually a separated gas phase (as already underscored in section 3.1.2, the latter is generally called vapor phase, due to the prevalence of water vapor);
(2) the sample collected at the surface (from a hydrothermal manifestation such as a thermal spring or a fumarole) is fully representative of the hydrothermal fluid present into the reservoir.

Hypothesis (2) is not always satisfied. The parent hydrothermal liquid, during the ascent towards the surface, either mixes with shallow waters or separates a vapor phase or precipitates some mineral phases or re-equilibrates at decreasing temperatures. The hydrothermal vapor, either present into the hydrothermal reservoir or produced through boiling (steam separation) of the parent hydrothermal liquid, experiences secondary processes such as steam condensation and air entrainment at shallow levels. It is rather obvious that we have to model the effects of these secondary processes for a correct application of geothermometric and geobarometric techniques.

Most geothermometers, including the Na-K and silica geothermometers were initially derived on a purely empirical basis. Long ago, geochemists observed a general decrease in Na/K ratio and a general increase in $SiO_2$ concentration of thermal waters with increasing temperatures and based the first geothermometers on these empirical correlations. Studies of hydrothermal alteration mineralogy developing in high-temperature hydrothermal systems (e.g., Browne, 1970), and modeling of the mineral-solution equilibria and of the irreversible mass transfer taking place during water-rock interaction (see sections 7 and 4.4.1) suggested that geothermometers are governed by equilibrium reactions between hydrothermal minerals and the aqueous solution under reservoir conditions. A new generation of geothermometric techniques was consequently proposed, based on both the solubility of different silica minerals (e.g., Fournier and Potter, 1982; Arnórsson et al., 1983; Giggenbach, 1991a) and mineral-solution exchange reactions. In the latter class of geothermometers it is worth to mention the Na-K geothermometers of Fournier (1979b) and Arnórsson et al. (1983), and the Na-K-Mg-Ca geoindicators of Giggenbach (1988). Finally a theoretical justification for ionic solutes geothermometers and $P_{CO2}$-indicators was found by Guidi et al. (1990b) and Chiodini et al. (1991a).

For what concerns gas equilibria, a great contribution was given by Giggenbach (1980), who introduced vapor-liquid gas distribution coefficients into equilibrium relations and demonstrated the importance of addition to or removal from equilibrium liquids of equilibrium vapors. The approach of Giggenbach (1980) was adapted to fumarolic gas discharges by Chiodini and Marini (1998). Besides, a geothermometric function based on the $H_2$/Ar ratio was proposed by Giggenbach (1991a), who

hypothesized that Ar is present in hydrothermal fluids in relative contents close to those of air-saturated groundwater. Following a similar approach, a $CO_2/N_2$ geothermometer was earlier suggested by Arnórsson (1987).

The purpose of this section is to review the main geothermometers and $P_{CO2}$-indicators, trying to emphasize advantages and limitations and to give practical hints to the user.

### *8.2. The silica geothermometers*

The solubilities of all silica minerals increase with increasing temperature. Plotting the logarithm of dissolved silica versus the inverse of the absolute temperature, the data for several silica minerals (quartz, chalcedony, α-cristobalite, opal-CT, and amorphous silica) lie along straight lines in the 20-250 °C range, even in the residual water after single-step steam separation at 100 °C or maximum steam loss (Fig. 8.1).

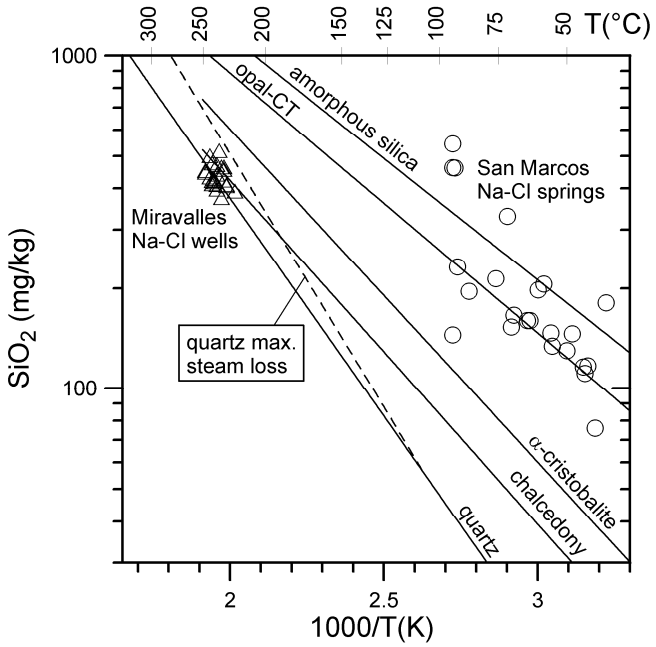


Fig. 8.1. Solubility of several silica minerals in water at the vapor pressure of the solution (from Fournier, 1973, 1991). Also shown are the deep Na-Cl geothermal liquids of Miravalles, Costa Rica (Marini et al., 2003b) and the Na-Cl thermal springs of San Marcos, Guatemala (Marini et al., 1998).

The equations of these straight lines are as follows, where $SiO_2$ indicates silica concentration in mg/kg (from Fournier, 1973, 1991):

$$T(°C) = \frac{1309}{5.19 - \log(SiO_2)} - 273.15, \text{ for quartz;} \quad (8.1)$$

$$T(°C) = \frac{1522}{5.75 - \log(SiO_2)} - 273.15, \text{ for quartz (maximum steam loss);} \quad (8.2)$$

$$T(°C) = \frac{1032}{4.69 - \log(SiO_2)} - 273.15, \text{ for chalcedony;} \quad (8.3)$$

$$T(°C) = \frac{1000}{4.78 - \log(SiO_2)} - 273.15 \text{, for } \alpha\text{-cristobalite;} \quad (8.4)$$

$$T(°C) = \frac{781}{4.51 - \log(SiO_2)} - 273.15 \text{, for opal-CT;} \quad (8.5)$$

$$T(°C) = \frac{731}{4.52 - \log(SiO_2)} - 273.15 \text{, for amorphous silica.} \quad (8.6)$$

The rate of quartz dissolution / precipitation depends strongly on temperature and is relatively fast at high temperatures and very slow at low temperature (Rimstidt and Barnes, 1980). This explains why: (1) in the geothermal reservoirs of constant, high temperature (generally > 180°C), liquids attain saturation with respect to quartz, after relatively long water-rock interaction (e.g., the deep Na-Cl geothermal liquids of Miravalles, Costa Rica, in Fig. 8.1) and (2) little dissolved silica polymerizes and precipitates during the relatively fast ascent of geothermal waters, even though saturation with respect to quartz is largely exceeded. On the other hand, amorphous silica precipitates relatively fast when saturation with respect to it is exceeded, although the lack of solubility and polymerization data at high temperatures, pH and in multi-component solutions limits the understanding of amorphous silica behavior (Chan, 1989). As a matter of fact, amorphous silica saturation poses an upper limit on the silica concentrations attainable in many natural aqueous environments (e.g., the Na-Cl thermal springs of San Marcos, Guatemala, in Fig. 8.1).

Below 300 °C and depths of some km, variations in hydrostatic pressure have small influence on the solubilities of quartz and amorphous silica (Fournier and Potter, 1982; Fournier and Rowe, 1977). The effects of added salts are significant only for concentrations greater than 2-3 wt% approximately (Marshall, 1980; Chen and Marshall, 1982; Fleming and Crerar, 1982; Fournier and Marshall, 1983; Fournier, 1985). However, above 300°C small variations in pressure and salinity becomes very important.

Since the $pK_A$ of the dissociation of silicic acid:

$$H_4SiO_4^\circ = H^+ + H_3SiO_4^- \quad (8.7)$$

varies between 10.3 and 8.8, in the 0-350°C range (Fig. 8.2), the solubility of silica is also affected by pH, for pH values above 7.8-9.3, depending on temperature. Besides, for pH < 2.5, acid-driven dissolution of Al-silicates may control dissolved silica at concentrations greater than solubilities of quartz and chalcedony, particularly for temperatures < 100-150 °C (Fournier, 1991). However, since the pH of geothermal reservoir liquids is generally constrained at values of 5-7 by water-rock reactions, corrections for pH-effects are rarely needed in geothermometric calculations.

For all these reasons, dissolved silica in solutions of near neutral pH from geothermal wells is a reliable geothermometer. The interpretation of dissolved silica from hot springs is somewhat ambiguous because of uncertainties about the mineral controlling dissolved silica and the amount of steam possibly separated (Fournier, 1991).

*8.2.1. The temperature dependence of isocoulombic reactions*

At this point, it is useful to make a digression on the temperature dependence of the dissociation constant of silicic acid. The pK – 1/T(K) relation is far from linear (Fig.

8.2a) because reaction (8.7) is not isocoulombic. An isocoulombic reaction has the same number of ionic species having the same charge on each side.

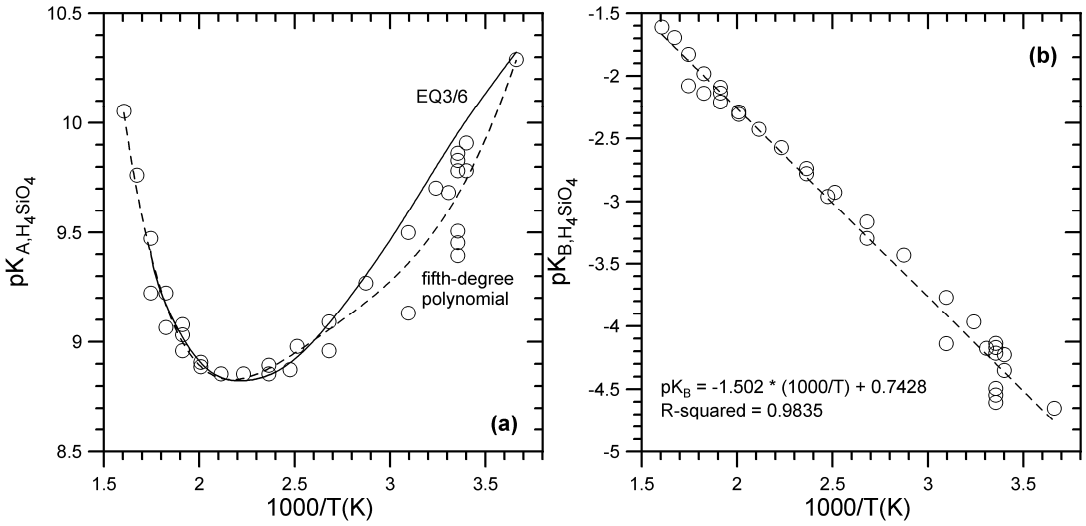


Fig. 8.2 Temperature dependence of the pK of (a) the silicic acid dissociation (reaction 8.7) and (b) the silicic acid neutralization (reaction 8.8), based on different experimental data (from Fleming and Crerar, 1982 and references therein).

Reaction (8.7) does not satisfy this condition, but it can be transformed into an isocoulombic reaction by summing the reaction of association of hydrogen ion and hydroxyl ion to give water, thus obtaining:

$$H_4SiO_4^\circ + OH^- = H_3SiO_4^- + H_2O. \qquad (8.8)$$

It is known that the reaction heat capacity, $\Delta C_P^\circ{}_r$, of isocoulombic reactions is close to zero (Anderson and Crerar, 1993). This implies that the enthalpy of isocoulombic reactions is nearly constant, independent of temperature, since the following relation holds:

$$\left(\frac{\partial\left(\Delta H_r^o\right)}{\partial T}\right)_P = \Delta C_{P,r}^o \qquad (8.9)$$

To gain more insights on this matter let us recall the van't Hoff equation:

$$\ln\frac{K_2}{K_1} = \int_{T_1}^{T_2}\frac{\Delta H_r^o}{RT^2}dT, \qquad (8.10)$$

which is easily integrated if $\Delta H^\circ_r$ is a constant, independent of temperature. The integrated result is:

$$-\log K_2 = -\log K_1 + \frac{\Delta H_r^o}{2.303R}\left(\frac{1}{T_2} - \frac{1}{T_1}\right) \qquad (8.11)$$

Subscript 1 usually refers to the reference temperature of 25°C. If this expression is obeyed, a straight line of slope [$-\Delta H^\circ_r$ / 2.303 R] and intercept [log $K_1$ + ($\Delta H^\circ_r$ / 4.576

$T_1$)] is obtained in a plot of log K versus 1/T(K). The linearity in such a plot is evidence that $\Delta H°_r$ is a constant, independent of temperature. As expected for isocoulombic reactions, linearity is observed in Fig. 8.2b. Incidentally, the slope of this plot allows one to evaluate the value of $\Delta H°_r$, which turns out to be $-1502 \times 2.303 \times 1.987165 = -6874$ cal/mol.

Revisiting Fig. 8.1 in the light of the insights gained so far, it is evident that the linear relation between log $SiO_2$ and 1/T for all the silica geothermometers is due to the fact that they refer to isocoulombic reactions of the type:

$$SiO_{2(s)} = SiO_{2(aq)}, \qquad (8.12)$$

where $SiO_{2(s)}$ is a solid phase of silica (either quartz, or chalcedony, or α-cristobalite, or opal-CT, or amorphous silica) and $SiO_{2(aq)}$ identifies dissolved silica.
We will see that most geothermometers relate to isocoulombic reactions as well.

*8.2.2. More on the quartz geothermometer*
Irrespective of these findings, Fournier and Potter (1982) proposed a mathematically different formulation of the quartz geothermometer:

$$T(°C) = -42.198 + 0.28831\ SiO_2 - 3.6686\ 10^{-4}\ SiO_2^2 + 3.1665\ 10^{-7}\ SiO_2^3 + 77.034 \log SiO_2, \qquad (8.13)$$

where $SiO_2$ is the silica concentration in mg/kg.

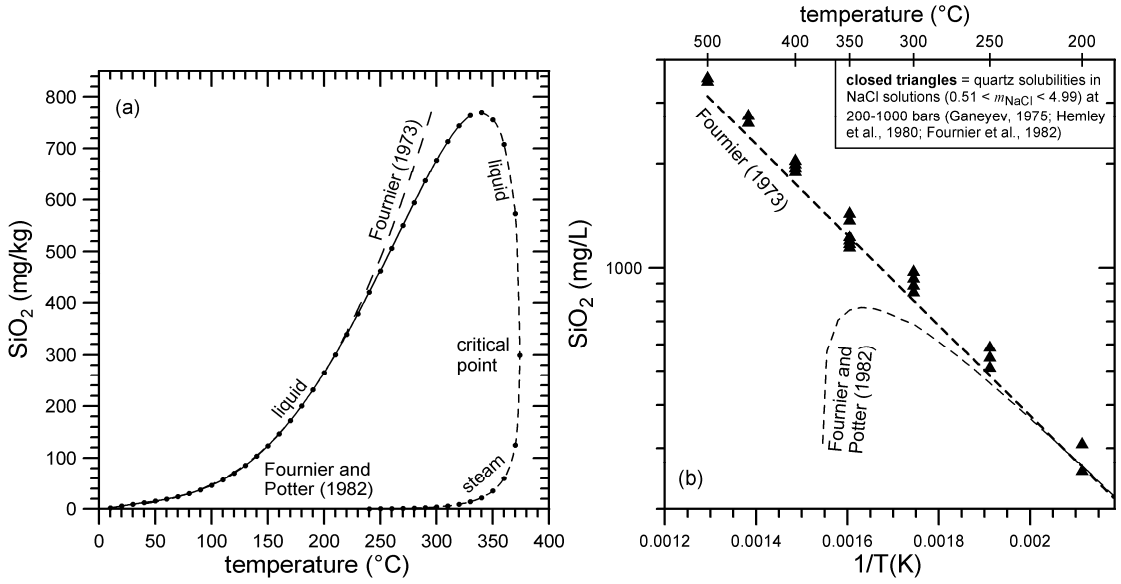


Fig. 8.3 (a) Solubility of quartz in water at the vapor pressure of the solution (from Fournier, 1991). Dots (from Fournier and Potter, 1982) are partly connected by a solid line (equation 8.13) and partly by a dashed line, beyond the range of applicability of equation (8.13). Also shown is the geothermometer by Fournier (1973, equation 8.1). (b) The quartz geothermometers of Fournier (1973) and Fournier and Potter (1982) (dashed lines) are compared with quartz solubilities in Na-Cl aqueous solutions with $0.51 < m_{NaCl} < 4.99$ (Ganeyev, 1975; Hemley et al., 1980; Fournier et al., 1982) at temperatures of 200-500°C and pressures of 200-1000 bars (triangles).

Equation (8.13) can be used in the range 20-330 °C, where it closely fits quartz solubility data in pure water. Linear functions in 1/T(K), such as equation (8.1), diverge significantly from equation (8.13) above 250 °C (Fig. 8.3a).

However, quartz solubilities measured in aqueous NaCl solutions with $0.51 < m_{NaCl} < 4.99$ (Ganeyev, 1975; Hemley et al., 1980; Fournier et al., 1982), at temperatures of 200-500°C and pressures of 200-1000 bars, i.e., above saturation conditions, lie along equation (8.1) as well (Fig. 8.3b). This indicates that changes in pressure and NaCl concentration have minor effects on quartz solubility, which is mainly governed by temperature (Fournier, 1983). Consequently, equation (8.1) can be safely used as a geothermometer up to temperatures of at least 500°C for concentrated and/or high-pressure aqueous solutions.

The choice of the "best" geothermometric function depends on the characteristics of the electrolyte solution under study.

*8.2.3. The chalcedony geothermometer*

Chalcedony is an aggregate of very tiny quartz grains. These small dimensions determine large surface energies, which make chalcedony more soluble than quartz. At T > 120-180 °C, chalcedony is unstable in contact with water and is quickly replaced by larger-sized quartz crystals. The size of quartz grains is controlled by several factors: temperature, time, fluid composition and origin, either re-crystallization of amorphous silica or direct precipitation of quartz. It turns out that in some places quartz controls dissolved silica at temperaturs as low as 100 °C, for instance where water has been in contact with rocks for comparatively long lapses of time. In other places, chalcedony governs dissolved silica up to 180 °C, especially in portions of geothermal systems recently affected by fracturing.

Therefore, it is recommendable (Fournier, 1991) to compute both quartz temperatures and chalcedony temperatures, below 180 °C, by means of either equations (8.1) or (8.13) and (8.3). The latter is quite similar to that derived empirically by Arnorsson et al. (1983) for chalcedony:

$$T(°C) = \frac{1112}{4.91 - \log(SiO_2)} - 273.15\,, \qquad (8.14)$$

where $SiO_2$ is the silica concentration in mg/kg.

*8.2.4. The silica vs. enthalpy diagram*

Rather than inspecting a table reporting the temperatures calculated by means of the silica geothermometers, it is advisable to construct and investigate a plot of silica vs. enthalpy, where both the solubility of quartz and other silica minerals are reported together with the analyzed waters.

As already noted, most geothermal liquids have sufficiently low salinities, so that enthalpies of pure water can be used to construct the silica vs. enthalpy diagram. Fournier and Potter (1982) have proposed the following relationships to relate the enthalpies of liquid water ($H_L$) and vapor ($H_V$) to temperature (T, in °C), at the vapor pressure of the solutions, in the temperature range 50 to 340 °C (complete dataset from Keenan et al., 1969):

$$H_L = 418.84 + 10.286\,T - 0.05092\,T^2 + 2.6309\,10^{-4}\,T^3 - 6.9303\,10^{-7}\,T^4 + 7.4566\,10^{-10}\,T^5 - 1209.8\,T^{-1} + 11.99\,T^{-2} - 353.76\log T \qquad (8.15)$$

$$H_V = 2035 - 5.0499\,T + 0.057399\,T^2 - 3.0426\,10^{-4}\,T^3 + 7.909510^{-7}\,T^4$$

$$-8.6968\ 10^{-10}\ T^5 + 1342.4\ T^{-1} - 13.298\ T^{-2} + 396.29 \log T \qquad (8.16)$$

From 0 to 50°C, $H_L$ is closely approximated by the following relationship, which must be used instead of equation (8.15):

$$H_L = 4.1868\ T. \qquad (8.17)$$

The solubility of quartz in liquid water at vapor pressure of the solutions is related to enthalpy (for $H_L < 1670$ J/g) by the following function (Fournier and Potter, 1982):

$$SiO_2 = -3.5532 + 0.146\ H_L - 4.927\ 10^{-4}\ H_L^2 + 1.2305\ 10^{-6}\ H_L^3 - 4.9421\ 10^{-10}\ H_L^4 \qquad (8.18)$$

where $SiO_2$ is the silica concentration in mg/kg.
Use of equations (8.15)-(8.18) allows the construction of a silica vs. enthalpy diagram such as that of Fig. 8.4.

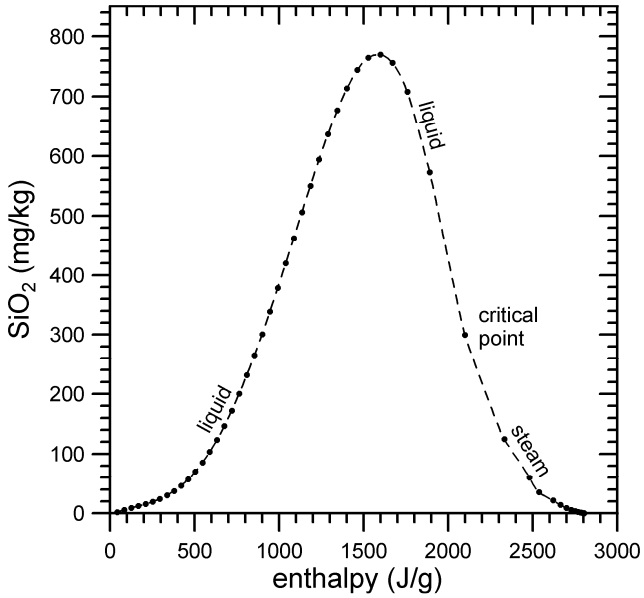


Fig. 8.4. Solubility of quartz in water at vapor pressure of the solutions as a function of enthalpy (from Fournier, 1991).

Relating the solubility of quartz to enthalpy instead of temperature has several advantages.
(1) The solubility of quartz in water (liquid and steam) is represented by a bell-shaped symmetrical curve, which reaches a maximum of 770 mg/kg at 1594 J/g (corresponding to 340°C) and decreases with a further increase in enthalpy. Therefore, at a given enthalpy, there is only one value of dissolved silica, while at a given temperature there are two values of dissolved silica, one for the liquid and one for the steam (compare Fig. 8.4 with Fig. 8.3a).
(2) If iso-enthalpic boiling occurs (which is a realistic assumption for the irreversible adiabatic processes taking place in geothermal wells and high-flow rate natural geothermal manifestations), the silica vs. enthalpy plot allows a quick determination of the silica concentration and enthalpy of the initial liquid before boiling assuming (a) single-step steam loss and (b) that dissolved silica is controlled by quartz solubility.

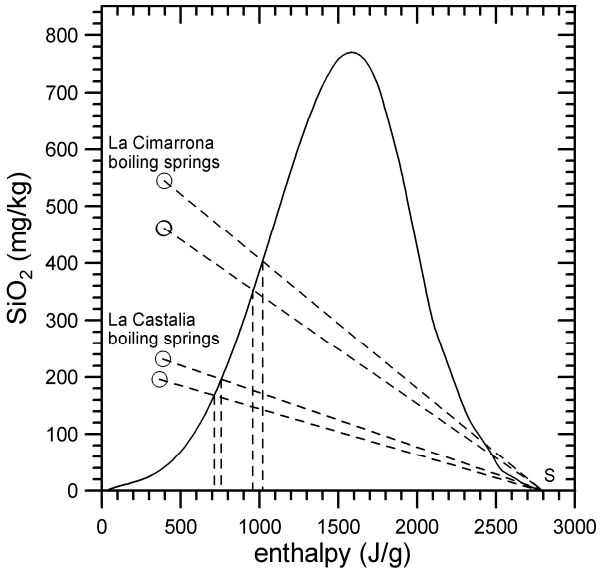


Fig. 8.5 Enthapy-silica plot showing that the enthalpy and silica content of the initial liquids before boiling are given by the intersection of the quartz solubility curve with the line joining the steam point at 100°C, 1.013 bar (S) and the boiled liquids (circles, data from Marini et al., 1998). Adapted from Fournier (1991).

This graphical exercise, shown in Fig. 8.5 for some boiling springs of San Marcos, Guatemala (Marini et al., 1998), corresponds to solve a system constituted by equation (8.18) rewritten as follows:

$$SiO_{2,O} = -3.5532 + 0.146\, H_O - 4.927\, 10^{-4}\, H_O^2 + 1.2305\, 10^{-6}\, H_O^3 - 4.9421\, 10^{-10}\, H_O^4, \quad (8.18a)$$

the mass balance:

$$SiO_{2,O} = SiO_{2,L}\,(1 - y) + SiO_{2,V}\, y, \quad (8.19)$$

and the enthalpic balance (no balance can be written for temperature):

$$H_O = H_L\,(1 - y) + H_V\, y, \quad (8.20)$$

where indices O, L, and V refer to the deep water, the separated liquid, and the separated steam and y is the steam fraction. Note that, assuming steam separation at 100°C and $SiO_{2,V} = 0$, equations (8.19) and (8.20) reduce to

$$SiO_{2,O} = SiO_{2,L}\,\frac{2676 - H_O}{2257}. \quad (8.21)$$

For La Cimarrona springs with $SiO_{2,L}$ of 545 and 462 mg/kg, $H_O$ turns out to be 1014 and 958 J/g, corresponding to quartz equilibrium temperatures of 235 and 223°C, respectively. For La Castalia springs with $SiO_{2,L}$ of 196 and 232 mg/kg, $H_O$ is 715 and 759 J/g, corresponding to quartz equilibrium temperatures of 169 and 179°C, respectively. These temperature values are only slightly smaller than those proposed by Marini et al. (1998), i.e., 240°C for La Cimarrona and 185°C for La Castalia.

(3) In a binary mixture, the concentration, $C_M$, of any conservative constituent is given by equation (6.1). If the two waters mix without loss or gain of heat, the combined enthalpies are conserved (neglecting second-order effects, such as the heat of dilution) in proportions dictated by the enthalpy balance (equation 6.2). Again, no balance can be written for temperature. Therefore, under the hypothesis stated above, enthalpy can be treated similar to mass, which makes the silica vs. enthalpy plot a good tool to investigated iso-enthalpic mixing. In fact, if iso-enthalpic mixing takes place without silica precipitation before and after mixing and without steam loss, this plot can be used to determine the temperature of the hot-water component (Truesdell and Fournier, 1977): the straight line drawn from the cold endmember through the mixtures to the intersection with the quartz solubility curve gives the initial silica content and enthalpy of the hot-water endmember (Fig. 8.6).

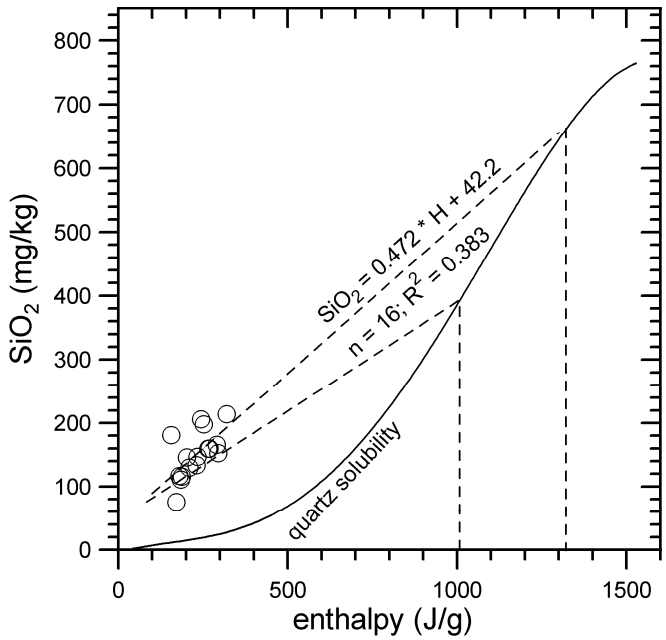


Fig. 8.6 Enthapy-silica plot illustrating the application of the silica mixing model (Truesdell and Fournier, 1977) to the Na-Cl unboiled thermal springs of San Marcos (data from Marini et al., 1998).

However, if conductive cooling took place, the inferred enthalpy of the hot-water endmember will be too high. This is the case of the Na-Cl unboiled thermal springs of San Marcos, whose linear regression equation in the silica vs. enthalpy plot intersects the quartz solubility curve for an enthalpy of ~1320 J/g, corresponding to a temperature of 295°C for the hot-water component. This value does not make sense for this geothermal site. However, the eyeball line drawn through the springs less affected by heat loss leads to estimate an enthalpy of ~1000 J/g for the hot-water component. This corresponds to a temperature close to 235°C, which agrees with the results of other geothermometric methods.

### *8.3. The ionic solutes geothermometers and $P_{CO2}$-indicators*

#### *8.3.1. The Na-K geothermometer*

As already recalled, a general decrease in Na/K ratios of thermal waters with increasing temperatures was observed long ago (White, 1957; Ellis and Wilson, 1960; Ellis and Mahon, 1964). The initial attempts to derive, from these observations, an empirical Na-

K geothermometer led to equations (White, 1965, Ellis and Mahon, 1967) with relatively small temperature dependences, due to the inclusion in the data sets of poorly equilibrated spring waters.

A calibration equation with a higher temperature dependence was proposed by Fournier and Truesdell (1973), evidently because they took into account experimental data on cation exchanges between coexisting Na- and K-feldspars (Orville, 1963; Hemley, 1967). The relationships proposed later by Truesdell (1975) and Arnorsson et al. (1983) did not led to substantial modifications (Fig. 8.7).

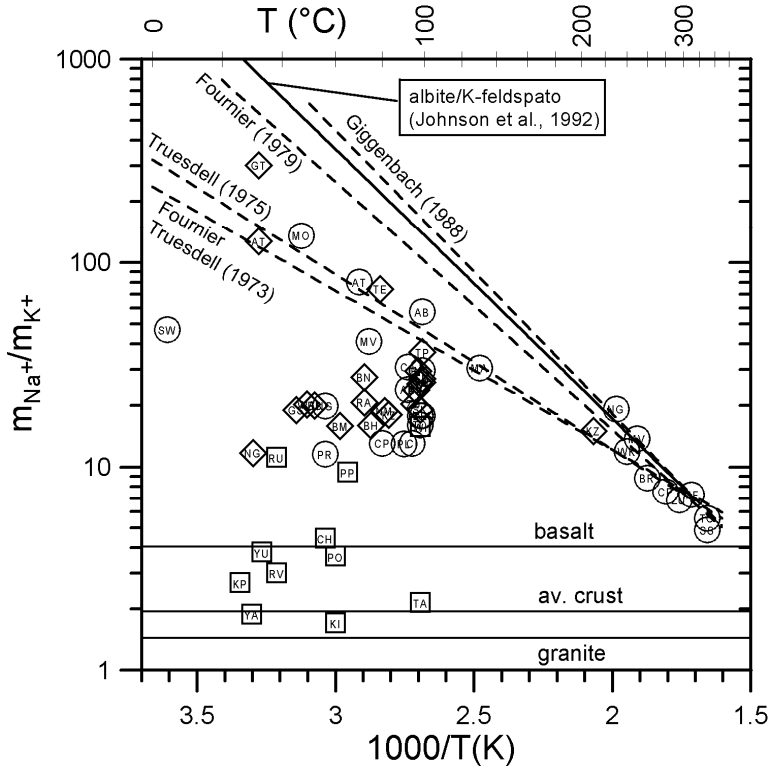


Fig. 8.7. Empirical, theoretical and analytical Na/K molal ratios of geothermal liquids as a function of temperature (from Giggenbach, 1988, modified); squares = acid sulfate waters; diamonds = Na-bicarbonate waters; circles= neutral chloride waters.

A step forward was done by Fournier (1979b), who carried out an empirical calibration based on well-equilibrated water discharges from deep geothermal wells and oil field brines. In fact, the equation proposed by Fournier (1979b) (concentration in mg/kg):

$$T_{NaK}(°C) = \frac{1217}{1.483 + \log(Na/K)} - 273.15 \qquad (8.22)$$

closely approach that computed by means of thermodynamic data of Na- and K-feldspars (Johnson et al., 1992).

An other empirical relationship, characterized by a slightly steeper temperature dependence, was suggested by Giggenbach et al. (1983) and Giggenbach (1988) (concentration in mg/kg):

$$T_{NaK}(°C) = \frac{1390}{1.75 + \log(Na/K)} - 273.15\,, \qquad (8.23)$$

again based on well-equilibrated aqueous solutions.

In addition to the empirical formulations of the Na-K geothermometer and the theoretical albite-K-feldspar coexistence, which are representative of partial or complete equilibration with these mineral phases, three horizontal lines representative of rock dissolution (average basalt, average granite, and average crustal rock) are also given in Fig. 8.7, together with selected water compositions on a molal base (Table 1).

Interestingly, neutral chloride waters from deep geothermal wells (circles, T>200°C) and the Na-bicarbonate water from a deep borehole of Kizildere (diamond, T of 210°C) plot close to the theoretical albite-K-feldspar coexistence suggesting attainment of mineral-solution equilibrium. Sodium-Cl springs (circles, T<100°C) have Na-K equilibrium temperatures equal to or slightly lower than corresponding well discharges, suggesting that Na/K ratios are essentially quenched at depth. This agrees with the slow kinetics, below 300°C, of the Na-K exchange between alkali feldspars and aqueous solutions, as indicated by both experiments (Orville, 1963; Hemley, 1967) and well discharges, where the Na/K ratio usually re-equilibrates more slowly than the quartz geothermometer upon temperature changes in response to production (Fournier, 1991). In Fig. 8.7, the Na/K ratio of most acid waters from crater lakes (squares) is consistent with rock dissolution. However the two samples from Ruapehu (Ru) and Popocatepetl (PP) plot above the rock dissolution region, likely due to preferential leaching of Na or uptake of K in alunite. Sodium-bicarbonate spring waters (diamonds) occupy positions intermediate between rock dissolution and equilibration, which might be due to either (i) preferential leaching of Na or uptake of K in clays or (ii) attainment of equilibrium with feldspars at temperatures significantly higher than outlet temperature.

*8.3.2. The K-Mg geothermometer*

It was recognized long ago that Mg contents of thermal waters are strongly dependent on temperature, and this relationship was early attributed to equilibration of geothermal liquids with chlorites (Ellis, 1971) or other Mg-bearing minerals, e.g., montmorillonites and saponites. According to Giggenbach (1988), the behavior of Mg in well-equilibrated geothermal waters is described by the reactions:

$$0.8 \text{ muscovite} + 0.2 \text{ clinochlore} + 5.4 \text{ chalcedony} + 2\ K^+ = 2.8 \text{ K-feldspar} + 1.6 \text{ water} + Mg^{2+} \quad (8.24)$$

and

$$0.8 \text{ muscovite} + 0.2 \text{ clinochlore} + 5.4 \text{ chalcedony} + 2\ Na^+ = 2 \text{ albite} + 0.8 \text{ K-feldspar} + 1.6 \text{ water} + Mg^{2+}. \quad (8.25)$$

The corresponding equilibrium constants are plotted in Figs. 8.8 and 8.9, both for activity of the solid phases equal to 1 and for different values of $AP = 0.8 \log (a_{muscovite}) + 0.2 \log(a_{clinochlore})$ to take into account the effect of the incorporation of muscovite and clinochlore into natural illites and chlorites.

The $Mg/Na^2$ molal ratios of liquids from geothermal wells plot close to the theoretical lines, indicating substantial attainment of mineral-solution equilibrium (Fig. 8.8). A similar position is observed for associated Na-Cl spring waters (and some Na-bicarbonate waters as well), suggesting re-adjustment of mineral-solution equilibrium upon water ascent towards the surface. A notable exception is represented by La Cimarrona spring, Guatemala (CI), whose $Mg/Na^2$ ratio is apparently quenched at a temperature much higher than outlet temperature.

The $Mg/Na^2$ molal ratios of acid waters and some Na-bicarbonate waters are largely controlled by rock dissolution of crustal rocks, indicating that the high Na/K ratios of Fig. 8.7 (with respect to crustal rock composition) are due to uptake of K in alunite or clays rather than preferential leaching of Na.

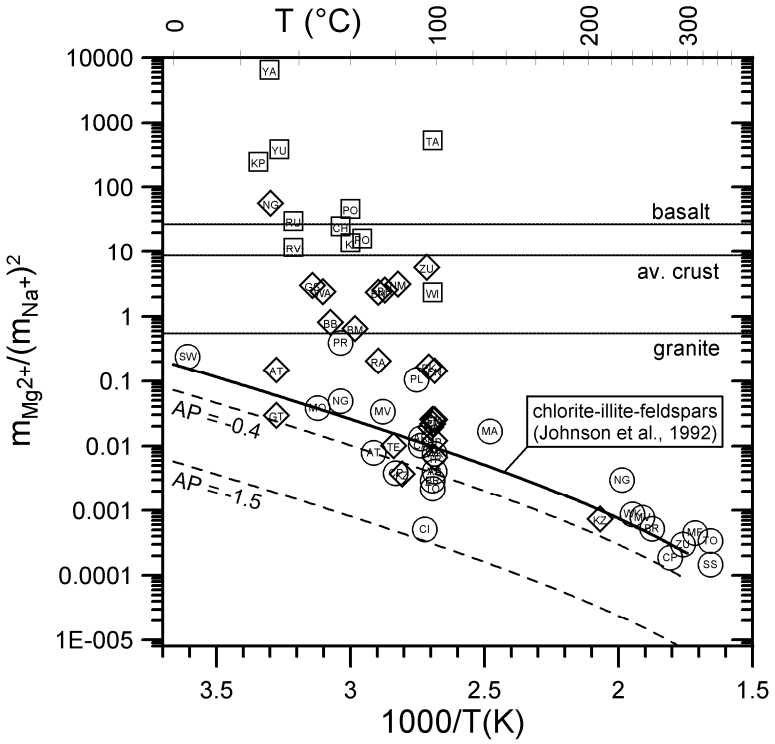


Fig. 8.8 Empirical, theoretical and analytical $Mg/Na^2$ molal ratios of geothermal liquids as a function of temperature (from Giggenbach, 1988, modified); squares = acid sulfate waters; diamonds = Na-bicarbonate waters; circles= neutral chloride waters.

Also the $Mg/K^2$ molal ratios of liquids from geothermal wells plot close to the theoretical lines, indicating attainment of mineral-solution equilibrium, whereas associated springs are shifted to slightly higher values, and have Mg-K equilibrium temperatures somewhat lower than corresponding well discharges, suggesting that $Mg/K^2$ ratios are partly quenched at depth (Fig. 8.9).

Figure 8.9 shows that the compositional ranges of rock dissolution coincide with equilibrium compositions in the low to intermediate temperature range. Acid waters plot either in this range of $Mg/K^2$ ratios or above, due to precipitation of K-rich mineral phases. Bicarbonate waters plot also close to the theoretical lines, indicating that the K-Mg system approaches mineral-solution equilibrium at temperatures as low as 25°C. This implies a fast response of this system upon cooling.

The $Mg/K^2$ ratio represents, therefore, the suitable basis for a geothermometer, which was, in fact, proposed by Giggenbach et al. (1983) and later slightly revised by Giggenbach (1988), who reported the following equation (concentrations in mg/kg):

$$T_{KMg}(°C) = \frac{4410}{14.0 - \log(K^2/Mg)} - 273.15. \qquad (8.26)$$

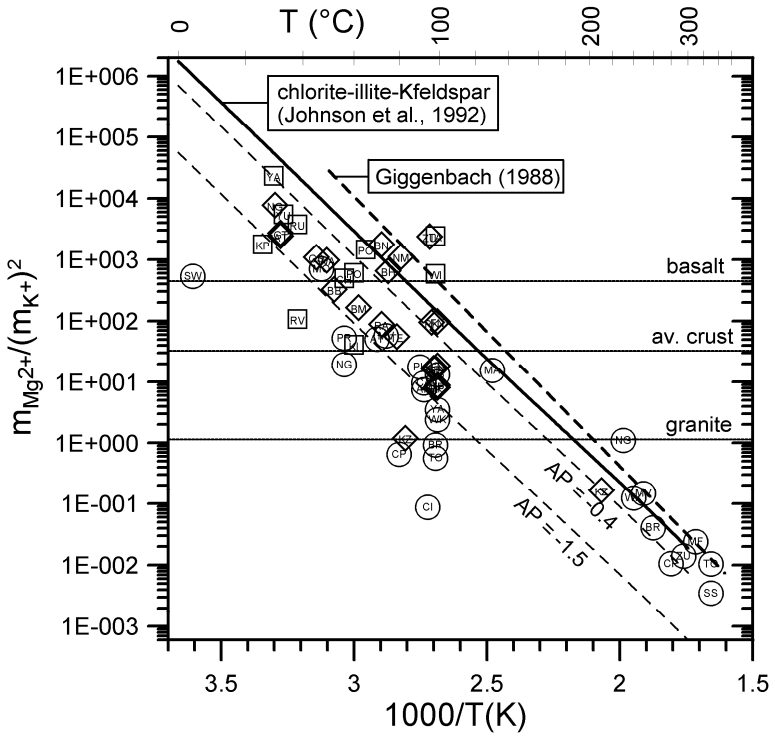


Fig. 8.9. Empirical, theoretical and analytical $Mg/K^2$ molal ratios of geothermal liquids as a function of temperature (from Giggenbach, 1988, modified); squares = acid sulfate waters; diamonds = Na-bicarbonate waters; circles= neutral chloride waters.

Combining the fast-responding K-Mg geothermometer with the slowly re-equilibrating Na-K geothermometer, by means of a triangular plot, Giggenbach (1988) suggested an excellent method to assess the degree of attainment of water-rock equilibrium (Fig. 8.10).

In this Na-K-$Mg^{1/2}$ plot, the two systems are presented by two sets of lines of constant Na/K ratios and $K/Mg^{1/2}$ ratios, radiating from the $Mg^{1/2}$ vertex and the Na vertex, respectively. Since at each value of the Na/K ratio and $K/Mg^{1/2}$ ratio corresponds a unique temperature value, each of these lines is an isotherm. The intersections of the Na-K and K-Mg isotherms, referring to the same temperatures, correspond to water compositions in equilibrium with the mineral phases controlling both geothermometers and delineate the so-called "full equilibrium" curve. The compositions of waters generated through isochemical dissolution of average crustal rocks, also shown in this triangular plot, delineate a rock dissolution area, which is well distinct from the "full equilibrium" curve.

Samples from deep geothermal wells generally plot on the full equilibrium curve, at temperatures slightly higher than those physically measured in these wells. Corresponding spring waters generally plot below the full equilibrium curve and are shifted towards the $Mg^{1/2}$ vertex, indicating that, upon cooling, Mg acquisition by thermal waters proceeds faster than Na acquisition.

Some bicarbonate waters indicate attainment of partial equilibrium, whereas other bicarbonate waters and acid waters are situated close to the $Mg^{1/2}$ vertex. These are the so-called "immature waters", which provide unreliable Na-K temperatures, whereas their K-Mg temperatures may still be valid, at least for not too acid waters.

This Na-K-$Mg^{1/2}$ plot is a powerful tool as it allows:
(i) the immediate distinction between waters suitable or unsuitable for the application of ionic solute geothermometers,

(ii) the assessment of deep equilibrium temperatures, and
(iii) the evaluation of re-equilibration and mixing effects on a large number of water samples.

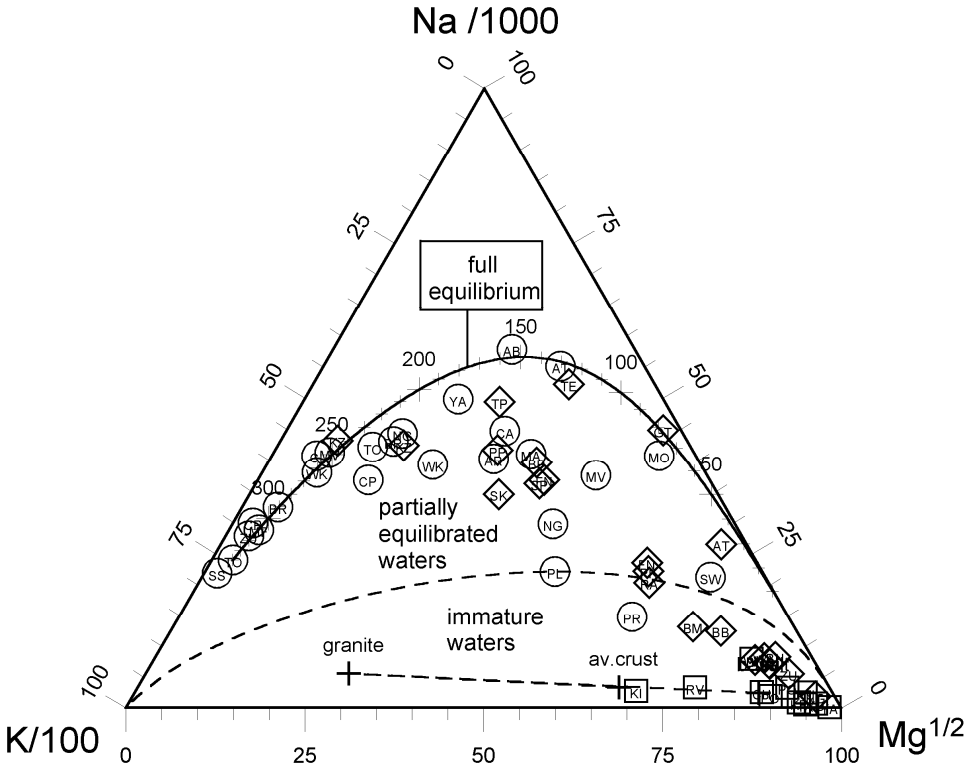


Fig. 10. The Na-K-$Mg^{1/2}$ triangular plot (from Giggenbach, 1988, modified); squares = acid sulfate waters; diamonds = Na-bicarbonate waters; circles= neutral chloride waters.

*8.3.3. The Na-K-Ca geothermometer*

The Na-K-Ca geothermometer (Fournier and Truesdell, 1973) is probably the most popular and used ionic solute geothermometer, although it is not a true geothermometer, as we will see below. The Na-K-Ca function is entirely empirical and assumes two different exchange reactions:

$$Na_{2/3}Ca_{1/6}\text{-solid} + K^+ = 1/6\ Ca^{2+} + 2/3\ Na^+ + K\text{-solid}, \qquad (8.27)$$

for T>100 °C, and:

$$Ca_{2/3}\text{-solid} + K^+ + 1/3\ Na^+ = 2/3\ Ca^{2+} + KNa_{1/3}\text{-solid} \qquad (8.28)$$

for T<100 °C. Fournier and Truesdell (1973) do not give the temperature dependence of each of these two separate reactions, but only the following equation (concentrations in ppm):

$$T_{NaKCa}(°C) = \frac{1647}{\log(Na/K) + \beta[\log(\sqrt{Ca}/Na + 2.06] + 2.47} - 273.15, \qquad (8.29)$$

where $\beta$=1/3 for waters equilibrating above about 100 °C and $\beta$=4/3 for waters equilibrating below about 100 °C. However $\beta$=1/3 for waters less than 100°C when log ($Ca^{1/2}$/Na) is negative, with molal concentrations.

The Na-K-Ca function gives erratic results below 200 °C due to high partial pressures of carbon dioxide (Paces, 1975) and to the occurrence of exchange reactions involving also Mg. This led Fournier and Potter (1979) to propose a quite complex Mg-correction to the Na-K-Ca function. In addition, precipitation of calcite causes an overestimation of the equilibrium temperature obtained by means of the Na-K-Ca function.

According to Tonani (1980), the Na-K-Ca geothermometer can be split into three temperature functions, based on the Na/K, $Ca^{1/2}$/Na, and $Ca^{1/2}$/K ratios, of which only two are mutually independent.

Giggenbach (1988) summarized the results of several investigations, which were carried out for providing both theoretical and experimental justifications to this technique, and concluded that many problems in the use of the Na-K-Ca geothermometer are connected with its sensitivity to differences in the $CO_2$ contents of geothermal fluids (see also Chiodini et al., 1991a), especially at relatively low temperatures. Therefore, rather than representing the basis for a geothermometer, Ca may be used to formulate a $P_{CO2}$-indicator. Actually, Ellis (1970) had already pointed out that Ca is a potential $CO_2$-indicator for thermal waters proposing a technique to evaluate deep $P_{CO2}$ on the basis of Na and Ca concentrations.

*8.3.4. The K-Ca $P_{CO2}$-indicator*

According to Giggenbach (1988), it is likely that the initial $CO_2$ contents of deep geothermal fluids are externally controlled by variable contributions of $CO_2$-rich magmatic fluids and $CO_2$-poor meteoric waters (see section 2). These fluids are expected to become reactive with respect to the conversion of Ca-Al-silicates to calcite, which involves the formation of either "acid clays":

$$\text{Ca-Al-silicate} + CO_2 + H_2O = 2(\text{H-Al-silicate}) + \text{calcite} \qquad (8.30)$$

or K-mica:

$$\text{Ca-Al}_2\text{-silicate} + \text{K-feldspar} + CO_2 = \text{K-mica} + \text{calcite}. \qquad (8.31)$$

The temperature dependence of reaction (8.31) is described by the following equation (Giggenbach, 1984; $P_{CO2}$ in bar, T in °C)

$$\log P_{CO2} = .0168\ T - 3.78. \qquad (8.32)$$

The univariant reaction (8.31) involves two constituents of the full equilibrium mineral assemblage, K-mica and K-feldspar, and represents the calcite/Ca-$Al_2$-silicate boundary. For a given temperature, calcite is stable for $P_{CO2}$ higher than that given by equation (8.32), whereas the Ca-$Al_2$-silicate mineral (either laumontite, epidote or wairakite, depending on temperature) is stable for $P_{CO2}$ lower than that given by equation (8.32). Arnorsson and Gunnlaugsson (1985) recognized that $P_{CO2}$ is governed, above ~230 °C, by a buffer comprising calcite, epidote, prehnite and quartz and proposed an empirical geothermometer that agrees closely with expression (8.32).

According to Giggenbach (1988), K-mica, K-feldspar, and calcite are also involved in the following reaction:

$$3\text{K-feldspar} + Ca^{2+} + CO_{2(g)} + H_2O = \text{K-mica} + \text{calcite} + 6\text{chalcedony} + 2K^+ \qquad (8.33)$$

whose log K is equal to log ($a_{K+}^2/a_{Ca++}$) - log $P_{CO2}$ if the solid phases and water are assumed to be pure. An other interesting property of this reaction is that its equilibrium constant is practically temperature independent, since in the temperature range 50-300°C, it is equal to either –1.66 ± 0.15 based on the thermodynamic data of Bowers et al. (1984) or –1.67 ± 0.07 (1σ) based on the thermodynamic data of Johnson et al. (1992). Therefore the $K^2$/Ca ratio acts as a $P_{CO2}$-indicator, as described by the following equation (Giggenbach, 1988; concentrations in mg/kg):

$$\log (K^2/Ca) = \log P_{CO2} + 3.0. \qquad (8.34)$$

A geothermometer adjusting with speed similar to that of the K-Ca $P_{CO2}$-indicator is required to correlate the $P_{CO2}$ obtained by means of equation (8.34) with temperature.

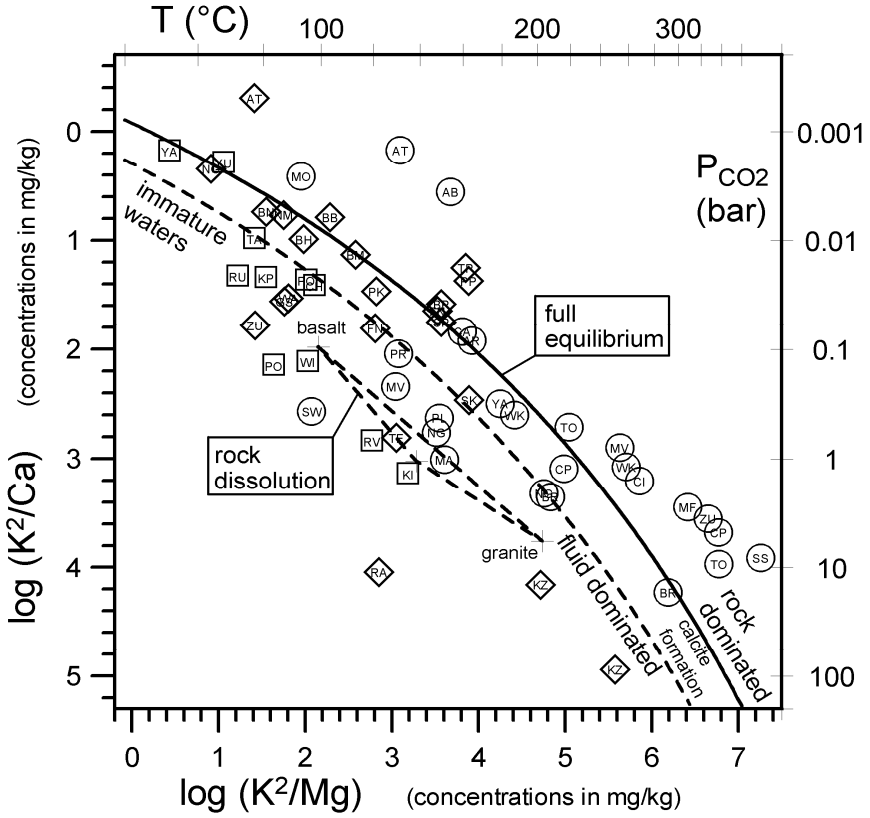


Fig. 8.11. Plot of log ($K^2$/Mg) vs. log ($K^2$/Ca), used to evaluate the $P_{CO2}$ of geothermal liquids. The full equilibrium line and the dissolution lines of basalt, granite and average crust are also shown (from Giggenbach, 1988, modified); squares = acid sulfate waters; diamonds = Na-bicarbonate waters; circles= neutral chloride waters.

Assuming that this is the K-Mg geothermometer, Giggenbach (1988) proposed to combine the two functions in a graphical method (Fig. 8.11) permitting the determination of both $CO_2$ contents and temperature of "last" water-rock equilibrium. The full equilibrium line, expressing coexistence of K-feldspar, illite, chlorite, chalcedony and calcite is drawn in Fig. 8.11. Data points below it have $P_{CO2}$ higher than full-equilibrium $P_{CO2}$, and can promote conversion of Ca-Al-silicates to calcite (reaction 8.31). On the other hand, the data points above it have low $CO_2$ contents, which drive this reaction in the opposite direction. All acid waters and some bicarbonate springs are situated below the full equilibrium line and their chemistry, again, appears to be controlled by rock dissolution rather than by mineral-solution equilibrium. Equation

(8.34) cannot be applied to these waters. Evaluation of $P_{CO2}$ by use of K-Ca contents is reliable only for points (either mature chloride waters or bicarbonate waters) plotting close to the full equilibrium line.

Taking into account Equations (8.26), (8.32), and (8.34) the full equilibrium condition can be drawn on the plot of 10 Mg/(10 Mg + Ca) vs. 10 K/(10 K + Na) (Fig. 8.12).

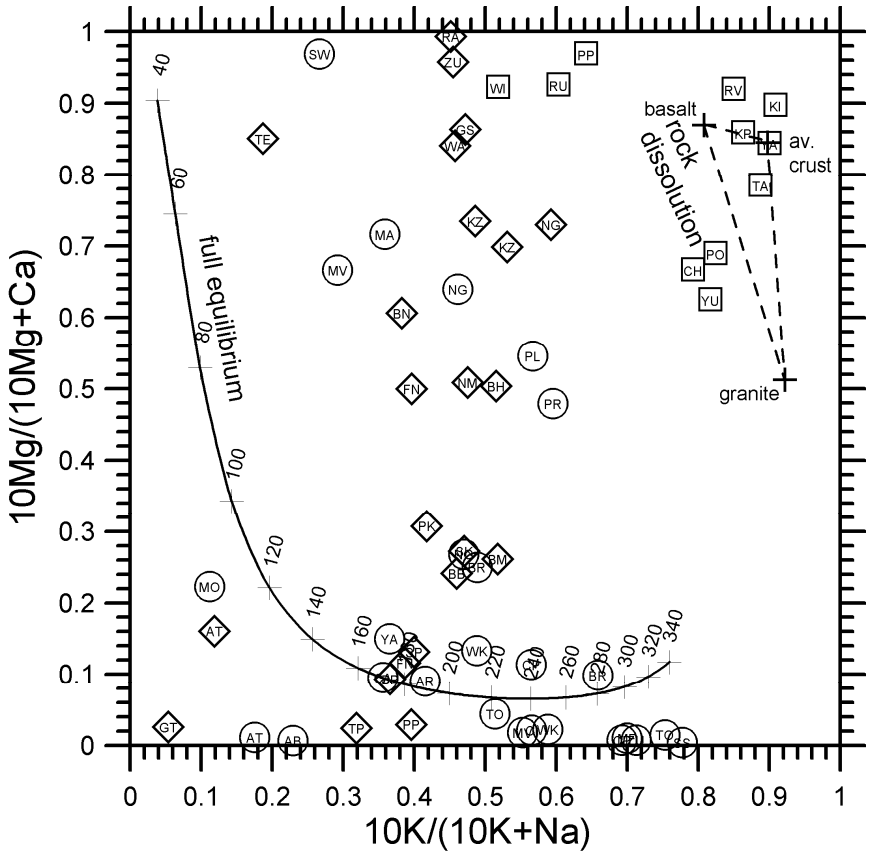


Fig. 8.12. Plot of 10 Mg/(10 Mg + Ca) vs. 10 K/(10 K + Na), showing the full equilibrium curve and the compositions produced through isochemical dissolution of crustal rocks (from Giggenbach, 1988, modified); squares = acid sulfate waters; diamonds = Na-bicarbonate waters; circles= neutral chloride waters.

In this plot the compositions of mature waters equilibrated under temperature, $P_{CO2}$ conditions of full equilibrium (equation 8.32) plot close to the full equilibrium line and are clearly separated from the compositions produced through isochemical dissolution of crustal rocks, such as basalt, granite and the average crust (Giggenbach, 1988). Mature waters equilibrated under $P_{CO2}$ either higher than those of full equilibrium (e.g., Kizildere, KZ) or lower than those of full equilibrium (e.g., Acqui Terme, AT) are situated above or below the full equilibrium line, as already recognised by Chiodini et al. (1993a).

An other useful graphical technique is obtained combining the two chemical subsystems responding most quickly and with comparable speed to changes in temperatures, that is those based on dissolved silica and on the $K^2$/Mg ratio (Giggenbach, et al., 1994, Fig. 8.13).

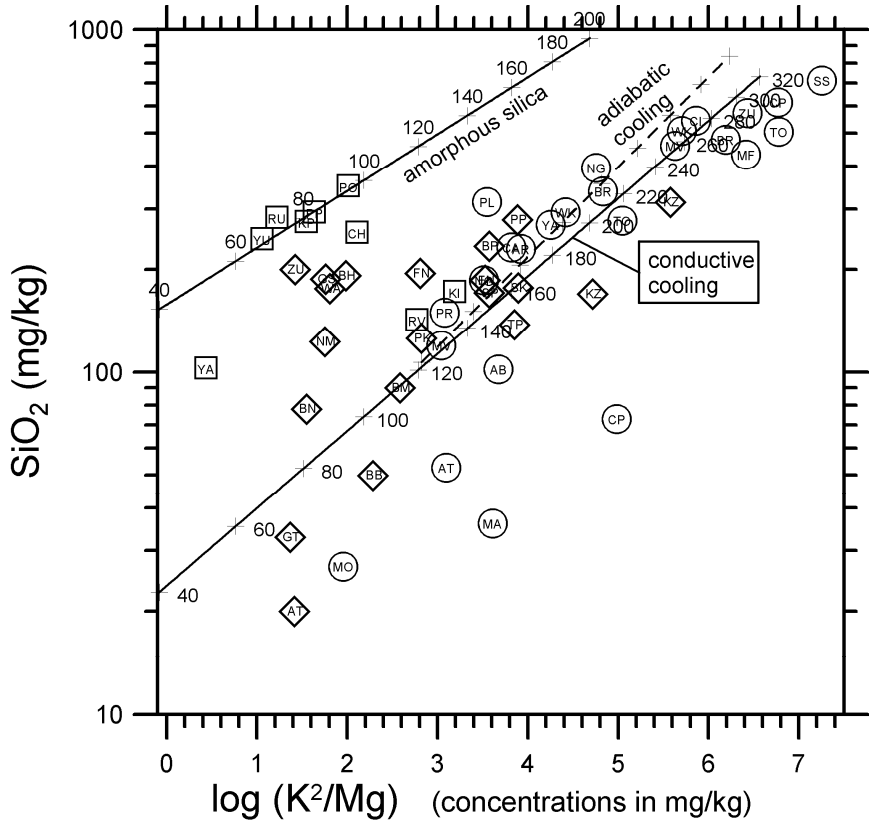


Fig. 8.13. Plot of $\log(K^2/Mg)$ vs. $\log(SiO_2)$ (from Giggenbach et al., 1994, modified); squares = acid sulfate waters; diamonds = Na-bicarbonate waters; circles= neutral chloride waters.

In Figure 8.13, equilibrium silica concentrations (in mg/kg) are obtained by means of the equation (Giggenbach et al., 1994):

$$\log(SiO_2) = 4.55 - \frac{1000}{T + 273.15} \ , \qquad (8.35)$$

whereas equilibrium $K^2/Mg$ ratios are computed by means of equation (8.26). These two equations apply if waters cool conductively, without steam loss or re-equilibration at decreasing temperatures. The corresponding full-equilibrium line is labelled "conductive cooling" in Fig. 8.13. The increase in solute concentrations caused by maximum steam separation from equilibrium temperature to 100°C (or maximum adiabatic cooling) can be suitably incorporated into equations (8.26) and (8.35) by means of simple mass and enthalpy balances (see equations 6.3 and 6.4), obtaining the following relations (Giggenbach et al., 1994):

$$\log(SiO_2)_b = 5.12 - \frac{1215}{T + 273.15} \ , \qquad (8.36)$$

$$\log(K^2/Mg)_b = 14.6 - \frac{4630}{T + 273.15} \ . \qquad (8.37)$$

The corresponding full-equilibrium line is marked "adiabatic cooling" in Figure 8.13.

Most neutral Na-Cl waters and some Na-bicarbonate waters plot close to these two full-equilibrium lines. However, important deviations are also observed, especially for low-temperature chloride and bicarbonate springs, possibly due to loss of silica, which moves data points downwards, and loss of Mg, which moves data points to the right. It is therefore difficult to identify the prevailing reason of disequilibrium, in the lack of additional information. In the case of well Maui (MA), whose bottom-hole temperature is 130°C, loss of silica is evidently the main cause of disequilibrium. Some Na-bicarbonate waters and some acid waters plot half-way between the full equilibrium line and the amorphous silica line, probably because aqueous silica concentrations are controlled by saturation with a silica polymorph of intermediate solubility. Amorphous silica solubility, the most soluble silica polymorph, represent the ultimate limit, which is active for some acid waters.

*8.3.5. Other ionic solutes geothermometers*

Other ionic solutes geothermometers include:

(i) The $Li/Mg^{1/2}$ geothermometer (Kharaka and Mariner, 1989) and the Li/Na geothermometer (Fouillac and Michard, 1981), whose general utilization is questionable, because of the variable fraction of the Li-endmember in the solid-mixtures taking part to the exchange reactions governing these geothermometers.

(ii) The Ca/Mg and $SO_4/F^2$ geothermometers (Marini et al., 1986; Chiodini et al., 1995b), which are specific for waters coming from carbonate-evaporite reservoirs. They have stimulated the investigation of the influence of ion complexing on geothermometers and $P_{CO2}$-indicators, which is considered in the next section.

### *8.4. A theoretical investigation of geothermometers and $P_{CO2}$-indicators for high-temperature geothermal liquids*

Guidi et al. (1990b) and Chiodini et al. (1991a) investigated the possible geothermometers and $P_{CO2}$-indicators for aqueous solutions coming from high-temperature (150-300°C) geothermal systems. They used a mineral-solution equilibrium model to calculate the concentrations of dissolved compatible constituents, which are fixed by equilibrium with a defined mineral assemblage at given T, $P_{CO2}$ and concentrations of mobile constituents (chloride only in their approach). The mineral-solution equilibrium model has the same computational structure of the model by Michard et al. (1981) but takes into account the effects of ion complexing. The following aqueous species are considered in the model: $H_2O°$, $H^+$, $OH^-$, $Na^+$, $NaCl°$, $NaSO_4^-$, $NaCO_3^-$, $NaF°$, $NaOH°$, $K^+$, $KCl°$, $KSO_4^-$, $KHSO_4°$, $Ca^{2+}$, $CaSO_4°$, $CaCO_3°$, $CaHCO_3^+$, $CaF^+$, $CaOH^+$, $Mg^{2+}$, $MgSO_4°$, $MgCO_3°$, $MgHCO_3^+$, $MgF^+$, $MgOH^+$, $H_2CO_3°$, $HCO_3^-$, $CO_3^{2-}$, $SO_4^{2-}$, $F^-$, $Cl^-$, $H_4SiO_4°$, $H_3SiO_4^-$, $Al(OH)_4^-$, $Al^{3+}$, $Al(OH)^{2+}$, $Al(OH)_2^+$. The model finds the roots of a polynomial equation of $H^+$ activity, which is obtained considering: the electroneutrality equation, the thermodynamic constants of the dissolution reaction of relevant mineral phases and gaseous $CO_2$, and the thermodynamic constants of dissociation equilibria of complex aqueous species.

In the light of the available information on high-temperature geothermal systems:

(i) $Na^+$, $K^+$, $Ca^{2+}$, $Mg^{2+}$, $Al(OH)_4^-$, $H_4SiO_4°$, $SO_4^{2-}$, $F^-$, and $HCO_3^-$ were chosen as compatible dissolved species;

(ii) the hydrothermal mineral assemblage was assumed to be made up of albite, K-feldspar, either a Ca-Al-silicate and/or calcite (depending on the $P_{CO2}$), clinochlore, muscovite, quartz, anhydrite, and fluorite;

(iii) $P_{CO2}$ was considered an externally controlled parameter fixing the activity of $HCO_3^-$ ion.

The expected composition of the equilibrium aqueous solutions was calculated, at different T, $P_{CO2}$ and chloride molalities. The satisfactory agreement between calculated and observed contents supports the adopted mineral-solution equilibrium model.
In the framework of this review, the chemical speciation of a hydrothermal aqueous solution in equilibrium with albite, K-feldspar, clinozoisite, calcite, clinochlore, muscovite, quartz, anhydrite, and fluorite at 250°C and variable Cl concentration (from 0.003 to 3 mol/kg) was computed by means of the computer code EQ3NR, version 7.2b (Wolery, 1992). Reference was made to the COM thermodynamic database, which includes a large number of solid, aqueous, and gaseous species, whose thermodynamic properties are mostly derived from Johnson et al. (1992). The aqueous species considered in speciation computations are listed in Table 2. In spite of same differences in the considered aqueous species and in some thermodynamic data, results are comparable with those of Guidi et al. (1990b).

*8.4.1. Complexing in hydrothermal aqueous solutions.*
As discussed by Guidi et al. (1990b) and Chiodini et al. (1991a), ion association in hydrothermal aqueous solutions has different effects mainly depending on the absolute value and sign of the ionic charge. These effects can be summarized as follows.

*Sodium and potassium* (Fig. 8.14): Although the concentrations of Cl-complexes increase with total Cl molality, the free ions $Na^+$ and $K^+$ are always the dominant species of dissolved sodium and potassium; therefore total (analyzed) Na and K contents are always representative of free ions contents.

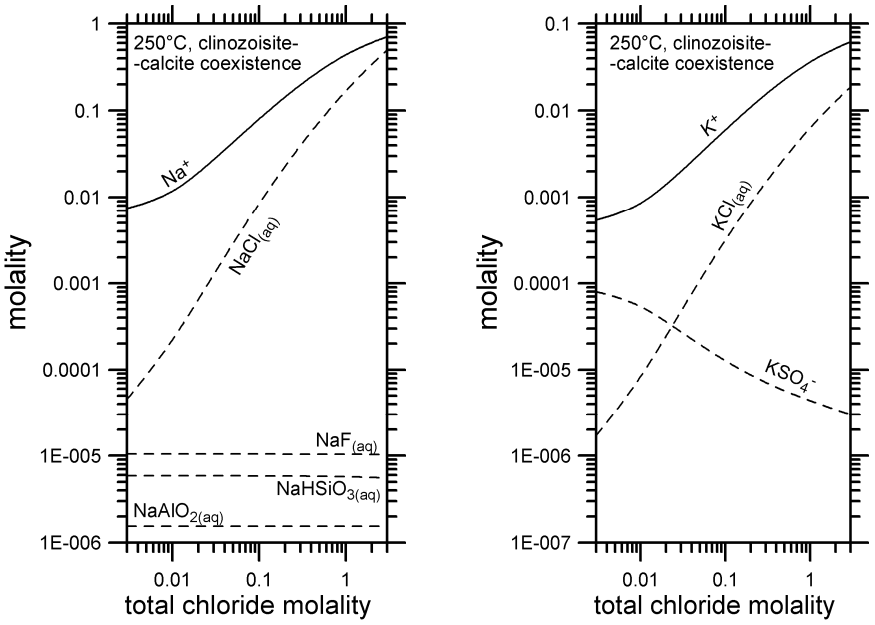


Fig. 8.14. Distribution of sodium and potassium species in a hydrothermal aqueous solution in equilibrium with albite, K-feldspar, clinozoisite, calcite, clinochlore, muscovite, quartz, anhydrite, and fluorite at 250°C and variable Cl concentration. $P_{CO2}$ is fixed by coexistence of calcite and clinozoisite (from Guidi et al., 1990b, modified).

*Magnesium and calcium* (Fig. 8.15): The free ion $Ca^{2+}$ is the dominant species only in Cl-rich solutions (apart from very high concentrations, approaching 3 mol/kg Cl, where Cl-complexes dominate), whereas $CaSO_4°$ prevails over other Ca-species at low Cl concentrations. The free ion $Mg^{2+}$ is never the main dissolved Mg-species, as $MgSO_4°$ dominates at low Cl concentrations and $MgCl^+$ prevails in Cl-rich solutions. Nevertheless the relative proportion of $Mg^{2+}$ increases with total Cl molality.

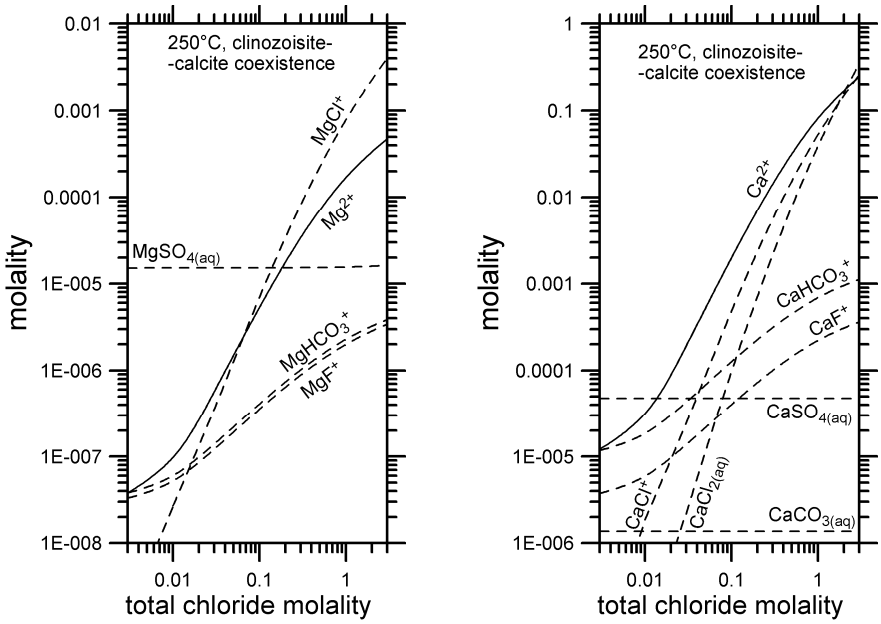


Fig. 8.15. Distribution of magnesium and calcium species in a hydrothermal aqueous solution in equilibrium with albite, K-feldspar, clinozoisite, calcite, clinochlore, muscovite, quartz, anhydrite, and fluorite at 250°C and variable Cl concentration. $P_{CO2}$ is fixed by coexistence of calcite and clinozoisite (from Guidi et al., 1990b, modified).

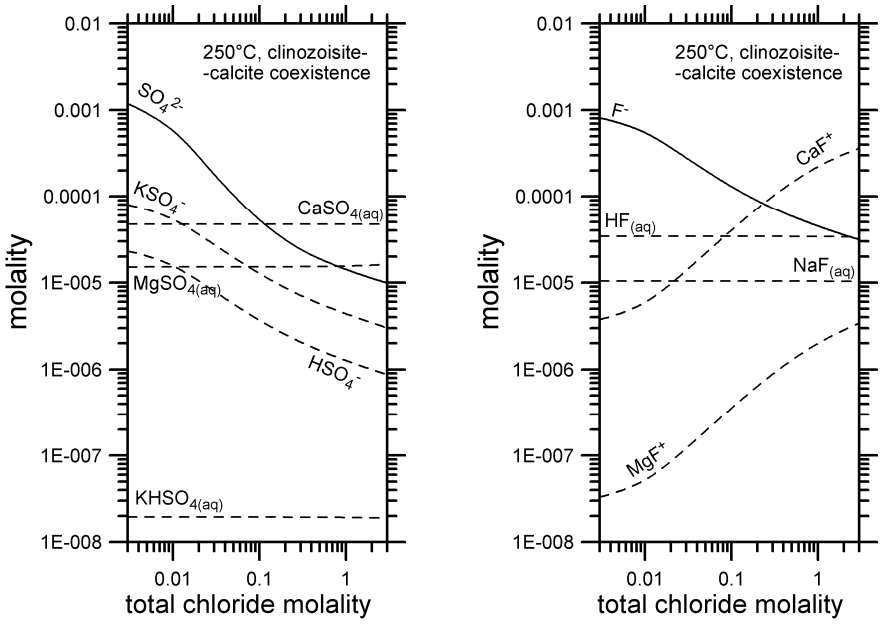


Fig. 8.16. Distribution of sulfate and fluoride species in a hydrothermal aqueous solution in equilibrium with albite, K-feldspar, clinozoisite, calcite, clinochlore, muscovite, quartz, anhydrite, and fluorite at 250°C and variable Cl concentration. $P_{CO2}$ is fixed by coexistence of calcite and clinozoisite (from Guidi et al., 1990b, modified).

*Sulfate and fluoride* (Fig. 8.16). Free ions $SO_4^{2-}$ and $F^-$ are the prevailing species only in Cl-poor solutions, while $CaSO_4°$ and $CaF^+$ are the dominant species at high Cl concentrations. Therefore total (analyzed) sulfate and fluoride contents are representative of free ions contents only in Cl-poor solutions.

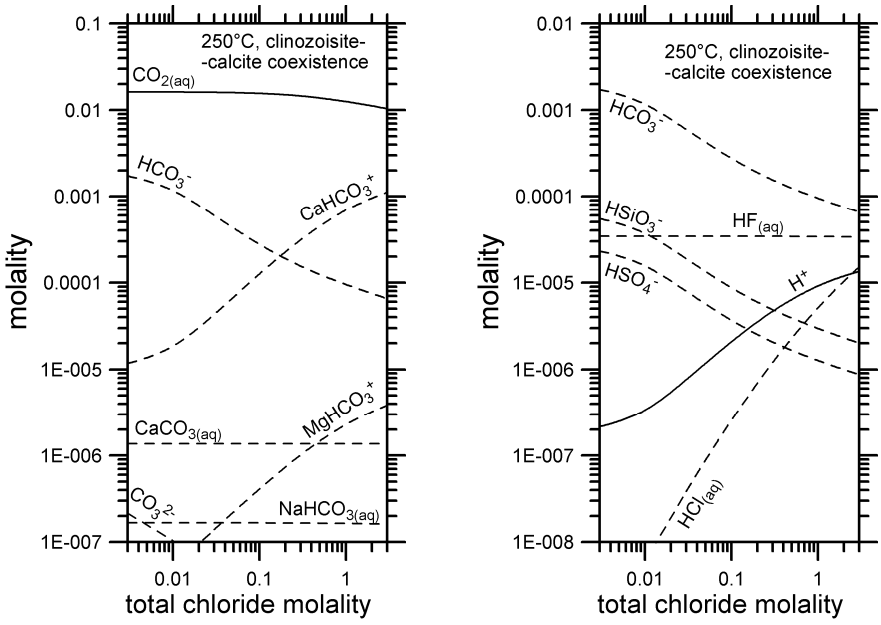


Fig. 8.17. Distribution of carbonate species and proton donors and $H^+$ in a hydrothermal aqueous solution in equilibrium with albite, K-feldspar, clinozoisite, calcite, clinochlore, muscovite, quartz, anhydrite, and fluorite at 250°C and variable Cl concentration. $P_{CO2}$ is fixed by coexistence of calcite and clinozoisite.

*Carbonate species* (Fig. 8.17): the main dissolved carbonate species is aqueous $CO_2$ (or carbonic acid, $H_2CO_3$) at all total Cl molalities. Similar to what has been observed for sulfate and fluoride, free $HCO_3^-$ ion is the main bicarbonate species at low Cl concentrations only, whereas the ion complex $CaHCO_3^+$ prevails in Cl-rich aqueous solutions.

*Proton donors and $H^+$* (Fig. 8.17): Bicarbonate is the main acid at all total Cl molalities. The concentration of $H^+$ ion increases with Cl concentrations, because it is buffered by coexistence of aluminosilicate minerals as already pointed out by Ellis (1970). For, instance, referring to the simplified system albite-muscovite-chalcedony-aqueous solution, it is easy to verify that if the $Cl^-$ concentration increases, the concentrations of $Na^+$ and $K^+$ have to increase accordingly to maintain the electroneutrality condition. This determines an increase in $H^+$ molality due to the equilibrium constraint dictated by the following reaction:

$$3 \text{ albite} + K^+ + 2H^+ = \text{muscovite} + 6 \text{ chalcedony} + 3 Na^+ . \qquad (8.38)$$

Due to the effects of ion complexing, total (analytical) concentration ratios of compatible cations ($Na^+$, $K^+$, $Ca^{2+}$ and $Mg^{2+}$) and compatible anions ($SO_4^{2-}$, $F^-$, and $HCO_3^-$) diverge, to variable amounts, from free ions activity ratios, which are uniquely fixed, at either a given T or a given T, $P_{CO2}$ condition, by mineral-solution equilibrium.

For instance, Figure 8.18 shows that: (i) these effects are minor on the Na/K ratio as both Na and K total (analyzed) concentrations are always (at all T, $P_{CO2}$, Cl conditions) representative of free ions concentrations and activity coefficients of $Na^+$ and $K^+$ ions are similar; (ii) large deviations are observed for the $K^2$/Mg ratio, due to the contrasting behavior of K and Mg, whose total (analyzed) concentration is always higher than free ion concentration; these deviations are particularly important at low total Cl molality where the effects of ion complexing on Mg are overwhelming.

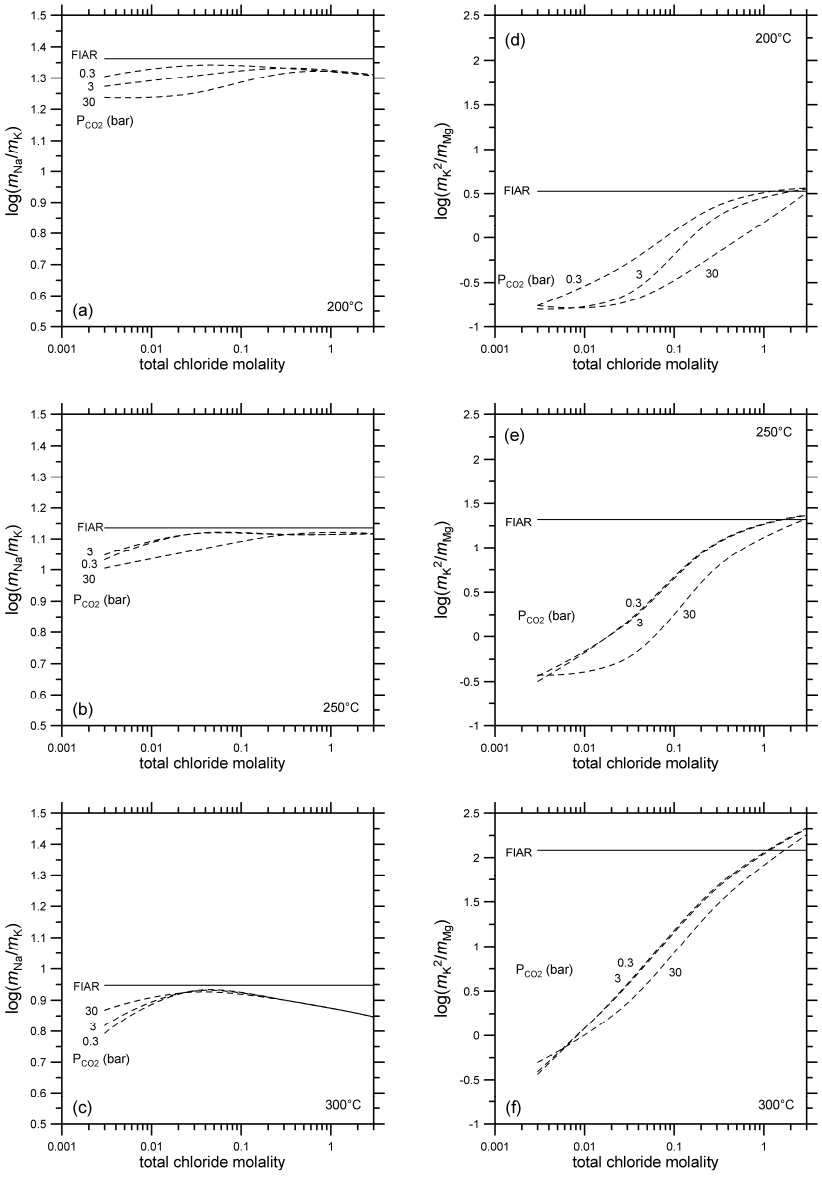


Fig. 8.18. Na/K and $K^2$/Mg total concentration ratios against total chloride concentration at different T, $P_{CO2}$ conditions (dashed lines). Corresponding free ions activity ratios (FIAR) are represented by solid lines (from Chiodini et al., 1991a, modified).

Chiodini et al. (1991a) treated the logarithms of total concentrations of compatible constituents and their log-ratios as dependent variables in multiple stepwise regression analysis, in which 1/T, log $P_{CO2}$ and log Σeq (Σeq is total ionic salinity in eq/kg) were taken as independent variables. Final regression equations for total concentrations and total concentration ratios of compatible constituents are reported in Table 3. Inspection of this table shows that:
(i) Na/K, $K^2$/Mg, and $SO_4/F^2$ ratios as well as $SO_4$ and F contents are mainly controlled by temperature and are therefore potential geothermometers;
(ii) $K^2$/Ca, Ca/Mg, $HCO_3$/F, and $(HCO_3)^2/SO_4$ ratios as well as $HCO_3$ contents are largely controlled by $P_{CO2}$ and are therefore potential $P_{CO2}$-indicators.
(iii) $Na^2$/Mg and $Na^2$/Ca ratios, the concentrations of other constituents, and pH are mainly constrained by total ionic salinity and are therefore less suitable, in principle, as either geothermometers or $P_{CO2}$-indicators.

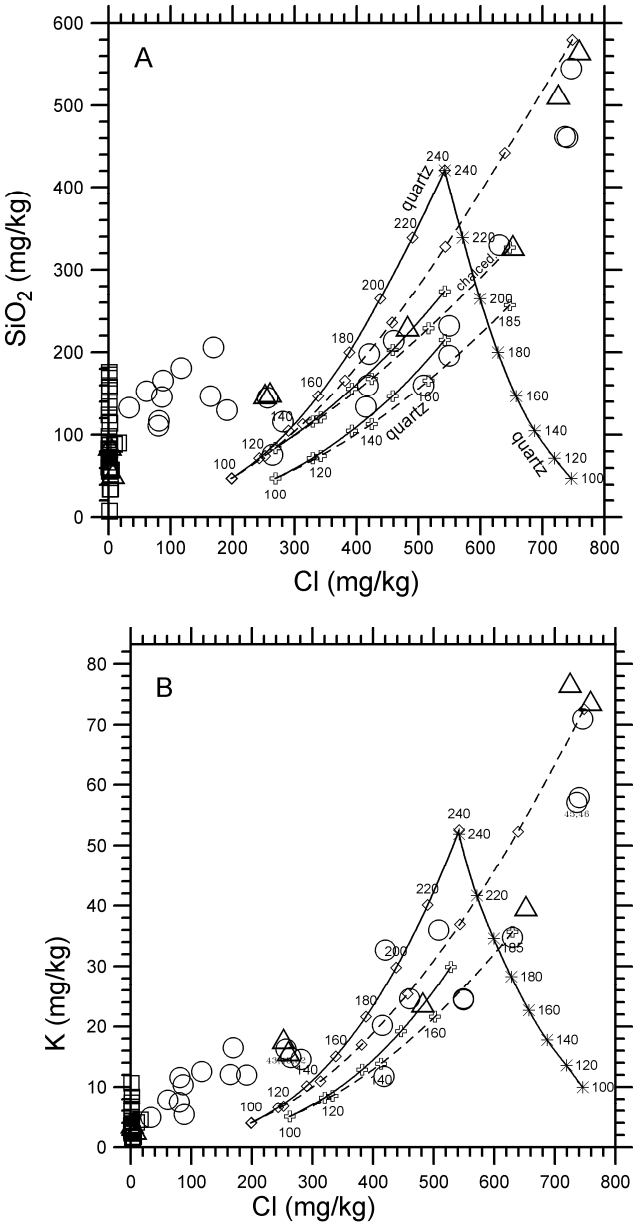


Fig. 8.19. Plots of (A) $SiO_2$ and (B) K vs Cl for the water discharges of San Marcos, Guatemala. Curves with small diamonds and crosses refer to the La Cimarrona (initial temperature 240°C) and La Castalia (initial temperature 185°C) geothermal endmembers, respectively; they report the compositions expected for geothermal water-groundwater isoenthalpic mixtures that are allowed to equilibrate with the hydrothermal paragenesis typical of most geothermal systems, and reach the surface after either no steam loss (solid curve) or maximum steam loss (dashed curve). The curve with asterisks represents the theoretical composition for the La Cimarrona geothermal liquid after boiling and equilibration at decreasing temperatures (from Marini et al., 1998).

These studies found a theoretical justification for ionic solutes geothermometers and $P_{CO2}$-indicators, which were originally derived on a purely empirical basis. In addition the functions of Table 3 allows one to investigate the behavior of each solute upon mixing and re-equilibration, as attempted by Marini et al. (1998) for the thermal waters of the San Marcos area (Guatemala).

It was shown that $SiO_2$ and K play a key role in unravelling mixing, boiling and re-equilibration phenomena (Fig. 8.19). On the other hand, dissolved magnesium does

not seem to be constrained by equilibrium with chlorites, at least in the mixed Na-Cl waters of the San Marcos area, possibly because Mg-bearing montmorillonites and saponites are more abundant than chlorites at temperatures below 200°C. If so, the use of the K-Mg geothermometer might be in error, especially below ~175°C, as pointed out by Fournier (1991).

Theoretical geothermometers and $P_{CO2}$-indicators for aqueous solutions coming from hydrothermal systems of medium-low temperature hosted into carbonate-evaporite rocks were derived by Chiodini et al. (1995b) following the same approach of Chiodini et al. (1991a).

### *8.5. Effects of mixing on the geothermometers*

The effects of mixing between thermal waters and cold waters on the silica (quartz) geothermometer has been already discussed in section 8.2.4, referring to the silica vs. enthalpy plot. As shown above, the main disadvantage of the iso-enthalpic mixing model is the possible occurrence of conductive heat losses, which determine an overestimation of the calculated temperature of the hot-water endmember.

To get rid of this possible problem, we will try to develop mixing models which do not assume enthalpy (heat) conservation but mass conservation only. It might seem obvious, but first the occurrence of mixing must be established by means of suitable plots between mobile species (see section 6.2). It is also useful to examine plots between the pairs of species involved in ionic solutes geothermometers, e.g., the Na-K and the K-Mg geothermometers, as done in Figure 8.20 for the waters of San Marcos, Guatemala. This exercise shows that, if the cold water has low salinity, the Na-K geothermometer is practically unaffected by dilution, whereas the K-Mg geothermometer is significantly influenced by mixing. In fact: (i) in the Na vs. K plot, the mixing line, as well as the different isotherms, are straight lines passing through the origin, whereas (ii) in the K vs. log Mg plot the isotherms have parabolic shape; the mixing line is not a straight line, as the log-scale has been used to show the large changes in Mg concentrations (use linear scales, if possible !).

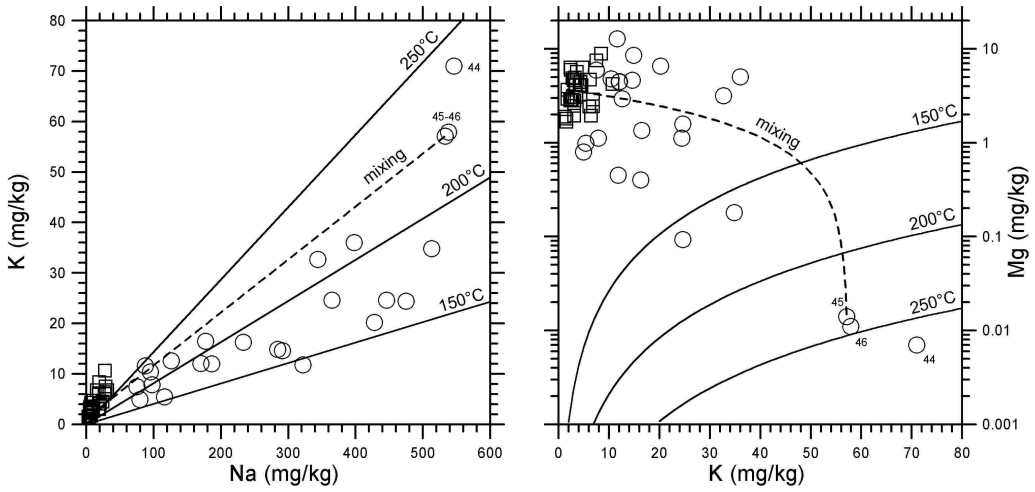


Fig. 8.19. Plots of (left) K vs Na and (right) Mg vs K for the water discharges of San Marcos, Guatemala, showing relevant isotherms and the mixing line of sample 45 from La Cimarrona with local groundwater (from Marini et al., 1998).

How to calculate the equilibrium temperature of the pure thermal endmember? Some hypotheses are needed. They are: (i) existence of overall equilibrium in the reservoir; this means that different geothermometers (e.g. the Na/K and quartz

geothermometers) indicate the same temperature for the pure thermal endmember; (ii) neither gain nor loss of matter occur upon mixing and cooling (which is not the case at San Marcos, Fig. 8.19); (iii) the chemical composition of the cold component is known. Let us now select two samples which are representative of the mixed water, M, and of the cold water, C. The sodium, potassium and silica concentrations in the pure thermal endmember, T, are related to those in the mixed water and in the cold water by the following mass balances:

$$C_{Na,T}x = C_{Na,M} - C_{Na,C}(1-x) \tag{8.39}$$

$$C_{K,T}x = C_{K,M} - C_{K,C}(1-x) \tag{8.40}$$

$$C_{SiO_2,T}x = C_{SiO_2,M} - C_{SiO_2,C}(1-x) \tag{8.41}$$

where x indicates the weight fraction of the thermal component in the mixture. The Na/K ratio of the pure thermal endmember is obtained dividing Eqn. (8.39) by Eqn. (8.40), while the silica concentration of the thermal component is simply obtained dividing Eqn. (8.41) by x.

$$\frac{C_{Na,T}}{C_{K,T}} = \frac{C_{Na,M} - C_{Na,C}(1-x)}{C_{K,M} - C_{K,C}(1-x)} \tag{8.42}$$

$$C_{SiO_2,T} = \frac{C_{SiO_2,M} - C_{SiO_2,C}(1-x)}{x} \tag{8.43}$$

Expressions (8.42) and (8.43) are then inserted in the Na/K and quartz geothermometers, obtaining a system of two equations and two unknowns (T and x), which can be solved. Once x is computed it can be inserted back in the mass balance equations (Eqns. 8.39-8.41) to calculate the composition of the pure thermal endmember. Similar mixing models can be based upon any two geothermometers.

Alternatively, the concentrations of Na, K, Mg, and $SiO_2$, i.e., all the constituents involved in the geothermometers of interest (Na-K, K-Mg, and quartz, in this case) are regressed against Cl. If the concentrations of the considered constituents in the mixed waters are governed by mixing between a thermal water and a cold water, data should fit straight lines and simple linear equations ($C_{Na} = a_1\, C_{Cl} - b_1$, $C_K = a_2\, C_{Cl} - b_2$, $C_{Mg} = a_3\, C_{Cl} - b_3$, $C_{SiO2} = a_4\, C_{Cl} - b_4$) should be obtained. These are inserted in the quartz, Na-K, and K-Mg geothermometers (e.g., Eqns. 8.1, 8.22, and 8.26), obtaining simple T-Cl functions, such as:

$$Tqz(°C) = \frac{1309}{5.19 - \log(a_4 C_{Cl} - b_4)} - 273.15 \tag{8.44}$$

$$T_{NaK}(°C) = \frac{1217}{1.483 + \log(a_1 C_{Cl} - b_1) - \log(a_2 C_{Cl} - b_2)} - 273.15 \tag{8.45}$$

$$T_{KMg}(°C) = \frac{4410}{14.0 - 2\log(a_2 C_{Cl} - b_2) + \log(a_3 C_{Cl} - b_3)} - 273.15\,. \tag{8.46}$$

Then, Na-K-, K-Mg- and qz-temperatures are calculated for increasing Cl concentrations and plotted against it. If overall equilibrium is satisfied for the thermal endmember, the three functions converge, indicating the Cl concentration and overall equilibrium temperature of the thermal component. This approach has been used for the thermal waters of Plymouth, Montserrat by Chiodini et al. (1996; Fig. 8.21) and Aguilera et al. (2004).

Ternary mixtures can be modeled by means of models involving three geothermometers (Antrodicchia et al., 1985) or two geothermometers and the conservation of enthalpy (Cioni et al., 1992).

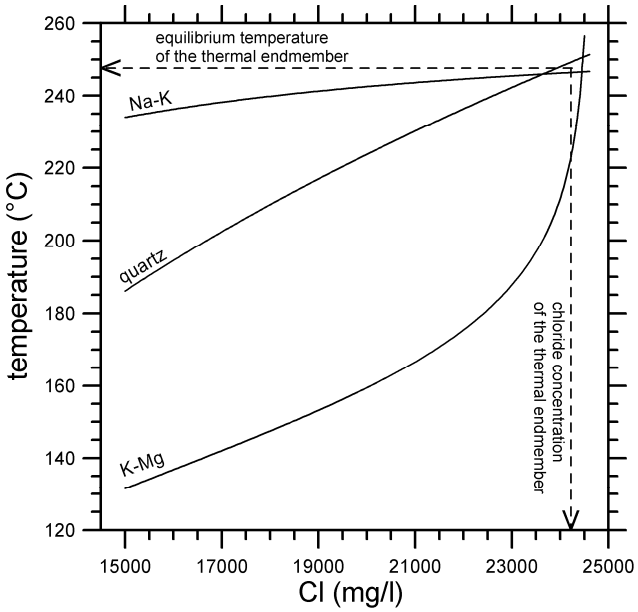


Fig. 8.21. Variations of Na/K temperature, $K^2$/Mg temperature and quartz temperature vs. Cl contents along the mixing line of Plymouth discharges (from Chiodini et al., 1996, modified).

### *8.6. Affinity to equilibrium and log(Q/K) vs. T diagrams*

The degree of attainment of equilibrium may be monitored by using the concept of thermodynamic affinity to equilibrium: since a reaction proceeds minimizing the Gibbs free energy of the system, for a generic reaction j occurring at constant T,P, the thermodynamic affinity, $A_j$, is defined as follows:

$$A_j = \left(\frac{\partial G}{\partial \xi_j}\right)_{P,T} = 2.303 \cdot R \cdot T \cdot \log\left(\frac{Q_j}{K_j}\right), \qquad (8.47)$$

where $\xi_j$ is the progress variable for the j-th reaction, $K_j$ is the equilibrium constant and $Q_j$ is the corresponding activity product. The affinity has the magnitude of an energy (i.e., kJ/mole, kcal/mol) and represents the energy driving towards the equilibrium condition in a chemical potential field.

Restricting our attention to the specific case of dissolution/precipitation of a given mineral in an aqueous solution, three general situations are possible. If $A_j > 0$, the aqueous solution is oversaturated with respect to the solid phase. If $A_j = 0$, the aqueous solution is saturated with respect to the mineral, i.e., in equilibrium with it. If $A_j < 0$, the

aqueous solution is undersaturated with respect to the solid phase. Many authors prefer to work with the adimensional variable log (Q/K), which is called saturation index, SI, rather than with thermodynamic affinity, but the two approaches are totally equivalent.

Reed and Spycher (1984) showed that calculation, for a given geothermal water, of SI's (or affinities to equilibrium) with respect to a number of plausible hydrothermal alteration minerals, at varying temperature, can be used as an effective geothermometric tool. Saturation indices are initially calculated at outlet temperature and measured pH. Temperature is then changed iteratively and the SI's recomputed. Computed SI's are then plotted against temperature, obtaining plots such as that reported in Fig. 8.22.

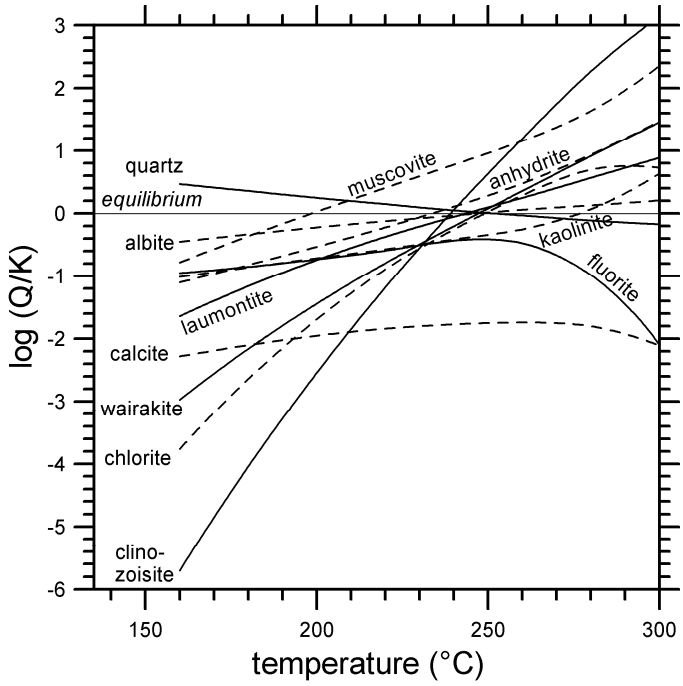


Fig. 8.22. Changes in the saturation indices of hydrothermal minerals, as a function of temperature, for one of the La Cimarrona thermal springs, San Marcos, Guatemala (from Marini et al., 1998).

If the geothermal water is in equilibrium with the considered minerals at a given temperature, all the SI curves converge to 0 at that temperature. If loss of $CO_2$ takes place, the SI curves for minerals sensitive to changing pH are shifted to lower values (e.g., calcite in Fig. 8.22). If the geothermal water mixes with a water of low salinity, all the SI curves are shifted downward into the undersaturation field, but the intersection cluster remains, indicating the approximate temperature of equilibrium. In spite of these perturbations brought about by mixing and $CO_2$ loss (Pang and Reed, 1998), the SI vs. T plot is a powerful tool to investigate the equilibrium temperature of geothermal waters.

In order to calculate the SI's, the chemical speciation in the aqueous solution have to be reconstructed first, taking into account all ion complexes. This is a great step forward with respect to simple geothermometers. Of course, calculations have to be carried out with the aid of a computer program, such as the EQ3/6 software package (Wolery, 1979, 1992; Wolery and Daveler, 1992) or SOLVEQ (Reed, 1982), which was specifically implemented for this purpose (Reed and Spycher, 1984).

Since most hydrothermal minerals are Al-silicates, the aluminum concentration in the aqueous solution has to be introduced in the computations. Unfortunately, monomeric Al concentrations are rarely measured in geothermal liquids and sometimes

poorly representative values of even total Al are obtained, because finely dispersed Al-oxyhydroxides pass through the membrane filters (Kennedy and Zellweger, 1974; Laxen and Chandler, 1982). However, the absence or the poor analytical quality of Al data can be circumvented assuming that aluminum concentrations are constrained by equilibrium with a given Al-silicate (Pang and Reed, 1998).

## 9. Geothermal gases

In general, the major component of geothermal gases is $H_2O$, which is followed by $CO_2$ and $H_2S$ in order of decreasing importance. Other gas species present in lower concentrations are $N_2$, $H_2$, $CH_4$, CO, $NH_3$, Ar, and He. Strongly acid gases, i.e., $SO_2$, HCl, and HF, which are typical of fluids degassed from magma bodies (Giggenbach, 1987; Chiodini et al, 1993b), are virtually absent in geothermal fluids (Giggenbach, 1980).

Sulfur dioxide was detectable only in some mixed magmatic-geothermal fumarolic discharges from active volcanic areas, such as Guagua Pichincha crater, Ecuador (Marini et al., 1991) and Forgia Vecchia of Vulcano, Italy (Chiodini et al., 1995a).

Besides, geothermal gases are characterized by $CH_4$ contents much greater than CO concentrations (Chiodini et al., 1992).

Similar to what is done for waters, for which a first classification step is needed before investigating mineral-solution equilibria, also for gases it is convenient to carry out an initial evaluation involving the less reactive constituents, with the aim to get information on the possible origin of fluid components, on the main processes controlling their distribution and on the secondary processes possibly interfering with gas equilibria evaluations. The most obvious constituents to use are $N_2$, Ar, and He, as suggested by Giggenbach (1991a).

### *9.1. Relative concentrations of He, Ar, and $N_2$*

Ar and He are chemically inert noble gases. Although $N_2$ is reactive (see below), in general its contents are not perturbed by chemical reactions since it is by far the predominant nitrogen species. Considering a large number of gas analyses coming from different tectonic settings, Giggenbach (1991a, 1992b) showed that the relative concentrations of He, Ar, and $N_2$ delineate the following major source components.

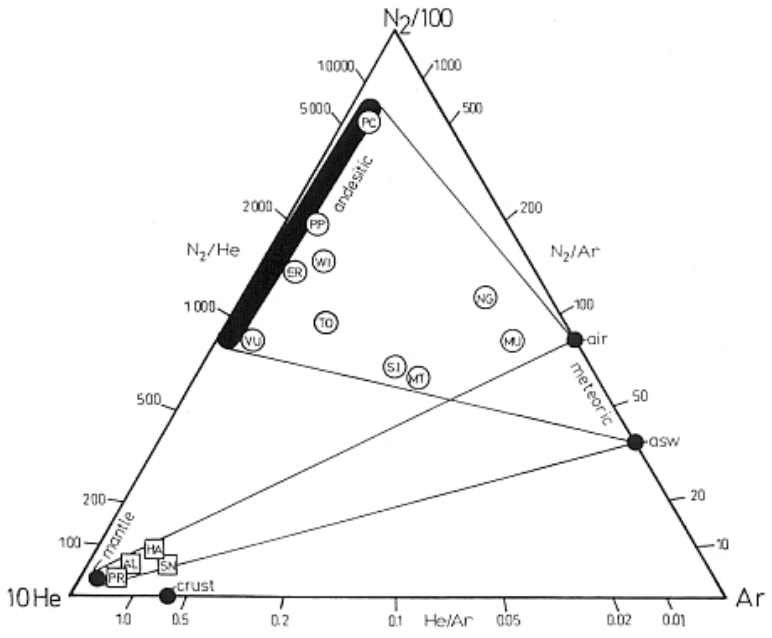


Fig. 9.1. Relative concentrations of He, Ar, and $N_2$ in several geothermal gases coming from different tectonic settings (from Giggenbach, 1996).

(1) A *meteoric* component represented by air-saturated groundwater (asw), which is characterized by $N_2$/Ar ratios of ~38 or somewhat higher due to possible entrainment of air bubbles. The He/Ar ratio is less than 0.001.
(2) A *magmatic "andesitic"* component with $N_2$/Ar ratios of 800-2000, which are typical of gas discharges from geothermal and volcanic centers along convergent plate boundaries (see also Giggenbach, 1997a and references therein). These relatively high $N_2$/Ar ratios were attributed to addition of $N_2$, mostly from the thermal decomposition of organic material contained in subducted sediments (Matsuo et al., 1978). However, this ratio is highly variable, possibly due to differences in the amounts of marine sediments reaching the zones where andesitic magmas are generated (Kita et al., 1993). Some systems situated along convergent plate boundaries (e.g., the volcanic islands of Nisyros, Milos and Kos belonging to the Hellenic island arc, Giggenbach, 1997a; La Ruffa et al., 1999; Kavouridis et al., 1999; Brombach et al., 2003) have low $N_2$/Ar ratios, comparable to those of mantle-derived gases, probably due to low contributions of $N_2$ from the subduction slab.
(3) A *magmatic "basaltic"* component, characterized by a helium content significantly higher than that of the meteoric component (He/Ar ≥ 0.1). Gases rich in this component, labeled mantle in Fig. 9.1, are typically found along divergent plate boundaries (sample PR) and in hot spot areas (e.g., SN and AL from the Galapagos and HA from the Hawaii).
(4) A *crustal* component, which is also rich in helium, because of addition of radiogenic He, i.e., $^4$He from radioactive decay of crustal U and Th. In principle, the $^3$He/$^4$He ratios could be used to discriminate the contributions of mantle and crustal gases. The $^3$He/$^4$He ratio of mantle gases, normalized to air, is usually close to 8 $R_A$ in mid-ocean ridge gases, but may exceed 20 $R_A$ in some hot spot gases. On the other hand, crustal gases usually have $^3$He/$^4$He ratios < 0.1 $R_A$. However, since the present understanding of the processes governing the $^3$He/$^4$He ratios in volcanic and geothermal fluids is still at a very qualitative-descriptive stage, inferences based on He isotopes are highly speculative in my opinion.

In spite of the care in sampling natural gas discharges, atmospheric air contamination cannot always be avoided, for instance when air is entrained in the upflow path of deep fluids upstream of the surface discharge. Air contamination might be indicated by the presence of $O_2$, but this is not a general rule, since $O_2$ is rapidly consumed through reaction with the reducing gas species (mainly $H_2S$) initially present in deep gases. In turn, air contamination may lead to partial or complete oxidation of reducing gas species. The occurrence of this process, therefore, invalidates the geothermometric-geobarometric techniques involving either reducing gas species or atmospheric gases (e.g., Ar).

## 10. Geothermal gas equilibria

Geothermal gas equilibria have been extensively investigated (e.g., Hulston and McCabe, 1962; Ellis, 1962; Glover, 1970; Tonani, 1973; Seward, 1974; D'Amore and Nuti, 1977; Giggenbach, 1980, 1991a, 1993; D'Amore and Panichi, 1980; D'Amore and Celati, 1983; Nehring and D'Amore, 1984; Arnorsson and Gunnlaugsson, 1985; Bertrami et al., 1985; Arnorsson, 1987, 1990; Chiodini and Cioni, 1989; Arnorsson et al., 1990; D'Amore, 1991; Chiodini et al., 1991b, 1992; Chiodini, 1994; Chiodini and Marini, 1998).

Based on earlier findings by Hulston and McCabe (1962), Giggenbach (1980) incorporated vapor-liquid gas distribution coefficients into equilibrium relationships, showing that the contents of $CO_2$, $H_2S$, $NH_3$, $H_2$, $N_2$, and $CH_4$ in the fluids discharged from the deep geothermal wells of the Wairakei, Kawerau, and Broadlands (New Zealand) and Manikaran (India) are closely approximated by two theoretical processes, either addition to or removal from an equilibrium liquid phase of an equilibrium vapor phase, defined as "vapor gain" and "vapor loss", respectively.

Giggenbach (1980) took into account the following three reactions:

$$CH_4 + 2H_2O = 4\ H_2 + CO_2 \qquad (10.1)$$

$$2\ NH_3 = N_2 + 3\ H_2 \qquad (10.2)$$

$$FeS_2 + H_2 + [H_2O] = [FeO] + 2\ H_2S \qquad (10.3)$$

and described the effects of vapor gain or loss with respect to the composition expected for the discharge of a pure equilibrium liquid phase by means of simple mass balances. These mass balances were suitably readjusted, referring to the vapor-liquid distribution coefficient of each gas species, $B_i$, which was defined above (Eqn. 6.6). The following equation was thus obtained for the theoretical concentration quotient of reaction (10.1):

$$K'_C = \frac{K_C \cdot P^2_{H_2O} \cdot D^{\pm 1}_{CO_2} \cdot D^{\pm 4}_{H_2} \cdot B_{CH_4}}{B_{CO_2} \cdot B^4_{H_2} \cdot D^{\pm 1}_{CH_4}} \qquad (10.4)$$

where:
(i) $K_C$ is the equilibrium constant of reaction (10.1), and its logarithm can be expressed as a linear function of 1/T(K):

$$\log K_C = 10.76 - \frac{9323}{T(K)}; \qquad (10.5)$$

(ii) $P_{H2O}$ is the partial pressure of water, and its logarithm is also a linear function of 1/T(K) for liquid-vapor coexistence:

$$\log P_{H_2O} = 5.51 - \frac{2048}{T(K)}; \qquad (10.6)$$

(iii) log $B_i$'s are linear functions of T(°C), as expressed by equations (6.7)-(6.12);
(iv) $D_i$ is equal to $(1 - y + yB_i)$, with y expressing the fraction of equilibrium vapor either added to or separated from the deep liquid phase.

Instead of comparing these theoretical concentration quotients with the analytical counterparts

$$K'_C = \frac{X_{d,CO_2} \cdot X^4_{d,H_2} \cdot P^4_t}{X_{d,CH_4}} \tag{10.7}$$

where $X_{d,i}$ is the total (well discharge) mol fraction of the i-th species, Giggenbach preferred to get rid of total pressure, by means of the following approximated expression:

$$P_t = \frac{P_{H_2O}}{1 - X_g \cdot y_s \cdot B_{CO_2,280°}} \tag{10.8}$$

where $X_g$ is the gas fraction and $y_s$ is the steam fraction, thus obtaining:

$$K''_C = \frac{K'_C}{P^4_{H_2O}} = \frac{X_{d,CO_2} \cdot X^4_{d,H_2}}{X_{d,CH_4} \cdot \left(1 - X_g \cdot y_s \cdot B_{CO_2,280°}\right)} \tag{10.9}$$

These concentration quotients are shown in Fig. 10.1.

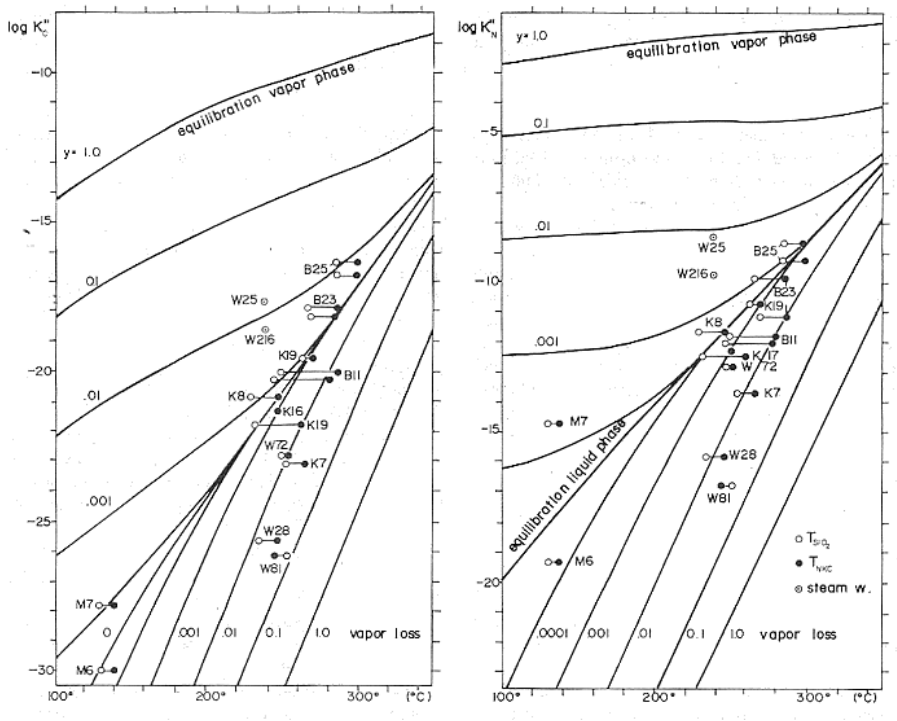


Fig. 10.1. Values of log K"$_C$ and log K"$_N$ as a function of temperature and y, which is the fraction of equilibrium vapor either added to or separated from the deep liquid phase. The corresponding analytical quotients for some geothermal wells of Wairakei (W), Broadlands (B), Kawerau (K), and Manikaran (M) are also plotted (from Giggenbach, 1980).

The approach by Giggenbach (1980), and other similar models (e.g., D'Amore and Celati, 1983; Arnorsson et al., 1990; D'Amore, 1991) are based on total fluid composition. It is also required that total fluid composition measured at the surface is fully representative of reservoir conditions (e.g., absence of gas-slip effects).

These "vapor gain" models cannot be applied to vapors discharged by fumaroles, which are usually generated through steam separation from boiling liquids. "Vapor gain" models cannot be applied also to geothermal wells of which only the composition of the separated vapor phase is known. Recently, the geochemical techniques proposed by Giggenbach (1980) have been adapted to fumarolic gas discharges by Chiodini and Marini (1998). Besides, Chiodini et al. (2001b) investigated the effects of gas solubility in aqueous solutions of high salinity on relevant gas equilibria.

Following Chiodini and Marini (1998), this presentation is largely based on the equilibria in the $H_2O$-$H_2$-$CO_2$-CO-$CH_4$ system, which plays a pivotal role for geothermal gas discharges. First, the theoretical compositions of gaseous mixtures in chemical equilibrium under fixed temperature-pressure-redox or temperature-pressure conditions are computed. The results of these calculations are expressed in suitable graphics, also showing the effects of possible processes (boiling and steam condensation) experienced by deep fluids during the upflow towards the surface. Then, the analytical data are compared with theoretical data.

## *10.1. Gas equilibria in the $H_2O$-$H_2$-$CO_2$-CO-$CH_4$ system*

### *10.1.1. Variables controlling gas equilibria in the $H_2O$-$H_2$-$CO_2$-CO-$CH_4$ system*

To calculate the theoretical composition of geothermal gases, the fugacity of $H_2O$ and, depending on the approach, the fugacities of $CO_2$ and $O_2$ as well, have to be known at the temperatures of interest.

Depending on P, T conditions, the main component of geothermal fluids, $H_2O$, can be present in different physical states, i.e., liquid, gas (called here 'superheated vapor' to avoid misunderstanding) and saturated liquid + vapor. For coexisting vapor and liquid water, changes of log $f_{H2O}$ with temperature are closely approximated by equation (10.6). Water fugacity is not constrained by temperature alone, and becomes an additional external variable, both for a single liquid phase at pressures higher than saturation and for a single vapor phase at pressures lower than saturation.

As discussed above, $CO_2$ fugacity in "full equilibrium" geothermal systems is fixed, at any given temperature, by univariant reactions involving calcite, a Ca-Al-silicate, K-feldspar, K-mica and chalcedony (Giggenbach, 1984, 1988). Under these peculiar conditions, fugacity of $CO_2$ and temperature are linked by Eqn. (8.32).

According to Giggenbach (1987) the most suitable parameter describing redox potentials of most natural fluids is:

$$R_H = \log r_H = \log \frac{f_{H_2}}{f_{H_2O}} \cong \log \frac{X_{H_2}}{X_{H_2O}} \qquad (10.10)$$

He proposed that the redox potentials of geothermal systems are governed by the (FeO)-($FeO_{1.5}$) couple, which controls also the redox state of basaltic and andesitic magmas as earlier recognized by Fudali (1965). Referring to the (FeO)-( $FeO_{1.5}$) buffer, $R_H$-values are fixed by the reaction:

$$H_2O + 2(FeO) = H_2 + 2(FeO_{1.5}) \quad (10.11)$$

the equilibrium constant of which is equal to $R_H$ and is practically temperature independent at -2.82 ± 0.02. Considering formation of water from $H_2$ and $O_2$, reaction (10.11) can be rewritten as:

$$2(FeO) + ½\ O_2 = 2(FeO_{1.5}) \quad (10.12)$$

and log $f_{O2}$ can be linked to temperature through the following equation:

$$\log f_{O_2} = 10.736 - \frac{25414}{T(K)}. \quad (10.13)$$

Similar equations relating $f_{O2}$'s and temperatures in geothermal environments were proposed by many authors (e.g., Tonani, 1973; D'Amore and Nuti, 1977; D'Amore and Panichi, 1980; D'Amore and Gianelli, 1984). For the purpose of the following discussion, we report here the empirical relationships of D'Amore and Panichi (1980):

$$\log f_{O_2} = 8.20 - \frac{23643}{T(K)}. \quad (10.14)$$

*10.1.2. Attainment of chemical equilibrium in a single vapor phase*

It is initially assumed that the considered gas species attain chemical equilibrium in a single vapor phase. The following three reactions provide the equilibrium constraints in the $H_2O$-$H_2$-$CO_2$-CO-$CH_4$ system:

$$H_2O = H_2 + ½\ O_2 \quad (10.15)$$

$$CO_2 = CO + ½\ O_2 \quad (10.16)$$

$$CO_2 + 2H_2O = CH_4 + 2O_2 \quad (10.17)$$

Production of $CH_4$ could take place also through reaction of elemental C and $H_2$. Although elemental C (graphite) may be present in some natural geothermal systems such as Cerro Prieto, Mexico (Nehring and D'Amore, 1984) and in Northern Latium, Italy (Chiodini, 1994), these are probably peculiar cases rather than the general situation. The most general approach, i.e., equation (10.17) is preferred here.
The equilibrium constants of reactions (10.15)-(10.17) can be written as:

$$\log f_{H_2} = \log K_{H_2} - \frac{1}{2}\log f_{O_2} + \log f_{H_2O} \quad (10.18)$$

$$\log f_{CO} = \log K_{CO} - \frac{1}{2}\log f_{O_2} + \log f_{CO_2} \quad (10.19)$$

$$\log f_{CH_4} = \log K_{CH_4} - 2\log f_{O_2} + 2\log f_{H_2O} + \log f_{CO_2} \quad (10.20)$$

The temperature dependence of the thermodynamic constants $K_{H2}$, $K_{CO}$ and $K_{CH4}$ is given by the following equations, based on the thermodynamic data by Stull et al. (1969):

$$\log K_{H_2} = 2.548 - \frac{12707}{T(K)} \tag{10.21}$$

$$\log K_{CO} = 5.033 - \frac{14955}{T(K)} \tag{10.22}$$

$$\log K_{CH_4} = 0.527 - \frac{42007}{T(K)}\,. \tag{10.23}$$

*Theoretical fugacities of $H_2$, CO and $CH_4$.* To solve equations (10.18) to (10.20), the fugacities of $H_2O$, $CO_2$ and $O_2$ have to be known at the temperatures of interest. Assuming that $f_{CO2}$ is constrained by equation (8.32), $f_{O2}$ is governed by a suitable buffer, e.g., equations (10.13) or (10.14), and treating $f_{H2O}$ as either a simple temperature function, for coexisting liquid plus vapor (Eqn. 10.6), or an externally fixed parameter, for single phase environments, equations (10.18) to (10.20) allow one to compute fugacities of $H_2$, CO and $CH_4$ at different temperatures (Fig. 10.2).

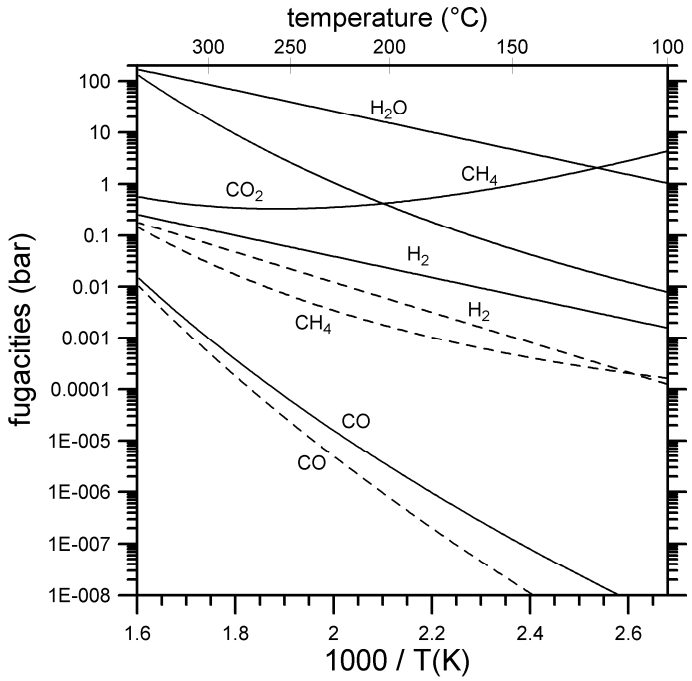


Fig. 10.2. Fugacities of $H_2$, CO and $CH_4$ at different temperatures, for a vapor phase coexisting with an infinitesimally small amount of liquid water, calculated assuming that $f_{CO2}$ is constrained by the full equilibrium function of Giggenbach (1984, 1988), and $f_{O2}$ is governed by either the FeO-$FeO_{1.5}$ hydrothermal buffer of Giggenbach (1987, solid lines) or the $f_{O2}$-buffer of D'Amore and Panichi (1980, dashed lines). Fugacities of $H_2O$ and $CO_2$, which are simple temperature functions, are also shown (from Chiodini and Marini, 1998).

Use of the two $O_2$-buffers of Giggenbach (1987) and D'Amore and Panichi (1980) leads to different theoretical fugacities of $H_2$, CO and $CH_4$. Carbon monoxide shows the

largest changes with temperature, and it is, therefore, the best geothermometer. However, since fugacities of single gas species are practically impossible to be determined for fumarolic effluents and only with limited accuracy for well discharges, Fig. 10.2 cannot be used to compare theoretical and analytical compositions.

*Theoretical log-ratios $H_2/H_2O$, $CO/CO_2$, and $CH_4/CO_2$*. Most of the disadvantages of referring to fugacities of single gas species are overcome by working with isomolar concentration ratios, which can be analytically determined on both fumarolic fluids and well discharges. In order to meet these requirements, the equilibrium constants of reactions (10.15)-(10.17) can be re-formulated as:

$$\log\frac{f_{H_2}}{f_{H_2O}} = \log K_{H_2} - \frac{1}{2}\log f_{O_2} = \log\frac{X_{H_2}\Gamma_{H_2}}{X_{H_2O}\Gamma_{H_2O}} \qquad (10.24)$$

$$\log\frac{f_{CO}}{f_{CO_2}} = \log K_{CO} - \frac{1}{2}\log f_{O_2} = \log\frac{X_{CO}\Gamma_{CO}}{X_{CO_2}\Gamma_{CO_2}} \qquad (10.25)$$

$$\log\frac{f_{CH_4}}{f_{CO_2}} = \log K_{CH_4} - 2\log f_{O_2} + 2\log f_{H_2O} = \log\frac{X_{CH_4}\Gamma_{CH_4}}{X_{CO_2}\Gamma_{CO_2}}. \qquad (10.26)$$

For gas phases largely made up of water vapor, i.e., when $X_{H2O} > 0.8$, the ratios of fugacity coefficients $\Gamma_{H2}/\Gamma_{H2O}$, $\Gamma_{CO}/\Gamma_{CO2}$, and $\Gamma_{CH4}/\Gamma_{CO2}$ do not deviate significantly from 1, in the typical P,T range of geothermal systems, 100-374 °C and 1-220 bar (Ryzhenko and Volkov, 1971; Ryzhenko and Malinin, 1971; Naumov et al., 1974). Therefore use of ratios of mole fractions in the vapor phase, $X_i$'s, introduces negligible errors (Giggenbach, 1987). The theoretical values obtained from equations (10.24)-(10.26) are reported as vapor lines and superheated vapor grids in Figs. 10.3 and 10.4. It must be underscored that equilibrium values of $\log(X_{H2}/X_{H2O})$ and $\log(X_{CO}/X_{CO2})$ depend upon the temperature and the redox potential in the gas equilibration zone only, whereas theoretical $\log(X_{CH4}/X_{CO2})$ ratios are also controlled by water fugacity. As a consequence, $\log(X_{H2}/X_{H2O})$ and $\log(X_{CO}/X_{CO2})$ in pure saturated vapors are equal to those in superheated vapors at any T and redox condition (vapor lines in Fig. 10.3), whereas $\log(X_{CH4}/X_{CO2})$ in pure saturated vapors (vapor lines in Fig. 10.4) are different from those in superheated vapors (superheated vapor grids in Fig. 10.4).

*Theoretical sums of log-ratios $H_2/H_2O$, $CO/CO_2$, and $CH_4/CO_2$*. Geoindicators independent on the redox potential can be derived summing reactions (10.15) to (10.17) in order to eliminate $O_2$. This exercise produces the following 5 reactions, each including 4 and excluding 1 of the considered 5 constituents:

$$CO_2 + H_2 = CO + H_2O \qquad (10.27)$$

$$CH_4 + 2H_2O = 4\,H_2 + CO_2 \qquad (10.28)$$

$$3CO_2 + CH_4 = 4CO + 2H_2O \qquad (10.29)$$

$$CH_4 + H_2O = 3H_2 + CO \qquad (10.30)$$

$$CH_4 + CO_2 = 2H_2 + 2CO \qquad (10.31)$$

Only 2 of these 5 reactions are mutually independent, as all the 5 constituents are involved in any 2 of these reactions.

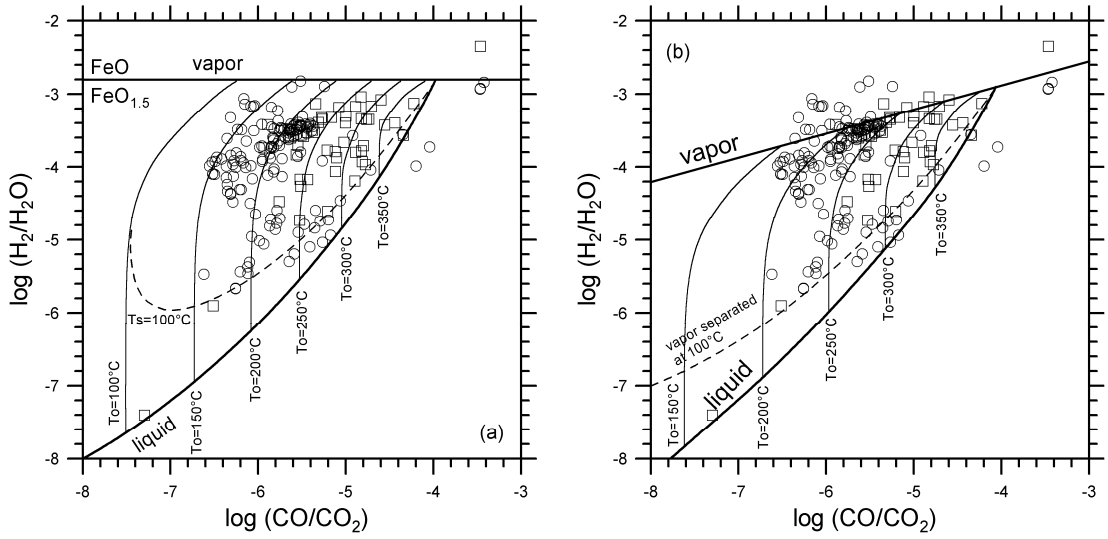


Fig. 10.3. Plot of $\log(X_{H2}/X_{H2O})$ vs $\log(X_{CO}/X_{CO2})$. The theoretical grid assumes that redox conditions in the gas equilibration zone are controlled by either (a) the FeO-$FeO_{1.5}$ hydrothermal buffer of Giggenbach or (b) the $f_{O2}$-buffer of D'Amore and Panichi. Compositions of both the vapor and liquid phases (thick solid lines) are shown. Compositions of the vapor phase separated in a single-step at different temperatures from a liquid phase initially at To = 150°, 200°, 250°, 300° and 350 °C are also shown (thin solid lines) as well as the compositions resulting from single-step vapor separation at 100°C starting from any initial temperature (dashed lines). Circles = fumarolic vapors; squares = vapors from geothermal wells (from Chiodini and Marini, 1998).

Let us consider, for instance, reactions (10.27) or water-gas shift reaction WGS and (10.29) here indicated with the acronym CCC. Their equilibrium constant expressions are:

$$\log\frac{f_{CO}}{f_{CO_2}} - \log\frac{f_{H_2}}{f_{H_2O}} = K_{WGS} \cong \log\frac{X_{CO}}{X_{CO_2}} - \log\frac{X_{H_2}}{X_{H_2O}} \qquad (10.32)$$

$$3\log\frac{f_{CO}}{f_{CO_2}} + \log\frac{f_{CO}}{f_{CH_4}} = K_{CCC} - 2\log f_{H_2O} \cong 3\log\frac{X_{CO}}{X_{CO_2}} + \log\frac{X_{CO}}{X_{CH_4}} \qquad (10.33)$$

The temperature dependence of the thermodynamic constants $K_{WGS}$ and $K_{CCC}$ is given by the following equations:

$$\log K_{WGS} = 2.485 - \frac{2248}{T(K)}. \qquad (10.34)$$

$$\log K_{WGS} = 19.605 - \frac{17813}{T(K)}. \qquad (10.35)$$

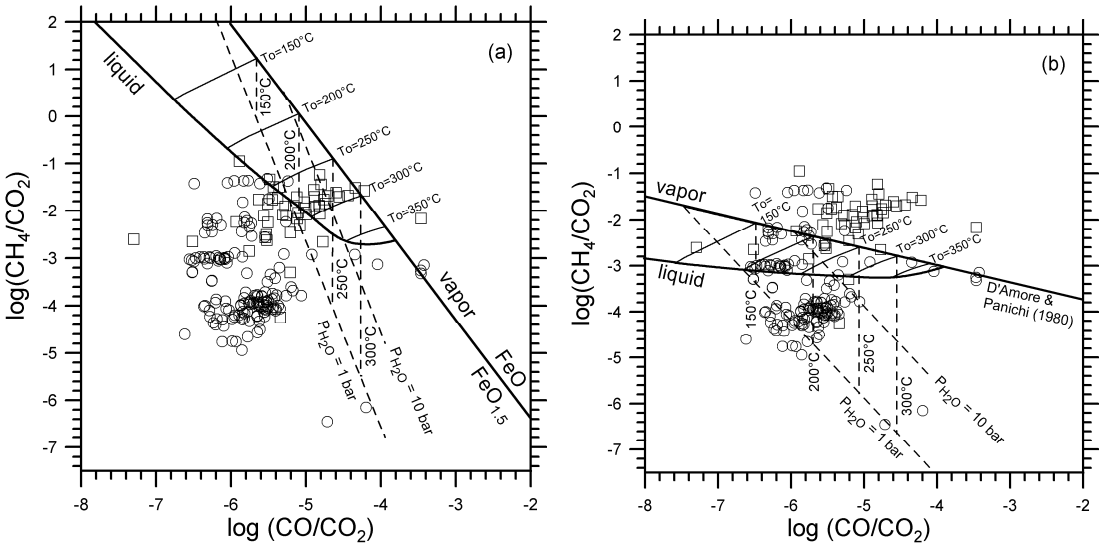


Fig. 10.4. Plot of $\log(X_{CH4}/X_{CO2})$ vs $\log(X_{CO}/X_{CO2})$. Theoretical grids for coexisting liquid and vapor phases (solid lines) and superheated vapors (dashed lines) are calculated assuming that redox potentials in the gas equilibration zone are controlled by either (a) the FeO-$FeO_{1.5}$ hydrothermal buffer or (b) the $f_{O2}$-buffer of D'Amore and Panichi. Symbols as in Fig. 10.3 (from Chiodini and Marini, 1998).

Equilibrium values of $\log(X_{CO}/X_{CO2})$ - $\log(X_{H2}/X_{H2O})$ depend upon the temperature in the gas equilibration zone only, whereas theoretical values of $3\log(X_{CO}/X_{CO2})$ + $\log(X_{CO}/X_{CH4})$ are also controlled by water fugacity. Theoretical values of these sums of log-ratios are shown as vapor lines and superheated vapor grids in Fig. 10.5.

*10.1.3. Attainment of chemical equilibrium in a single saturated liquid phase*

Equilibrium gas contents in a single saturated liquid phase are conveniently computed using the vapor-liquid distribution coefficient, $B_j$, which is defined as the ratio between the concentration of gas j in the vapor phase and the concentration of the same gas in the liquid phase (Eqn. 6.6). The temperature dependence of vapor-liquid distribution coefficients for the gas species of interest is described, in the 100-340 °C range, by equations (6.9, 6.10, 6.11, and 6.13). Above 340 °C, distribution coefficients are obtained interpolating between the value at 340 °C and 1, i.e., the theoretical value at 374°C for all gas species.

Insertion of Eqn. (6.6) in equations (10.24), (10.25), (10.26), (10.32), and (10.33) leads to the following relationships:

$$\log\left(\frac{X_{H_2}}{X_{H_2O}}\right)_L = \log K_{H_2} - \frac{1}{2}\log f_{O_2} - \log B_{H_2} \qquad (10.36)$$

$$\log\left(\frac{X_{CO}}{X_{CO_2}}\right)_L = \log K_{CO} - \frac{1}{2}\log f_{O_2} - \log\frac{B_{CO}}{B_{CO_2}} \tag{10.37}$$

$$\log\left(\frac{X_{CH_4}}{X_{CO_2}}\right)_L = \log K_{CH_4} - 2\log f_{O_2} + 2\log f_{H_2O} - \log\frac{B_{CH_4}}{B_{CO_2}} \tag{10.38}$$

$$\log\left(\frac{X_{CO}}{X_{CO_2}}\right)_L - \log\left(\frac{X_{H_2}}{X_{H_2O}}\right)_L = \log K_{WGS} - \log\frac{B_{CO}}{B_{CO_2}} + \log B_{H_2} \tag{10.39}$$

$$3\log\left(\frac{X_{CO}}{X_{CO_2}}\right)_L + \log\left(\frac{X_{CO}}{X_{CH_4}}\right)_L = \log K_{CCC} - 2\log f_{H_2O} - 3\log\frac{B_{CO}}{B_{CO_2}} - \log\frac{B_{CO}}{B_{CH_4}} \tag{10.40}$$

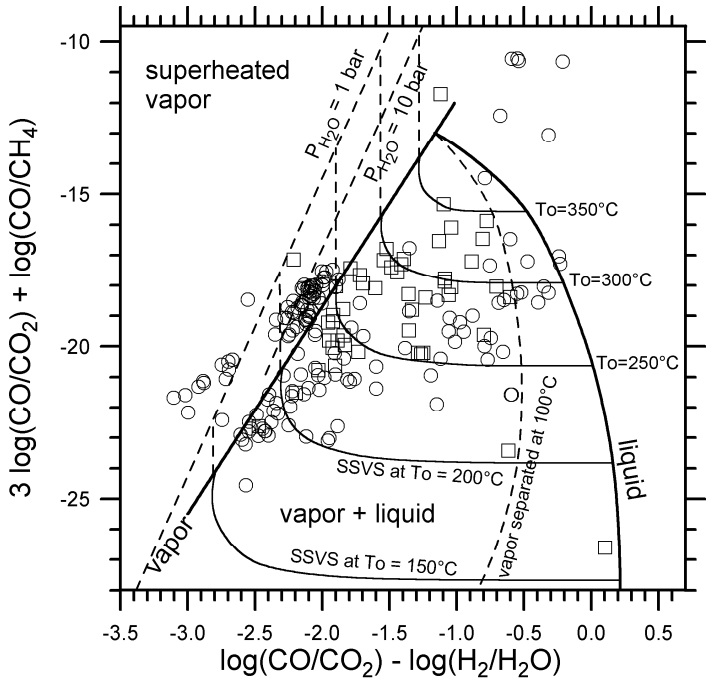


Fig. 10.5. Plot of $3\log(X_{CO}/X_{CO2}) + \log(X_{CO}/X_{CH4})$ vs. $\log(X_{CO}/X_{CO2}) - \log(X_{H2}/X_{H2O})$, showing the theoretical grids for coexisting liquid and vapor phases (solid lines) and superheated vapors (dashed lines). Also shown are the compositions of vapors separated in a single-step at different temperatures from a liquid phase initially at To = 150°, 200°, 250°, 300° and 350 °C (thin solid lines) and the compositions resulting from single-step vapor separation at 100°C starting from any initial temperature (dashed lines). Symbols as in Fig. 10.3 (from Chiodini and Marini, 1998).

Compositions described by equations (10.36)-(10.40) can be reached in fumaroles and steam wells only through complete isothermal evaporation of an equilibrated liquid. This process requires a considerable supply of heat from an external source and it is possible under peculiar situations only, usually absent in most 'normal' geothermal systems. Nevertheless they represent a useful reference, and would be applicable to any unflashed samples of a deep liquid phase. The theoretical values of $\log(X_{H2}/X_{H2O})_L$, $\log(X_{CO}/X_{CO2})_L$, $\log(X_{CH4}/X_{CO2})_L$, $\log(X_{CO}/X_{CO2})_L - \log(X_{H2}/X_{H2O})_L$, and $3\log(X_{CO}/X_{CO2})_L + \log(X_{CO}/X_{CH4})_L$ are reported as liquid lines in Figs. 10.3-10.5.

*10.1.4. Steam produced through boiling of an equilibrated liquid phase*

To compare theoretical and measured data, the effect of secondary phenomena affecting rising geothermal fluids have to be taken into account. Since it is not possible to separate the effects of two or more secondary phenomena for a given sample, we implicitly assume that only one of these phenomena is important in each case. Among these secondary phenomena, boiling and steam condensation (for computing the effects of the latter process see Chiodini and Marini, 1998), can bring about large chemical changes, due to distribution of different gas species between separating liquid and vapor phases. To calculate the effects of boiling on the theoretical values of $\log(X_{H2}/X_{H2O})_L$, $\log(X_{CO}/X_{CO2})_L$, $\log(X_{CH4}/X_{CO2})_L$, $\log(X_{CO}/X_{CO2})_L - \log(X_{H2}/X_{H2O})_L$, and $3\log(X_{CO}/X_{CO2})_L + \log(X_{CO}/X_{CH4})_L$, it is assumed attainment of chemical equilibrium in a single saturated liquid phase at initial (equilibrium) temperature To, followed by adiabatic single-step steam separation at temperature Ts. Under these assumptions, the mole fractions of the gas species of interest in the separated vapor phase are constrained by simple mass balances (e.g., Eqn. 6.14) and enthalpy balance (Eqn. 6.4). The following relations are obtained inserting expression (6.14) into equations (10.36) – (10.40):

$$\log\left(\frac{X_{H_2}}{X_{H_2O}}\right)_{Ts} = \log K_{H_2} - \frac{1}{2}\log f_{O_2} - \log B_{H_2,To} - \log\left(y + \frac{1-y}{B_{H_2,Ts}}\right) \qquad (10.41)$$

$$\log\left(\frac{X_{CO}}{X_{CO_2}}\right)_{Ts} = \log K_{CO} - \frac{1}{2}\log f_{O_2} - \log\frac{B_{CO,To}}{B_{CO_2,To}} - \log\left(y + \frac{1-y}{B_{CO,Ts}}\right) + \log\left(y + \frac{1-y}{B_{CO_2,Ts}}\right) \qquad (10.42)$$

$$\log\left(\frac{X_{CH_4}}{X_{CO_2}}\right)_{Ts} = \log K_{CH_4} - 2\log f_{O_2} + 2\log f_{H_2O} - \log\frac{B_{CH_4,To}}{B_{CO_2,To}} - \log\left(y + \frac{1-y}{B_{CH_4,Ts}}\right) + \log\left(y + \frac{1-y}{B_{CO_2,Ts}}\right) \qquad (10.43)$$

$$\log\left(\frac{X_{CO}}{X_{CO_2}}\right)_{Ts} - \log\left(\frac{X_{H_2}}{X_{H_2O}}\right)_{Ts} = \log K_{WGS} - \log\frac{B_{CO,To}}{B_{CO_2,To}} + \log B_{H_2,To}$$
$$- \log\left(y + \frac{1-y}{B_{CO,Ts}}\right) + \log\left(y + \frac{1-y}{B_{CO_2,Ts}}\right) + \log\left(y + \frac{1-y}{B_{H_2,Ts}}\right) \quad (10.44)$$

$$3\log\left(\frac{X_{CO}}{X_{CO_2}}\right)_{Ts} + \log\left(\frac{X_{CO}}{X_{CH_4}}\right)_{Ts} = \log K_{CCC} - 2\log f_{H_2O} - 3\log\frac{B_{CO,To}}{B_{CO_2,To}}$$
$$- \log\frac{B_{CO,To}}{B_{CH_4,To}} - 4\log\left(y + \frac{1-y}{B_{CO,Ts}}\right) + 3\log\left(y + \frac{1-y}{B_{CO_2,Ts}}\right) + \log\left(y + \frac{1-y}{B_{CH_4,Ts}}\right) \quad (10.45)$$

The theoretical log ratios and sums of log ratios values in the vapor phase separated at different temperatures from a liquid phase initially at 150°, 200°, 250°, 300° and 350 °C are shown in Figs. 10.3-10.5 as single-step vapor separation lines. In Figs. 10.3 and 10.5 the theoretical values of vapor separated at 100°C starting from any initial temperature are also reported.

*10.1.5. Comparison between theoretical and analytical compositions*

Analytical data spread throughout the theoretical grids in the $\log(X_{CO}/X_{CO2})$ vs $\log(X_{H2}/X_{H2O})$ plot (Fig. 10.3), which is slightly affected by the choice of redox buffer.

In the $\log(X_{CH4}/X_{CO2})$ vs $\log(X_{CO}/X_{CO2})$ plot (Fig. 10.4), the field of saturated vapors overlaps that of superheated vapors, thus complicating the interpretation of measured data. In addition, a large number of analytical data plot outside the theoretical grid, using either the redox buffer by Giggenbach (1987) or that of D'Amore and Panichi (1980). As the $CH_4/CO_2$ ratio is strongly affected by redox conditions in the gas equilibration zone, this disagreement between measured and theoretical values suggests that no unique redox buffer is active in all the geothermal environments. Alternatively, $CH_4$ might be out of equilibrium with the other gases due to kinetic reasons. An attempt to quantify the kinetics of chemical equilibration between $CO_2$ and $CH_4$ was presented by Giggenbach (1997b). Assuming that the conversion of $CO_2$ to $CH_4$ may be described by a pseudo-first order reaction, the reaction half-time would be about 12a at 300°C, 500a at 200°C and 160ka at 100°C. However, these are very preliminary estimates based on limited experimental data and further researches are needed to clarify the kinetics of conversion of $CO_2$ to $CH_4$ in the presence of catalysts occurring in natural environments (Giggenbach, 1997b).

The diagrams that make use of 2 sums of log-ratios [e.g., $\log(X_{CO}/X_{CO2})$ - $\log(X_{H2}/X_{H2O})$, and $3\log(X_{CO}/X_{CO2}) + \log(X_{CO}/X_{CH4})$, Fig. 10.5] are independent of redox conditions. In addition, the weight of $CH_4$ on these functions is relatively small and these sums of log-ratios are mainly controlled by the $CO/CO_2$ and $H_2/H_2O$ ratios. These functions gave reasonable estimates of the equilibrium temperature and, therefore, can be used as effective geoindicators in most geothermal systems. It must be pointed out, however, that application of CO-based geothermometers may be complicated by fast re-equilibration of this minor species (Brombach et al., 2002, 2003).

### *10.2. Geothermal gas equilibria in the $H_2O$-$H_2$-$H_2S$ system*

Giggenbach (1980) showed that the $H_2S$ fugacity in hydrothermal environments is controlled by coexisting pyrite, an unspecified Fe-Al-silicate (indicated as [FeO], probably chlorite or epidote in natural systems) and the corresponding Al-silicate in its protonated, Fe-free form, [$H_2O$], as expressed by the following reaction (after Giggenbach, 1980, modified):

$$FeS_2 + H_2O + [H_2O] = [FeO] + 1/2\ O_2 + 2\ H_2S, \qquad (10.46)$$

whose equilibrium constant is conveniently written as:

$$\log\left(\frac{X_{H_2S}}{X_{H_2O}}\right) = \frac{1}{2}\log K_S - \frac{1}{4}\log f_{O_2} - \frac{1}{2}\log f_{H_2O}. \qquad (10.47)$$

As indicated by Eqn. (10.47), equilibrium $X_{H2S}/X_{H2O}$ ratios depend upon temperature, redox potential and water fugacity in the gas equilibration zone. The temperature dependence of the thermodynamic constant $K_S$ is given by the following equation:

$$\log K_S = 2.388 - \frac{13211.8}{T(K)}, \qquad (10.48)$$

which is based on an empirical correlation by Giggenbach (1980) and on the thermodynamic constant of water formation from elements (Stull et al., 1969). Assuming that redox conditions in the gas equilibration zone are fixed by either Eqns. (10.13) or (10.14) and water fugacity is constrained by Eqn. (10.6), the temperature dependence of the theoretical $X_{H2S}/X_{H2O}$ ratio in a single saturated vapor phase can be easily computed.

### *10.3. Geothermal gas equilibria in the $H_2O$-$H_2$-$N_2$-$NH_3$ system*

Ammonia and $N_2$ are involved in the following redox reaction (Giggenbach, 1980, modified):

$$N_2 + 3\ H_2O\ = 2\ NH_3 + 3/2\ O_2 \qquad (10.49)$$

whose equilibrium constant can be written as

$$L_N = \log\left(\frac{X_{NH_3}}{X_{N_2}}\right) + \log\left(\frac{X_{NH_3}}{X_{H_2O}}\right) = \log K_N - \frac{3}{2}\log f_{O_2} + 2\log f_{H_2O}. \qquad (10.50)$$

Eqn. (10.50) indicates that theoretical $L_N$ values are controlled by temperature, redox conditions and water fugacity in the gas equilibration zone. On the basis of the thermodynamic data of Stull et al. (1969), the temperature dependence of the thermodynamic constant $K_N$ is described by:

$$\log K_N = -3.996 - \frac{32863}{T(K)}. \qquad (10.51)$$

Again, assuming that redox conditions in the gas equilibration zone are fixed by suitable $f_{O2}$-buffers, e.g., Eqns. (10.13) or (10.14), and water fugacity is constrained by Eqn. (10.6), the temperature dependence of the theoretical $L_N$ values in a single saturated vapor phase can be easily computed.

### *10.4. The $H_2$-Ar geoindicator*

Giggenbach (1991a) derived a $H_2$-Ar geoindicator which is based on the strong dependence of $f_{H2}$ on temperature and on the assumption that the Ar content of hydrothermal fluids derives almost entirely from air-saturated meteoric waters involved in the recharge of these systems. A derivation slightly different from that of Giggenbach (1991a) is presented hereunder.

First of all, it is convenient to test the Giggenbach's hypothesis, i.e., to verify if the Ar contents of fumarolic fluids are equal to those of air-saturated groundwaters or not. This exercise is conveniently carried out by means of a $H_2O$-$N_2$-Ar triangular plot (Fig. 10.6), where the fumarolic samples are plotted together with the points representative of atmospheric air and air-saturated groundwaters at 5, 10, 15 and 20°C.

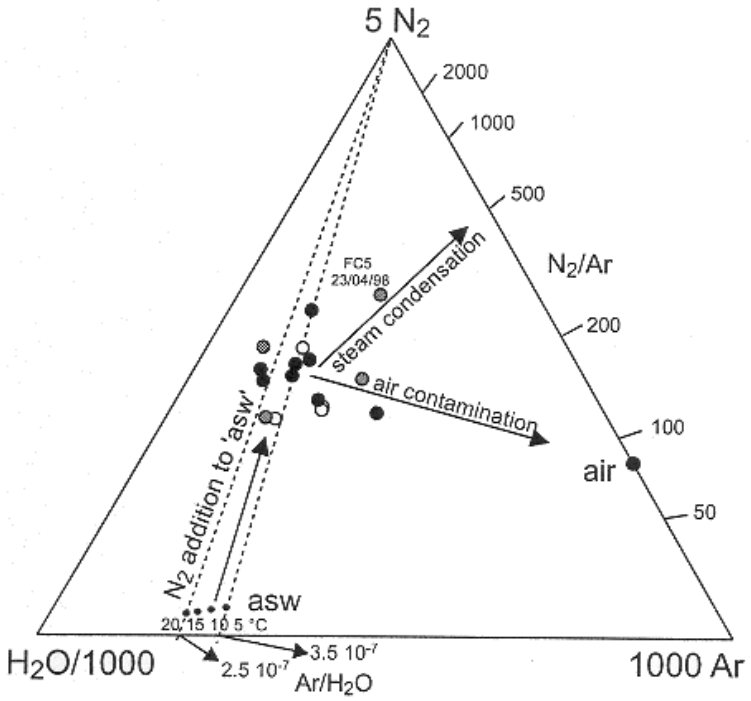


Fig. 10.6. Triangular plot $H_2O$-$N_2$-Ar, showing analytical data of Vesuvius fumaroles and the compositions of atmospheric air and of air-saturated groundwater at 5-20°C (from Chiodini et al., 2001b).

The composition air-saturated groundwaters is easily computed referring to the solubility data of Wilhelm et al. (1977) and considering that the average atmospheric partial pressures of Ar and $N_2$ are 0.00934 bar and 0.7808 bar, respectively. For instance, at 12°C $K_{H,Ar}$ = 31289 and $K_{H,N2}$ = 69013 bars (mole fraction)$^{-1}$; therefore log $X_{Ar}$ = -6.52 and log $X_{N2}$ = -4.95.

As already recalled, according to Giggenbach (1987), the log $(f_{H2}/f_{H2O}) \cong$ log $(X_{H2}/X_{H2O})_V$ of hydrothermal fluids is buffered by the (FeO) – ($FeO_{1.5}$) redox buffer of the rock system at –2.82, at any temperature of interest. Assuming that the $X_{Ar}/X_{H2O}$ ratio in the liquid phase is equal to that of average air saturated groundwater, and

admitting that $X_{H2O}$ is close to unity, both in the liquid and vapor phases, the $X_{Ar}/ X_{H2O}$ ratio in the vapor phase is given by:

$$\log\left(\frac{X_{Ar}}{X_{H_2O}}\right)_V = \log B_{Ar} + \log\left(\frac{X_{Ar}}{X_{H_2O}}\right)_L = \log B_{Ar} - 6.52. \qquad (10.52)$$

The theoretical $X_{H_2}/X_{Ar}$ ratio in the vapor phase is readily obtained as follows:

$$\log\left(\frac{X_{H_2}}{X_{Ar}}\right)_V = \log\left(\frac{X_{H_2}}{X_{H_2O}}\right)_V - \log\left(\frac{X_{Ar}}{X_{H_2O}}\right)_V = \qquad (10.53)$$
$$-2.82 - \log B_{Ar} + 6.52 = 3.7 - \log B_{Ar}.$$

The vapor-liquid distribution coefficient of Ar is related to temperature by the following linear equation (data from Naumov et al., 1974; T is in °C):

$$\log B_{Ar} = 6.4822 - 0.0160\ T. \qquad (10.54)$$

Therefore, the $H_2$/Ar ratio in the vapor phase is linked to temperature by this equation:

$$\log\left(\frac{X_{H_2}}{X_{Ar}}\right)_V = -2.78 + 0.016T. \qquad (10.55)$$

A similar expression holds true for the liquid phase, as already observed by Giggenbach (1991a):

$$\log\left(\frac{X_{H_2}}{X_{Ar}}\right)_L = -2.53 + 0.014T. \qquad (10.56)$$

The similarity of the two expressions is not surprising because the vapor-liquid distribution coefficients of $H_2$ and Ar are quite similar.

These two equilibrium relationships are used, together with equations (10.24) and (10.36), to construct the theoretical grid in the plot of $\log(X_{H2}/X_{H2O})$ vs $\log(X_{H2}/X_{Ar})$ of Fig. 10.7, also showing the analytical data of fumarolic gases, in this case from the island of Nisyros, Greece (from Brombach et al., 2003). Most points distribute close to the liquid composition, at temperatures close to 350°C, indicating that these thermal conditions are present in the roots of this geothermal system. Also shown in Fig. 10.7 are the effects of air contamination and steam condensation, which are presumably responsible for the department of some samples from the equilibrium composition in a liquid phase at ~350°C.

Applications of the $H_2$/Ar geothermometric function are promising, although it may be affected by loss of Ar from the hydrothermal reservoir through boiling. If this process takes place, Ar is lost once for all, whereas $H_2$ is contributed again by $H_2O$

dissociation. This leads to overestimation of equilibrium temperatures (Brombach et al., 2002, 2003).

Other uncertainties derive from the salinity of the geothermal liquid phase, which is typically unknown when dealing with fumarolic fluids. However, the solubility of the gas species of interest, including Ar, in high-salinity aqueous solutions can be estimated following the approach of Chiodini et al. (2001b). For instance, the plot of $\log(X_{H2}/X_{H2O})$ vs $\log(X_{H2}/X_{Ar})$ of Figure 10.8 was prepared for gases dissolving in 1 m NaCl (Gambardella, 2001).

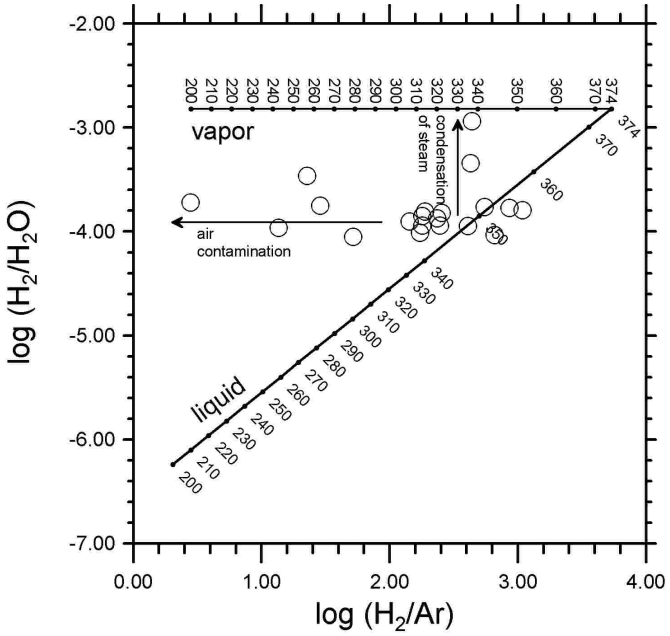


Fig. 10.7. Plot of $\log(X_{H2}/X_{H2O})$ vs $\log(X_{H2}/X_{Ar})$ for the fumarolic gases of Nisyros, Greece (from Brombach et al., 2003, modified).

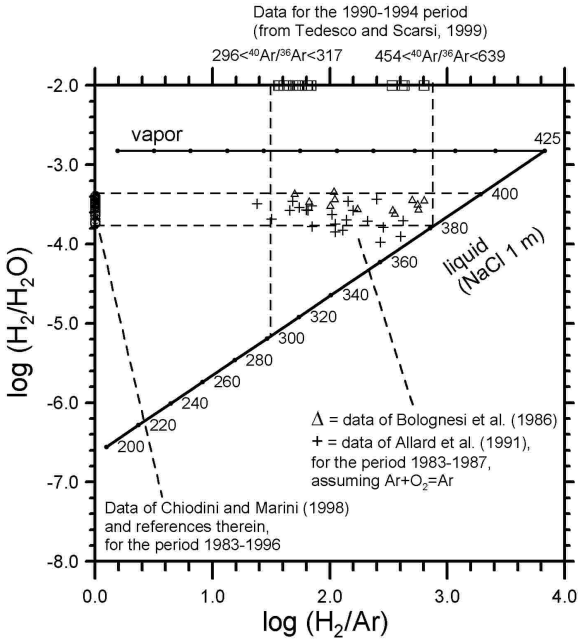


Fig. 10.8. Plot of $\log(X_{H2}/X_{H2O})$ vs $\log(X_{H2}/X_{Ar})$ for the fumarolic gases of La Solfatara, Italy (from Gambardella, 2001).

## 11. The δD and $\delta^{18}O$ values of geothermal fluids

The δD and $\delta^{18}O$ values of liquids circulating in deep, high-temperature geothermal systems are controlled by several processes, including (Giggenbach, 1991b): (1) rock-water $^{18}O$ exchange, (2) mixing of different waters (meteoric waters, marine waters, connate waters, magmatic waters, ...), and (3) steam separation (boiling).

### *11.1. The rock-water $^{18}O$ exchange*

The $^{18}O$ exchange between a geothermal liquid and a given mineral is governed, at equilibrium, by the fractionation factors $\alpha_{m-w}$, which is defined as follows:

$$\alpha_{m-w} = \frac{\left(\frac{^{18}O}{^{16}O}\right)_m}{\left(\frac{^{18}O}{^{16}O}\right)_w} \qquad (11.1)$$

Equilibrium isotope fractionation factors can be computed through the partition functions, i.e., mathematical relationships coming from statistical mechanics (e.g., Richet and Bottinga, 1976; Richet al al., 1977; Kieffer, 1982; O'Neil, 1986).

The $\alpha_{m-w}$ values increase with increasing strength of the chemical bonds holding oxygen atoms into a given mineral lattice. Quartz and calcite have high $\alpha_{m-w}$ values, whereas feldspars have low $\alpha_{m-w}$ values (see insert in Figure 11.1, where $\varepsilon_{m-w} = 1000 \ln\alpha_{m-w}$ is reported against temperature). In general, equilibrium isotope fractionation factors are temperature dependent and approach 1 (which means zero fractionation) with increasing temperature. However, the $\alpha_{m-w}$ values of quartz, calcite, and feldspars are significantly >1 ($\varepsilon_{m-w}$ >0) for temperatures lower than 400°C.

The decrease in temperature brings about also a quick decrease in the kinetics of the $^{18}O$ exchange between minerals and water. Therefore, $^{18}O$ enrichments in Na-Cl geothermal liquids with respect to meteoric waters (usually called "shifts") have been traditionally considered as indicators of high temperatures (>150 °C) in the geothermal reservoirs of provenance (e.g., Truesdell and Hulston, 1980 and references therein). However, the $^{18}O$ shifts depend also on the initial isotope composition of the liquid and solid phases involved in the exchange process as well as on the water/rock ratio, or on system dynamics (Giggenbach, 1991b, see below).

These $^{18}O$ shifts are not accompanied by hydrogen isotope shifts because (i) rock minerals contain little hydrogen and (ii) water/rock ratios are usually relatively high and, consequently, the hydrogen of rock minerals is not a significant fraction of the total hydrogen of the water-rock system, which is dominated by water.

Referring to the geothermal systems of New Zealand, Giggenbach (1991b) underscored the differences between Ngawha and Wairakei (Fig. 11.1).

At Ngawha (temperatures up to 320°C), the least diluted water is remarkably enriched in $^{18}O$ with respect lo local meteoric waters and it is only 5‰ lighter than rocks. Besides altered rocks have $\delta^{18}O$ values, which are not much different from those of unaltered rocks. Water approaches isotopic equilibrium with rocks, since the system is almost stagnant and rock-dominated.

At Wairakei (temperatures close to 260°C) the $^{18}O$ enrichment of the geothermal liquids with respect lo local meteoric waters is small, ~1.2 ‰, and altered rocks are, with $\delta^{18}O$ values of 2.5 to 5 ‰, much lighter than unaltered rocks, whose $\delta^{18}O$ values

range from 7 to 9 ‰. Wairakei appears to be a dynamic, water-dominated geothermal system, i.e., flushed by large water flows.

This distinction between stagnant, rock-dominated systems and dynamic, water-dominated (Giggenbach, 1991b) is more reasonable than that based on the water/rock ratio.

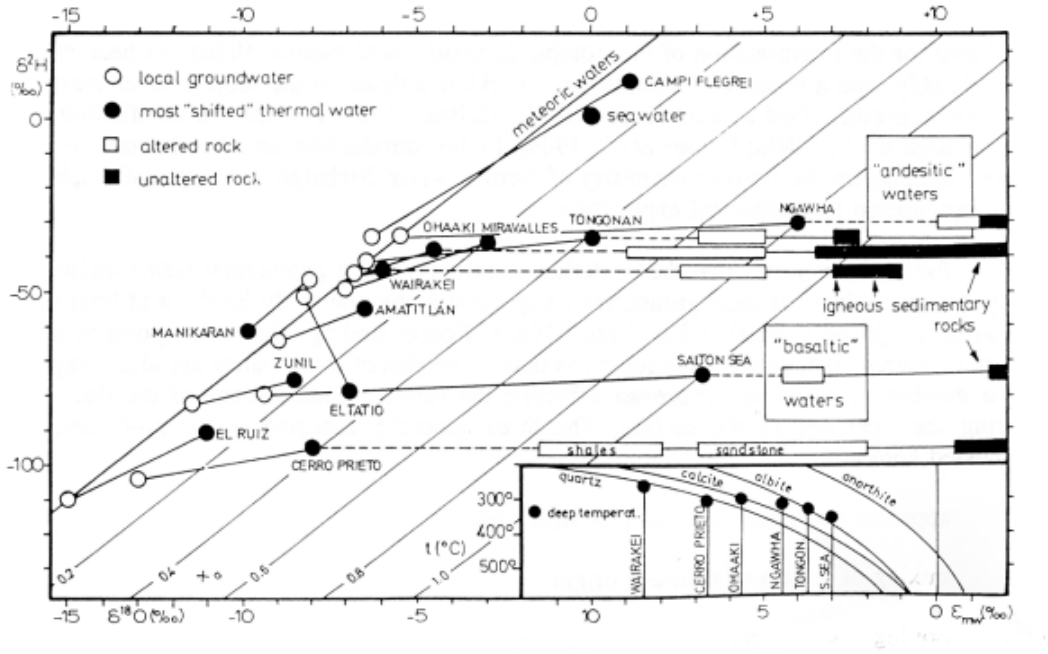


Figure 11.1. δD and $\delta^{18}O$ values of shallow and deep thermal waters and altered and unaltered rocks form different geothermal systems. In the insert the equilibrium fractionation factors between minerals and water are compared with those observed in some geothermal systems (from Giggenbach, 1991b).

### *11.2. Mixing of different waters*

A second type of processes affecting the δD and $\delta^{18}O$ values of geothermal liquids is mixing between local meteoric waters and waters of different origin, such as: (i) marine waters (e.g. Campi Flegrei in Fig. 11.1); (ii) high-salinity waters or connate waters, especially in sedimentary basins; examples of this class of waters are represented by the brines circulating in the geothermal systems of Salton Sea and Cerro Prieto, whose high salinity is ascribable to leaching of evaporite rocks; the interaction of these stagnant brines with fine grained sediments at temperatures close to 350°C explains their enrichment in $^{18}O$; (iii) magmatic waters, as anticipated in the Introduction.

The andesitic or arc-type magmatic water, which is characterized by δD values of -10 to -30 ‰, is found in all the geothermal areas located along convergent plate boundaries as well as in areas which were affected by subduction in a geologically recent past (e.g., Tyrrhenian Central-Southern Italy). In some of these volcanic areas (e.g., Amatitlan and Zunil, Guatemala, and Miravalles, Costa Rica), if the involvement of andesitic water is ruled out, dilution trends would imply that geothermal waters derived from rain waters infiltrating at low elevations mix with shallow groundwaters infiltrating at high elevations, which is a rather queer hydrogeological model.

It must be recalled that the isotopic ratios of any binary mixture made of, for instance, a thermal endmember and a cold endmember are constrained by the following general binary mixing equation (Faure, 1986):

$$\delta_M = \frac{\delta_T \cdot C_T \cdot x + \delta_F \cdot C_F \cdot (1-x)}{C_M} \qquad (11.2)$$

where subscripts M, T, and F identify the binary mixture, the thermal endmember and the cold endmember and x is the fraction of the thermal component in the mixture. If $C_T \neq C_F \neq C_M$ the binary mixing line is a hyperbola in $\delta$ - C and $\delta$ - $\delta$ spaces, but it becomes a straight line in the $\delta$ - (1/C) space. Since water is by far the major component of any aqueous solution, $C_T = C_F = C_M$, and Eqn. (11.2) reduces to:

$$\delta_M = \delta_T\, x + \delta_F\, (1\text{-}x) \qquad (11.3)$$

which is equivalent to Eqn. (6.1). As a consequence, mixing lines are straight lines in the $\delta$ - C and $\delta$ - $\delta$ spaces, but this is the exception, not the rule, a fact which cannot be forgotten when working with isotope ratios of chemical constituents different from water.

### *11.3. Steam separation*

Steam separation (boiling) takes place when the vapor pressure (plus the sum of the partial pressures of dissolved gases) of high-temperature (>>100 °C) geothermal waters uprising towards the surface exceeds the hydrostatic burden. This process brings about isotopic fractionation, with heavy isotopes concentrating in the liquid (at any temperature for $^{18}O$ and at temperatures below 229°C for deuterium in a pure water system) whereas the vapor phase is obviously depleted in heavy isotopes.

The isotopic fractionation factor decreases approaching the critical point both for $^{18}O$ and D. It is recalled that the critical point is 374°C, 221 bar for pure water, but depending on the salt content of the NaCl-$H_2O$ system (which is the obvious, simplest analogue of the complex, natural geothermal liquids), the critical point is shifted to pressures and temperatures significantly higher than those of pure water (e.g., Bischoff and Pitzer, 1989; Knight and Bodnar, 1989). Liquid-vapor fractionation factors of O and H isotopes for pure water from 0°C to the critical temperature are given by the following relationships (Horita and Wesolowski, 1994, T in K):

$$1000 \cdot \ln \alpha_{L-V(D)} = 1158.8 \frac{T^3}{10^9} - 1620.1 \frac{T^2}{10^6} + 794.84 \frac{T}{10^3} - 161.04 + 2.9992 \frac{10^9}{T^3} \qquad (11.4)$$

$$1000 \cdot \ln \alpha_{L-V(^{18}O)} = -7.685 + 6.7123 \frac{10^3}{T} - 1.6664 \frac{10^6}{T^2} + 0.35041 \frac{10^9}{T^3}. \qquad (11.5)$$

Computed values of 1000 ln $\alpha_{L\text{-}V}$ are approximated to ±1.2 ‰ (1 $\sigma$) for D and ±0.11 ‰ (1 $\sigma$) for $^{18}O$. Liquid-vapor fractionation factors for NaCl solutions from 0 to 5 m NaCl, are computed by means of the following equations (Horita et al., 1995):

$$1000 \cdot \ln \Gamma_{(D)} = m \cdot \left( 0.01680 \cdot T - 13.79 + \frac{3255}{T} \right) \qquad (11.6)$$

$$1000 \cdot \ln \Gamma_{(18O)} = m \cdot (-0.033 + 8.93\times10^{-7}\ T^2 - 2.12\times10^{-9}\ T^3) \qquad (11.7)$$

where:

$$1000 \ln \Gamma = 1000 \ln \alpha_{L\text{-}V(\text{pure water})} - 1000 \ln \alpha_{L\text{-}V(\text{salt soln.})}, \qquad (11.8)$$

m is the molality of the NaCl solution and T is in K. Computed values of 1000 ln $\alpha_{L\text{-}V}$ are approximated to ±0.9 ‰ (1 σ) for D and ±0.12‰(1 σ) for $^{18}O$. At temperatures above 350°C, the fractionation factors can be obtained interpolating between the value at 350 °C and 0 ‰, i.e., the theoretical value at the critical temperature. Since at these high temperatures the fractionation factors are relatively small (-10 to 0 ‰ for H isotopes and +1 to 0 ‰ for O isotopes), uncertainties in this interpolation have negligible effects on boiling calculations.

Fractionation of O and H isotopes between liquid water and vapor attains equilibrium almost immediately, even at temperatures close to 100°C. Isotopic fractionation depends also on the fraction of separated steam and the kind of separation (single step, multistep or continuous).

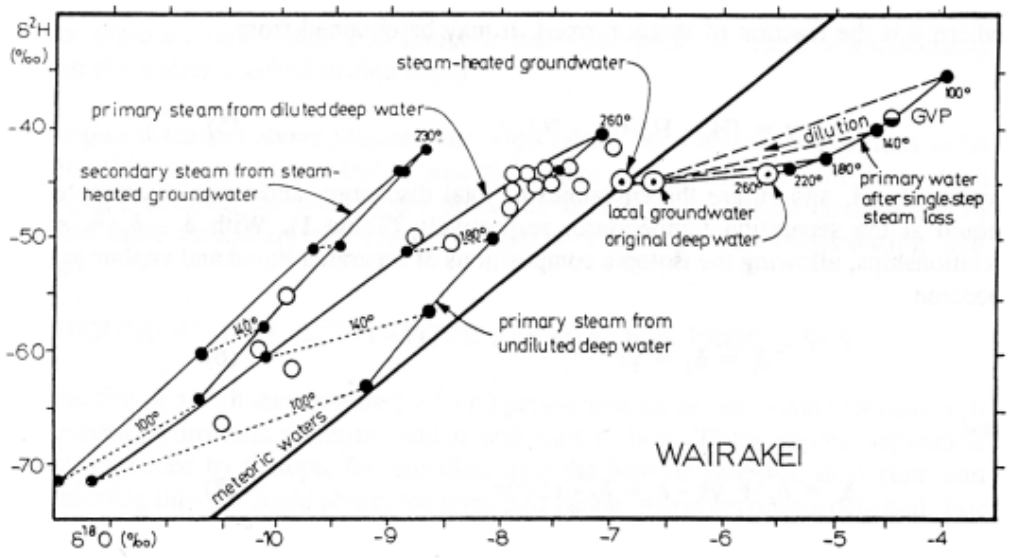


Fig. 11.2. δD vs. $\delta^{18}O$ plot comparing observed and theoretical isotope values of vapor and liquid produced through boiling of a parent geothermal liquid (from Giggenbach and Stewart, 1982).

In general, natural steam separation processes are satisfactorily approximated by the single step model (Truesdell et al, 1977; Giggenbach, 1978; Giggenbach and Stewart, 1982). In this case, the δ values of the separated vapor and liquid, $\delta_V$ e $\delta_L$, are related to that of the initial liquid, $\delta_T$, by the following mass balance:

$$\delta_T = \delta_L\ (1\text{-}y) + \delta_V\ y \qquad (11.9)$$

and by the approximate relationship:

$$1000 \ln\alpha_{L\text{-}V} = \delta_L - \delta_V. \qquad (11.10)$$

For isoenthalpic steam separation y is calculated through Eqn. (6.5). The following relationships are easily obtained from Eqns. (11.9) and (11.10):

$$\delta_L = \delta_T + y\ 1000\ \ln\alpha_{L\text{-}V} \tag{11.11}$$

$$\delta_V = \delta_T - (1\text{-}y)\ 1000\ \ln\alpha_{L\text{-}V} \tag{11.12}$$

They allow one to compute the theoretical δD and $\delta^{18}O$ values of the separated vapor and liquid during the evolution of the process. Further theoretical models involve boiling of diluted waters, absorption of maximum enthalpy steam in local groundwater (Giggenbach and Stewart, 1982), and condensation (Brombach et al., 2000). Theoretical values can be compared with observed values in a δD vs. $\delta^{18}O$ plot (Fig. 11.2).

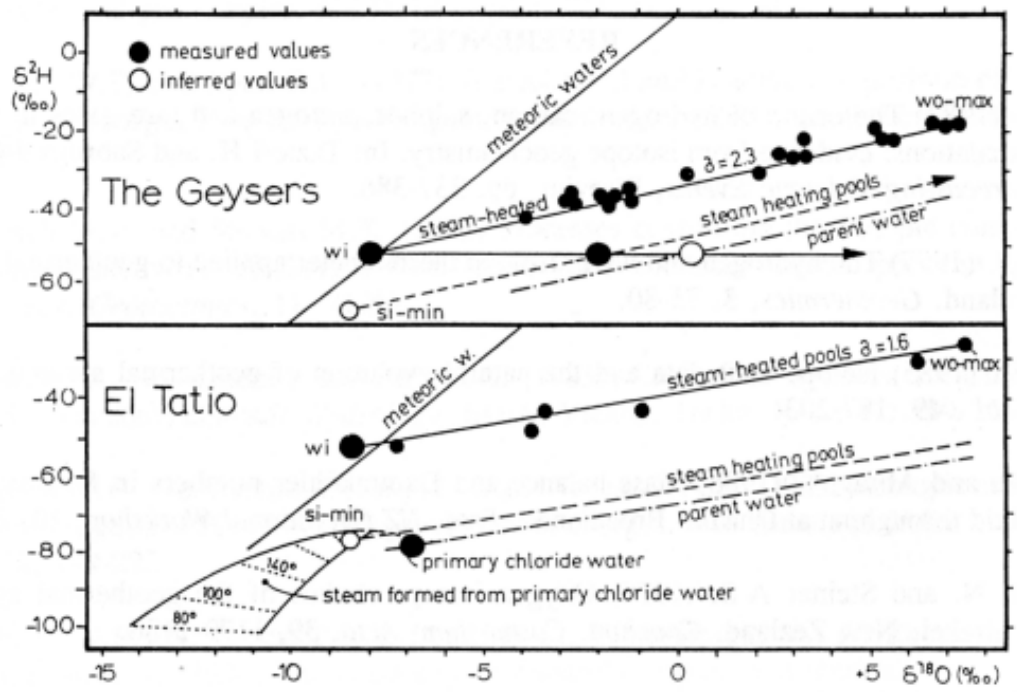


Fig. 11.3. δD vs. $\delta^{18}O$ plot showing the non-equilibrium surface evaporation effects of steam-heated pools (from Giggenbach and Stewart, 1982).

The isotope composition of acid sulfate waters of steam-heated pools (which are produced through input of steam in very shallow or stagnant surface waters) reflects instead non-equilibrium surface evaporation (Giggenbach and Stewart, 1982). This process brings about dramatic enrichments in heavy isotopes, with respect to local meteoric waters (Fig. 11.3). The slope of the straight line connecting data poins from steam-heated pools is given by:

$$\sigma_P = \frac{\delta D_{si} - \delta D_{wi} + \varepsilon_D}{\delta^{18}O_{si} - \delta^{18}O_{wi} + \varepsilon_{^{18}O}} \tag{11.13}$$

where the subscripts si and wi refer to the steam entering the pool and to local groundwater, respectively, whereas $\varepsilon_i$ is the average kinetic isotope fractionation factor,

which is close to 50 ‰ for D and 16‰ for $^{18}O$, according to Giggenbach and Stewart (1982).
In the previous discussion it was implicitly assumed that analytical δD and $\delta^{18}O$ values of water vapor are fully representative of its isotopic composition at any P,T condition. However, this is not always true.

Chiodini et al. (2000) showed that the $\Delta^{18}O_{CO2\text{-}H2O}$ for geothermal and volcanic vapors is very close to the theoretical oxygen isotope fractionation factor between $CO_{2(g)}$ and $H_2O_{(g)}$ at outlet temperatures, suggesting that these two species are in isotopic equilibrium at outlet conditions (Fig. 11.4).

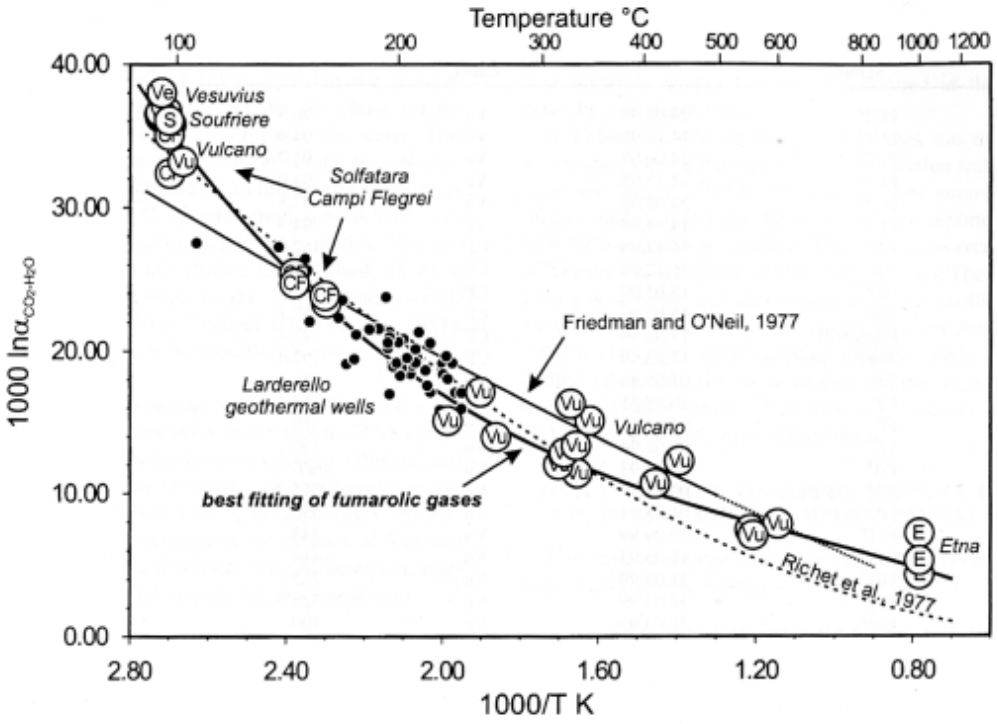


Fig. 11.4. The $\Delta^{18}O_{CO2\text{-}H2O}$ of vapors discharged from Italian volcanic and hydrothermal areas is plotted against outlet temperatures. Theoretical equilibrium fractionation factors according to Friedman and O'Neil (1977) and Richet et al. (1977) are shown for comparison.

This implies that the oxygen isotope exchange between $CO_{2(g)}$ and $H_2O_{(g)}$ is a quick process. Therefore the correct interpretation of the $\delta^{18}O$ values of geothermal vapors demands to correct the analytical $\delta^{18}O$ values of $H_2O$ for the isotopic exchange with $CO_2$. Obviously, this correction is important for $CO_2$-rich vapors. The initial $\delta^{18}O$ value of water, $\delta^{18}O_{H2O,i}$ (i.e., in the geothermal reservoir), is calculated from the final $\delta^{18}O$ value of water, $\delta^{18}O_{H2O,f}$ (i.e., at the surface discharge), combining a simple oxygen isotope mass balance with the oxygen isotope fractionation factors under both initial and final conditions, thus obtaining the following relationship:

$$\delta^{18}O_{H_2O,i} = \delta^{18}O_{H_2O,f} - \left[\frac{2 \cdot X_{CO_2}}{1 + X_{CO_2}} \cdot \left(1000 \cdot \ln \alpha_i - 1000 \cdot \ln \alpha_f\right)\right], \qquad (11.14)$$

where $\alpha$ identifies the oxygen isotope fractionation factor between $CO_{2(g)}$ and $H_2O_{(g)}$, whose temperature dependence is satisfactorily explained by this third order polynomial equation (Chiodini et al., 2000):

$$1000 \cdot \ln \alpha = -5.7232 + 20.303 \frac{10^3}{T} - 11.977 \frac{10^6}{T^2} + 3.7432 \frac{10^9}{T^3}, \qquad (11.15)$$

that closely fit the theoretical fractionation factors of Richet et al. (1977) below 400°C and those of Friedman and O'Neil (1977) at higher temperatures, up to 1000°C.

More information is needed to evaluate the possible fractionation effects between $H_2O$ and other H-species, mainly $H_2S$.

## 12. How much water and heat can be extracted from a geothermal system ?

At this point the reader has probably realized that there are many geochemical techniques, more or less sophisticated, to estimate the temperature and other intensive properties of fluids circulating in geothermal systems. The title of this section is, instead, a question which is difficult to be answered, but of crucial importance in the development of geothermal exploration-exploitation programs. Again, geochemistry can play a fundamental role.

### *12.1. Total natural discharge based on Cl balance*

It is common practice to estimate the total natural discharge (the fluxes of water and heat) of geothermal systems, by measuring the flowrate and chloride content of all the thermal springs present in the surveyed area (Ellis and Mahon, 1977). The natural heat discharge represents the minimum recoverable energy flow from the geothermal system, assuming that the system is close to steady state conditions, i.e., that there is a sort of balance between discharge and recharge.

First the chloride content and enthalpy of the parent geothermal liquid, $Cl_T$ and $H_T$, respectively, are reconstructed, by means of the enthalpy- chloride plot and other geothermometric techniques. The following step is the calculation of the flow of thermal component, $q_T$, contributed by each discharge of flowrate $q_M$:

$$q_T = q_M \, x, \tag{12.1}$$

where the fraction of the thermal component x is given by Eqn. (6.1):

$$x = \frac{Cl_M - Cl_F}{Cl_T - Cl_F} \tag{12.2}$$

which reduces to $x = Cl_M / Cl_T$, if $Cl_M >> Cl_F$. The total natural fluxes of water, $Q_T$, and heat, $\Phi_T$, are then obtained by means of the simple equations:

$$Q_T = \Sigma \, q_T \tag{12.3}$$

$$\Phi_T = H_T \, Q_T. \tag{12.4}$$

In general the results of these calculations underestimate the potential of the geothermal systems, and this is particularly true for concealed systems.

### *12.2. The distribution of leakage indicators in groundwaters*

A completely different approach was suggested by Tonani (1970), largely based on mining exploration strategy and on the transport of ammonia and boric acid in the vapor phase, which were described and explained by him at Larderello and The Geysers. Tonani proposed to study the distribution of these substances, which he called leakage indicators, in groundwaters, in order to detect processes of steam leakage from deep-seated geothermal systems and determine thereby their presence and extension. After application of this methodology to many systems throughout the world, it turned out that (i) ammonia is often controlled by fortuitous leaching of organic-rich sediments and (ii) boric acid anomalies caused by geothermal steam input are sometimes detectable in steam-heated pools but never in groundwaters.

On the other hand, a good correspondence was observed, in Tyrrhenian Central Italy (Marini and Chiodini, 1994; Chiodini et al., 1995c), between (i) surface areas of

high $CO_2$ fluxes, outlined on the basis of $P_{CO2}$ distribution in shallow waters and (ii) areal extension of geothermal reservoirs of high enthalpy (Monte Amiata and Latera), medium enthalpy (Torre Alfina) and low enthalpy (Viterbo). These geothermal reservoirs, which are mainly made up of permeable carbonate rocks and are covered by impervious fine grained clastic rocks, act as traps of deeply originated $CO_2$ (Fig. 12.1). Gases rich in $CO_2$ are released towards the surface even through the relatively impervious layers of the cover rocks: these gases dissolve in part in shallow waters, and in part reach the atmosphere mainly through diffuse soil degassing. Therefore, high $P_{CO2}$ values in groundwaters are effective indicators of the presence of geothermal reservoirs at depth and can be used to map their extension.

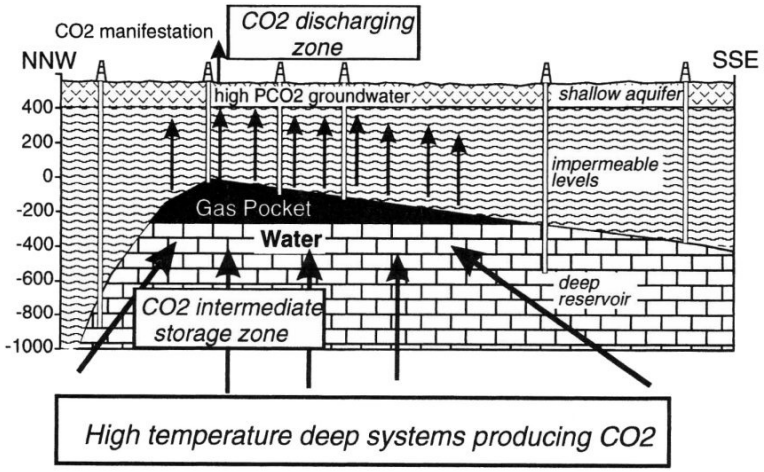


Figura 12.1. Conceptual geochemical model of the Torre Alfina geothermal field (from Barelli et al., 1978).

### *12.3. Diffuse $CO_2$ degassing through soil*

Both laboratory tests and field surveys have proven that the best method to measure the soil $CO_2$ flux in geothermal and volcanic areas is the accumulation chamber method, which allows one to obtain reliable values of $\varphi CO_2$ in the range 0.2 to over 10,000 g $m^{-2}$ $d^{-1}$, i.e., from the low $\varphi CO_2$ values sustained by decay of organic matter to the high $\varphi CO_2$ values typical of steaming grounds (Chiodini et al., 1998).

The average run time for a $\varphi CO_2$ measurement is about 1 minute. Thus detailed maps of $\varphi CO_2$ can be obtained in a relatively short time. The $\varphi CO_2$ is largely variable in space as shown by these maps that give prominence to active faults and fractures acting as uprising routes of deep $CO_2$-rich geothermal or magmatic gases. Maps of $\varphi CO_2$ can be used to estimate the total diffuse $CO_2$ output from the entire system provided that a sufficiently large numbers of measurements are performed. Moreover these maps allow one to select restricted areas where repeated measurements of $\varphi CO_2$ can be carried out to investigate the temporal evolution of the system.

Recent measurements of diffuse $CO_2$ degassing through soil in the fumarolic areas of the Lakki plain, Nisyros Island, Greece (Brombach, 2000; Brombach et al., 2001, 2002), and Solfatara di Pozzuoli, Campi Flegrei, Italy (Chiodini et al., 2001a), coupled with temperature measurements at 10 cm depth, have shown that there is a good correspondence between high $\varphi CO_2$ and high temperature areas (Fig. 12.2).

This suggests that both upflow of hot fluids from the underlying boiling hydrothermal reservoir and steam condensation in the subsoil are responsible for the high $\varphi CO_2$ values and the elevated soil temperatures. At Nisyros, a total hydrothermal

$CO_2$ flux of ~ 68 t $d^{-1}$ was calculated for the surveyed area of 1.3 $km^2$ in 1997. Assuming that the diffuse gas is derived from hydrothermal fluids having the same chemical composition of those discharged by nearby fumaroles and that their chemistry is not biased by steam condensation, it turns out that this hydrothermal $CO_2$ is accompanied by a flux of steam of 2200 t $d^{-1}$, corresponding to a heat flux of ~ 58 MW. Following the same approach, a heat flux of 88 MW was obtained for the Solfatara of Pozzuoli (Chiodini et al., 2001a), where the diffuse degassing area is ~0.5 $km^2$, the hydrothermal $CO_2$ flux is 1520 t $d^{-1}$ and the steam flux is 3350 t $d^{-1}$.

Both at Nisyros and Solfatara, the heat flux was also computed from thermal gradient measurements in the soil (0-40 cm), assuming a reasonable value for the thermal conductivity of soil. The fluxes of thermal energy computed from $\varphi CO_2$ data agree with those obtained from thermal gradient measurements, supporting the hypothesised conceptual model.

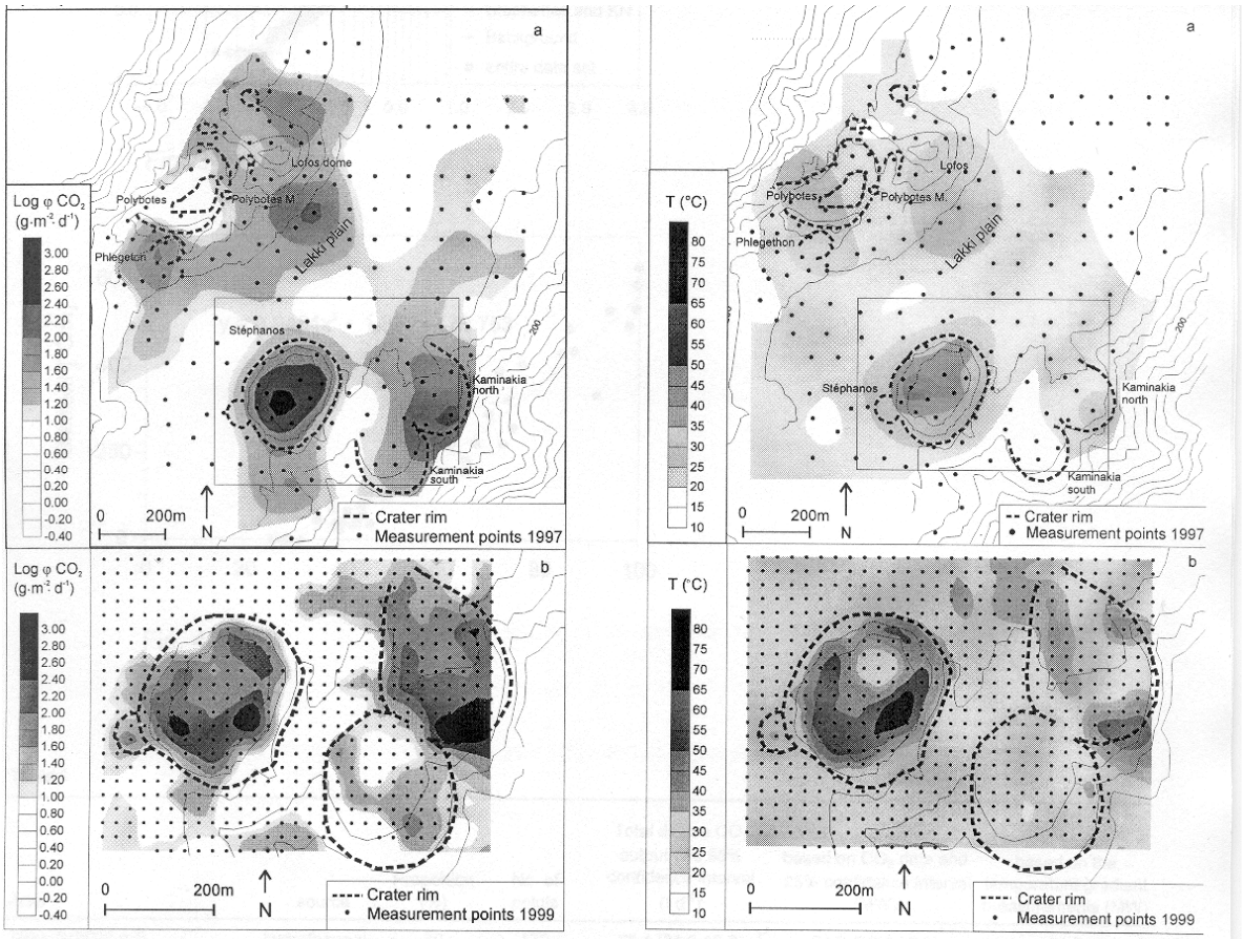


Fig. 12.2 Contour maps of log $\varphi CO_2$ (left) and temperature at 10 cm depth (right) for the southern part of the Lakki plain, Nisyros Island, Greece (from Brombach, 2000; Brombach et al., 2001)

These first results obtained at Nisyros and Solfatara show that the direct expulsion of hydrothermal gases from relatively small diffuse degassing areas is the main process through which these volcanic-hydrothermal systems dissipate thermal energy. $CO_2$ flux measurements constitute, therefore, a powerful tool to quantify these phenomena, which are of upmost importance in geothermal exploration.

**Table 1.** Chemical composition of selected geothermal and crater lake waters (concentrations in mg/kg, temperature in °C).

## Na-Cl waters

| Place | Code | T | pH | Na | K | Mg | Ca | Cl | $SO_4$ | $HCO_3$ | Ref |
|---|---|---|---|---|---|---|---|---|---|---|---|
| Ngawha NG-9, NZ | NG | 230 | 7.70 | 893 | 79 | 0.11 | 3 | 1260 | 18 | 185 | a |
| Jubilee Pool, NZ | NG | 56 | 7.20 | 842 | 72 | 1.6 | 9 | 1180 | 174 | 393 | a |
| Wairakei WK66, NZ | WK | 240 | 8.50 | 995 | 142 | 0.04 | 17 | 1675 | 30 | 0 | a |
| Champagne pool, NZ | WK | 99 | 8.00 | 1070 | 102 | 0.4 | 26 | 1770 | 26 | 76 | c |
| Broadlands BR-11, NZ | BR | 260 | 7.40 | 675 | 130 | 0.011 | 1 | 964 | 41 | 376 | a |
| Ohaki pool, NZ | BR | 98 | 7.10 | 860 | 82 | 0.1 | 3 | 1060 | 100 | 680 | c |
| Miravalles 10, C.Rica | MV | 250 | 7.80 | 1750 | 216 | 0.11 | 59 | 2910 | 40 | 27 | a |
| Sal.Bagaces, C.Rica | MV | 74 | 8.60 | 2063 | 85 | 6.6 | 33 | 2700 | 102 | 739 | a |
| Zunil ZQ-3, Guatemala | ZU | 295 | 8.10 | 563 | 139 | 0.007 | 9 | 1091 | 19 | 31 | a |
| Cerro Prieto 19A, Mexico | CP | 280 | 7.30 | 5600 | 1260 | 0.27 | 333 | 10500 | 14 | 40 | c |
| Spring N29, Mexico | CP | 80 | 7.60 | 5120 | 664 | 4.6 | 357 | 8790 | 31 | 65 | c |
| Tongonan, Philippines | TO | 330 | 7.00 | 3580 | 1090 | 0.2 | 128 | 6780 | 16 | 12 | c |
| Banati spr, Philippines | TO | 98 | 8.30 | 1990 | 210 | 0.4 | 86 | 3400 | 74 | 7 | c |
| Morere spring, NZ | MO | 47 | 7.00 | 6690 | 84 | 79 | 2750 | 15670 | nd | 28 | a |
| Salton Sea well, USA | SS | 330 | 5.20 | 38400 | 13400 | 10 | 22010 | 118400 | 4 | 140 | c |
| Seawater | SW | 4 | 7.80 | 10760 | 390 | 1290 | 410 | 19340 | 2710 | 140 | a |
| Araro spring, Mexico | AR | 92 | 8.10 | 705 | 50 | 0.3 | 30 | 1010 | 135 | 63 | b |
| Paraso spring, Solomon Is. | PR | 56 | 5.60 | 1210 | 178 | 26.6 | 289 | 2340 | 205 | 6 | b |
| Yasur spring, Vanuatu | YA | 99 | 8.80 | 1270 | 73 | 0.3 | 17 | 1690 | 280 | 75 | b |
| Maui well, NZ | MA | 130 | 7.50 | 7880 | 440 | 48 | 190 | 12600 | 18 | 630 | b |
| La Castalia spring, Guatemala | CA | 92 | 8.43 | 446 | 25 | 0.093 | 8.79 | 549 | 143 | 144 | d |
| La Cimarrona spring, Guatemala | CI | 94 | 8.43 | 546 | 71 | 0.007 | 3.14 | 746 | 166 | 137 | d |
| Acqui Terme spring, Italy | AT | 70 | 8.04 | 665 | 14 | 0.16 | 135 | 1130 | 230 | 23 | e |
| Plymouth spring, Montserrat | PL | 90 | 6.60 | 7880 | 1030 | 302 | 2510 | 18220 | 161 | 128 | f |
| Mofete 2 well, Italy | MF | 310 | 6.34 | 4900 | 1140 | 0.5 | 465 | 9790 | 6 | 39 | g |
| Abbe,Gibuti | AB | 99 | 7.65 | 989 | 29 | 0.18 | 240 | 1702 | 341 | 20 | h |

**Na-$HCO_3$ waters**

| Place | Code | T | pH | Na | K | Mg | Ca | Cl | $SO_4$ | $HCO_3$ | Ref |
|---|---|---|---|---|---|---|---|---|---|---|---|
| Waitangi, NZ | WA | 49 | 7.30 | 285 | 24 | 9 | 17 | 364 | 49 | 202 | a |
| Omapere, NZ | NG | 30 | 6.90 | 62 | 9 | 10 | 37 | 25 | nd | 295 | a |
| Golden Spr., NZ | GS | 45 | 7.00 | 224 | 20 | 7 | 11 | 51 | 8 | 670 | a |
| Radkersburg, Austria | RA | 72 | 8.90 | 2215 | 182 | 47 | 3 | 264 | 398 | 4130 | a |
| Te Aroha, NZ | TE | 79 | 8.10 | 2920 | 67 | 4 | 7 | 540 | 1260 | 6830 | a |
| Zunil spring, Guatemala | ZU | 95 | 7.00 | 384 | 32 | 39 | 17 | 172 | 234 | 635 | a |
| Fang spring, Thailand | FN | 99 | 9.00 | 122 | 8 | 0.10 | 1 | 27 | 22 | 145 | b |
| Acqui Terme spring, Italy | AT | 32 | 8.62 | 142 | 2 | 0.14 | 7.3 | 81 | 78 | 127 | e |
| Gotthard tunnel, Switzerland | GT | 32 | 9.70 | 60 | 0 | 0.005 | 1.86 | 12 | 52 | 62 | j |
| Ban Nong Khrok, Thailand | BN | 72 | 7.85 | 177 | 11 | 3.40 | 22.0 | 4 | 21 | 519 | i |
| Pong Kum | PK | 96 | 8.60 | 131 | 9 | 0.13 | 3.01 | 11 | 25 | 299 | i |
| San Kampaeng | SK | 98 | 9.20 | 159 | 14 | 0.026 | 0.68 | 28 | 45 | 305 | i |
| Tepanon, Thailand | TP | 99 | 8.90 | 117 | 5 | 0.004 | 1.68 | 10 | 13 | 238 | i |
| Nam Mae Mon, Thailand | NM | 81 | 8.45 | 108 | 10 | 1.7 | 16.4 | 14 | 33 | 293 | i |
| Ban Huai Mak Fai, Thailand | BH | 75 | 8.30 | 92 | 10 | 1.00 | 9.82 | 4 | 24 | 220 | i |
| Sop Pong, Thailand | SP | 98 | 8.85 | 106 | 7 | 0.013 | 0.88 | 11 | 22 | 220 | i |

**Na-$HCO_3$ waters**

| Place | Code | T | pH | Na | K | Mg | Ca | Cl | $SO_4$ | $HCO_3$ | Ref |
|---|---|---|---|---|---|---|---|---|---|---|---|
| Ban Pong Nam Ron, Thailand | BP | 97 | 8.90 | 143 | 8 | 0.018 | 1.76 | 20 | 48 | 238 | i |
| Ban Mae Chok Nai, Thailand | BM | 62 | 7.45 | 168 | 18 | 0.85 | 24.0 | 15 | 53 | 433 | i |
| Ban Ban Chen, Thailand | BB | 52 | 7.20 | 143 | 12 | 0.77 | 24.0 | 3 | 2 | 427 | i |
| Pa Pae, Thailand | PP | 99 | 9.20 | 90 | 6 | 0.005 | 1.46 | 8 | 19 | 177 | i |
| Fang, Thailand | FN | 99 | 9.20 | 124 | 8 | 0.018 | 1.38 | 19 | 25 | 220 | i |
| Tekke Hamam spring, KZ, Turkey | KZ | 83 | 7.59 | 1070 | 101 | 0.20 | 0.71 | 91 | 1040 | 1580 | k |
| Kizildere well, Turkey | KZ | 210 | 5.94 | 1070 | 121 | 0.039 | 0.17 | 90 | 535 | 2200 | k |

## Acid waters

| Place | Code | T | pH | Na | K | Mg | Ca | Cl | $SO_4$ | $HCO_3$ | Ref |
|---|---|---|---|---|---|---|---|---|---|---|---|
| El Chichon | CH | 56 | 0.56 | 607 | 232 | 424 | 2110 | 24030 | 3550 | nd | l |
| Kawa Idjen,Indonesia | KI | 60 | 0.60 | 1030 | 1020 | 680 | 770 | 21800 | 62400 | nd | a |
| Kawah Putih | KP | 26 | 0.62 | 65 | 41 | 48 | 78 | 6700 | 11965 | nd | m |
| Poas | PO | 60 | 0.00 | 500 | 234 | 536 | 2400 | 31300 | 64800 | nd | n |
| Popocatepetl | PP | 65 | 1.50 | 1835 | 329 | 2520 | 781 | 14200 | 23660 | nd | o |
| Mt Ruapehu, NZ | RU | 38 | 1.20 | 1120 | 170 | 1750 | 1380 | 13240 | 14700 | nd | a |
| Rincon de la Vieja | RV | 38 | 0.20 | 1630 | 920 | 1450 | 1250 | 30700 | 51300 | nd | p |
| Tamagawa, JP | TA | 98 | 1.30 | 38 | 30 | 35 | 95 | 2970 | 2300 | nd | a |
| White Island,NZ | WI | 98 | 0.60 | 5910 | 635 | 3800 | 3150 | 38700 | 4870 | nd | a |
| Yakeyama | YA | 30 | 2.20 | 2 | 2 | 1.2 | 2.2 | 1 | 378 | nd | q |
| Yugama | YU | 33 | 1.00 | 67 | 30 | 78 | 466 | 2620 | 3510 | nd | q |

---

**References** a: Giggenbach (1988); b: Giggenbach (1991a); c: Henley et al. (1984); d: Marini et al. (1998); e: Marini et al. (2000); f: Chiodini et al. (1996); g: Balducci et al. (1985); h: Geotermica Italiana (1983a); i: Geotermica Italiana (1983b); j: Pastorelli et al. (2001); k: Guidi et al. (1990a); l: Casadevall et al. (1984); m: Sriwana et al. (2000); n: Brantley et al (1987); o: Armienta et al. (2000); p: Kempter and Rowe (2000) ; q: Takano and Watanuki (1990).

**Table 2**. Aqueous species considered in speciation computations.

| | | | | | | | |
|---|---|---|---|---|---|---|---|
| $H_2O$ | $Al^{3+}$ | $Ca^{2+}$ | $H^+$ | $HCO_3^-$ | $K^+$ | $Mg^{2+}$ | $Na^+$ |
| $Cl^-$ | $Al(OH)_2^+$ | $CaCO_{3(aq)}$ | $HCl_{(aq)}$ | $CO_{2(aq)}$ | $KCl_{(aq)}$ | $MgCO_{3(aq)}$ | $NaAlO_{2(aq)}$ |
| $F^-$ | $AlO_2^-$ | $CaCl^+$ | $HF_{(aq)}$ | $CO_3^{2-}$ | $KHSO4_{(aq)}$ | $MgCl^+$ | $NaCO_3^-$ |
| $OH^-$ | $HAlO_{2(aq)}$ | $CaCl_{2(aq)}$ | $HF_2^-$ | | $KSO_4$- | $MgF^+$ | $NaCl_{(aq)}$ |
| $SO_4^{2-}$ | | $CaF^+$ | $HSO_4^-$ | | | $MgHCO_3^+$ | $NaF_{(aq)}$ |
| $SiO_{2(aq)}$ | | $CaHCO_3^+$ | $HSiO_3^-$ | | | $MgSO_{4(aq)}$ | $NaHCO_{3(aq)}$ |
| | | $CaSO_{4(aq)}$ | | | | | $NaHSiO_{3(aq)}$ |
| | | | | | | | $NaOH_{(aq)}$ |

**Table 3**. Dependence of total concentrations and total concentration ratios of compatible constituents in hydrothermal aqueous solutions on temperature, $P_{CO2}$ and salinity. The aqueous solution is assumed to be in equilibrium with albite, K-feldspar, either a Ca-Al-silicate and/or calcite (depending on the $P_{CO2}$), clinochlore, muscovite, quartz, anhydrite, and fluorite (from Chiodini et al. 1991a).

$$\log m_{Na} = -0.527 + 0.982 \log \Sigma eq + 78.9/T + 0.0119 \log P_{CO2}$$

$$\log m_{K} = +0.458 + 0.944 \log \Sigma eq - 1014/T + 0.0346 \log P_{CO2}$$

$$\log m_{Ca} = -1.116 + 1.302 \log \Sigma eq - 0.390 \log P_{CO2} - 443/T$$

$$\log m_{Mg} = -8.188 + 0.912 \log \Sigma eq + 2156/T + 0.356 \log P_{CO2}$$

$$\log m_{HCO_3} = -10.004 + 0.904 \log P_{CO2} + 3223/T - 0.489 \log \Sigma eq$$

$$\log m_{SO_4} = -12.503 + 4604/T + 0.501 \log P_{CO2} - 0.626 \log \Sigma eq$$

$$\log m_{F} = -5.069 + 798/T + 0.127 \log P_{CO2} - 0.0886 \log \Sigma eq$$

$$pH = +1.757 - 0.822 \log \Sigma eq + 1846/T - 0.0171 \log P_{CO2}$$

$$\log (m_{Na}/m_{K}) = -0.985 + 1093/T + 0.0384 \log \Sigma eq - 0.0228 \log P_{CO2}$$

$$\log (m_{K}2/m_{Mg}) = +9.104 - 4184/T + 0.975 \log \Sigma eq - 0.286 \log P_{CO2}$$

$$\log (m_{SO_4}/m_{F}2) = -2.364 + 3007/T - 0.449 \log \Sigma eq + 0.247 \log P_{CO2}$$

$$\log (m_{K}2/m_{Ca}) = +2.031 + 0.459 \log P_{CO2} + 0.585 \log \Sigma eq - 1584/T$$

$$\log (m_{Ca}/m_{Mg}) = +7.073 - 0.746 \log P_{CO2} - 2600/T + 0.390 \log \Sigma eq$$

$$\log (m_{HCO_3}2/m_{SO4}) = -7.506 + 1.307 \log P_{CO2} + 1843/T - 0.352 \log \Sigma eq$$

$$\log (m_{Na}2/m_{Mg}) = +7.134 + 1.052 \log \Sigma eq - 1999/T - 0.332 \log P_{CO2}$$

$$\log (m_{Na}2/m_{Ca}) = +0.061 + 0.662 \log \Sigma eq + 0.414 \log P_{CO2} + 601/T$$

## References


Anderson G.M., Crerar D.A. (1993) *Thermodynamics in Geochemistry. The Equilibrium Model*. Oxford University Press. New York, 588 p.

Aguilera E., Chiodini G., Cioni R., Guidi M., Marini L., Raco B. (2000). Water chemistry of Lake Quilotoa (Ecuador) and assessment of natural hazards. *J. Volcanol. Geotherm. Res*. **97**, 271-285

Aguilera E., Cioni R., Gherardi F., Magro G., Marini L. (2004) Geochemistry and isotope characteristics of the Chachimbiro geothermal fluids (Ecuador) *Geothermics* (in press).

Antrodicchia E., Cioni R., Chiodini G., Gagliardi R., Marini L. (1985). Geochemical temperatures of the thermal waters of Phlegraean Fields (Naples, Italy). *Geotherm. Res. Counc. Trans*. **9**, 287-292.

Armienta M.A., De la Cruz-Reyna S., Macías J.L. (2000) Chemical characteristics of the crater lakes of Popocatépetl, El Chichón, and Nevado de Toluca volcanoes, Mexico. In: J.C. Varekamp and G.L. Rowe Jr. (Editors), *Crater Lakes. J. Volcanol. Geotherm. Res.* **97**, 105-125.

Arnórsson S. (1987) Gas chemistry of the Krísuvík geothermal field, Iceland, with special reference to evaluation of steam condensation in upflow zones. *Jökull* **37**, 32-47.

Arnórsson S. (1990) Gas chemistry of geothermal systems. In *Geochemistry of Gaseous Elements and Compounds* (S.S. Augustithis Ed.), Theophrastus, Athens, 187-222.

Arnórsson S. and Gunnlaugsson E. (1985) New gas geothermometers for geothermal exploration - Calibration and application. *Geochim. Cosmochim. Acta* **49**, 1307-1325.

Arnórsson S., Björnsson S., Muna Z.W., Bwire-Ojiambo S. (1990) The use of gas chemistry to evaluate boiling processes and initial steam fractions in geothermal reservoirs with an example from the Olkaria field, Kenya. *Geothermics* **19**, 497-514.

Arnórsson S., Gunnlaugsson E., Svavarsson (1983) The chemistry of geothermal waters in Iceland. III. Chemical geothermometry in geothermal investigations. *Geochim Cosmochim Acta* **47**, 567-577

Balducci S., Chelini W., Ottonello G. (1985) *Definizione degli equilibri idrotermali nel campo geotermico di Mofete.* Agip S.p.A. - ESGE Report 411.

Barbier E. (1997) Nature and technology of geothermal energy: a review. *Renewable and Sustainable Energy Reviews*, **1**, 1-69.

Barelli A., Celati R., Manetti G. (1978) Gas-water interface rise during early exploitation tests in Alfina geothermal field (northern Latium, Italy) *Geothermics*, **6**, 199-208.

Bertrami R., Cioni R., Corazza E., D'Amore F., Marini L. (1985). Carbon monoxide in geothermal gases. Reservoir temperature calculations at Larderello (Italy). *Geotherm. Res. Counc. Trans*. **9**, 299-303.

Bischoff J.L. and Pitzer K.S. (1989) Liquid-vapor relations for the system NaCl-$H_2O$: summary of the P-T-X surface from 300°C to 500°C. *Am. J. Sci.* **289**, 1217-1248.

Bonham H.R. (1986) Models for volcanic-hosted epithermal precious metal deposits:a review. *Proc, 5$^{th}$ Int, Volcanology Cong*., Auckland, NZ, 13-17.

Bowers T.S., Jackson K.J., Helgeson H.C. (1984). *Equilibrium activity diagrams for coexisting minerals and aqueous solutions at pressures and temperatures to 5 kb and 600 °C*. Springer, 397 pp.

Brantley S.L., Borgia A., Rowe G., Fernandez J.F., Reynolds J.R. (1987) Poás volcano acts as a condenser for acid metal-rich brine. *Nature* **330**, 470-472.

Brombach T. (2000) *Fluid geochemistry of hydrothermal systems in volcanic island arcs: Guadeloupe (Lesser Antilles) and Nisyros (Greece).* Ph. D. Thesis. Université de Lausanne.

Brombach T., Marini L., Hunziker J.C. (2000) Geochemistry of the thermal springs and fumaroles of Basse-Terre island, Guadaloupe, Lesser Antilles. *Bull. Volcanol* **61**, 477-490.

Brombach T., Hunziker J.C., Chiodini G., Cardellini C., Marini L. (2001) Soil diffuse degassing and thermal energy fluxes from the southern Lakki plain, Nisyros (Greece). *Geophysical Research Letters*, **28**, 69-72.

Brombach T., Caliro S., Cardellini C., Chiodini G., Marini L., Dietrich V. (2002) Geochemical indicators of possible ongoing volcanic unrest at Nisyros Island (Greece). *Geophysical Research Letters*, **29** (16), 6-1/6-4.

Brombach T., Caliro S., Chiodini G., Fiebig J., Hunziker J.C., Raco B. (2003) Geochemical evidence for mixing of magmatic fluids with seawater, Nisyros hydrothermal system, Greece. *Bull. Volcanol.*, **65**, 505-516.

Browne P.R.L. (1970) Hydrothermal alteration as an aid in investigating geothermal fields. *Geothermics,* Spec. Issue **2**, 564-570.

Browne P.R.L. (1977) *Hydrothermal alteration in active geothermal fields*. N. Z. Geol. Surv., unpublished report M58, 57 pp.

Browne P.R.L. (1982) Mapping of geothermal discharge features. In *Introduction to geothermal prospecting* (M.P. Hochstein Ed.) Univ. of Auckland Publ., 67-69.

Casadevall T.J., De La Cruz-Reyna S., Rose W.I., Bagley S., Finnegan D.L., Zoller W.H. (1984) Crater lake and post-eruption hydrothermal activity, El Chichón volcano, Mexico. *J. Volcanol. Geotherm. Res*. **23**, 169-191.

Chan S.H. (1989) A review on solubility and polymerization of silica. *Geothermics* **18**, 49-56.

Chen C.T. and Marshall W.L. (1982) Amorphous silica solubilities – IV. Behavior in pure water and aqueous sodium chloride, sodium sulfate, magnesium chloride, magnesium sulfate solutions up to 350°C. *Geochim. Cosmochim. Acta* **46**, 279-287.

Chiodini G. (1994) Temperature, pressure and redox conditions governing the composition of the cold $CO_2$ gases discharged in north Latium (Central Italy). *Appl. Geochem*. **9**, 287-295.

Chiodini G. and Cioni R. (1989) Gas geobarometry for hydrothermal systems and its application to some Italian geothermal areas. *Appl. Geochem*. **4**, 465-472.

Chiodini G and Marini L (1998) Hydrothermal gas equilibria: The $H_2O$-$H_2$-$CO_2$-CO-$CH_4$ system. *Geochim. Cosmochim. Acta* **62**, 2673-2687.

Chiodini, G., Cioni, R., Guidi, M., Marini, L. (1991a) Chemical geothermometry and geobarometry in hydrothermal aqueous solutions: a theoretical investigation based on a mineral-solution equilibrium model. *Geochim. Cosmochim. Acta* **55**, 2709-2727.

Chiodini G., Cioni R., Raco B., Scandiffio G. (1991b) Carbonyl sulphide (COS) in geothermal fluids: an example from the Larderello field (Italy). *Geothermics* **20**, 319-327.

Chiodini G., Cioni R., Guidi M., Marini L., Raco B., Taddeucci G. (1992) Gas geobarometry in boiling hydrothermal systems: a possible tool to evaluate the hazard of hydrothermal explosions. *Acta Vulcanologica, Marinelli Vol.* **2**, 99-107.

Chiodini G., Cioni R., Leonis C., Marini L., Raco B. (1993a). Fluid geochemistry of Nisyros island, Dodecanese, Greece. *J. Volcanol. Geotherm. Res.*, **56**, 95-112.

Chiodini G., Cioni R., Marini L. (1993b) Reactions governing the chemistry of crater fumaroles from Vulcano Island, Italy, and implications for volcanic surveillance. *Appl. Geochem.* **8**, 357-371.

Chiodini G., Cioni R., Marini L., Panichi C. (1995a) Origin of the fumarolic fluids of Vulcano Island, Italy, and implications for volcanic surveillance. *Bull. Volcanol.* **57**, 99-110.

Chiodini G., Frondini F., Marini L. (1995b) Theoretical geothermometers and geobarometers for aqueous solutions coming from hydrothermal systems of medium-low temperature hosted into carbonate-evaporite rocks. Application to the thermal springs of the Etruscan Swell, Italy. *Appl. Geochem.* **10**, 337-346.

Chiodini G., Frondini F., Ponziani F. (1995c) Deep structures and carbon dioxide degassing in Central Italy. *Geothermics* **24**, 81-94

Chiodini G., Cioni R., Frullani A., Guidi M., Marini L., Prati F., Raco B. (1996). Fluid geochemistry of Montserrat Island, West Indies. *Bull. Volcanol.* **58**, 380-392.

Chiodini G., Cioni R., Guidi M., Raco B., Marini L. (1998) Soil $CO_2$ flux measurements in volcanic and geothermal areas. *Appl. Geochem.* **13**, 543-552.

Chiodini G., Allard P., Caliro S., Parello F. (2000) $^{18}O$ exchange between steam and carbon dioxide in volcanic and hydrothermal gases: isotopic and genetic implications. *Geochim. Cosmochim. Acta* **64**, 2479-2488

Chiodini G., Frondini F., Cardellini C., Granieri D. , Marini L., Ventura G. (2001a) $CO_2$ degassing and energy release at Solfatara volcano, Campi Flegrei, Italy. *Journal of Geophysical Research,* **106**, 16213-16222

Chiodini G., Marini L., Russo M. (2001b). Geochemical evidence for the existence of a high-temperature hydrothermal brines at Vesuvius volcano (Italy). *Geochimica et Cosmochimica Acta,* **65**, 2129-2147.

Christenson B.W. and Wood C.P. (1993) Evolution of a vent-hosted hydrothermal system beneath Ruapehu Crater Lake, New Zealand. *Bull. Volcanol*. **55**, 547-565.

Cioni R., Fanelli G., Guidi M., Kinyariro J.K., Marini L. (1992). Lake Bogoria hot springs (Kenya): geochemical features and geothermal implications. *J. Volcanol. Geotherm. Res.* **50**, 231-246.

Craig H. (1963) The isotopic geochemistry of water and carbon in geothermal areas. In *Nuclear geology in geothermal areas* (E. Tongiorgi, Ed.), Spoleto, 17-53.

D'Amore F. (1991) Gas geochemistry as a link between geothermal exploration and exploitation. In *Application of Geochemistry in Geothermal Reservoir Development*. (F. D'Amore, co-ordinator), UNITAR, 93-117.

D'Amore F. and Celati R. (1983) Methodology for calculating steam quality in geothermal reservoir. *Geothermics* **12**, 129-140.

D'Amore F. and Gianelli G. (1984) Mineral assemblages and oxygen and sulfur fugacities in natural water-rock interaction processes. *Geochim. Cosmochim. Acta* **48**, 847-857.

D'Amore F. and Nuti S. (1977) Notes on the chemistry of geothermal gases. *Geothermics* **6**, 39-45.

D'Amore F. and Panichi C. (1980) Evaluation of deep temperature of hydrothermal systems by a new gas-geothermometer. *Geochim. Cosmochim. Acta* **44**, 549-556.

Davis JC (1986) *Statistics and data analysis in geology*. 2nd Ed. Wiley.

Delfin Jr F.G., Sussman D., Ruaya R.G., Reyes A.G. (1992) Hazard assessment of the Pinatubo volcanic-geothermal system: clues prior to the June 15, 1991 eruption. *Geotherm. Res. Counc. Trans*. **16**, 519-527.

Delmelle P. and Bernard A. (1994) Geochemistry, mineralogy, and chemical modeling of the acid crater lake of Kawah Ijen Volcano, Indonesia. *Geochim. Cosmochim. Acta* **58**, 2445-2460.

Delmelle P., Bernard A. (2000) Volcanic Lakes. In: H. Sigurdsson, B.F. Houghton, S.R. McNutt, H. Rymer, J. Stix (Editors), *Encyclopedia of Volcanoes*. Academic Press, San Diego, pp. 877-895.

Dittman G.L. (1977) *Calculation of brine properties*. Lawrence Livermore Laboratory. Report UCID-17406.

Ellis A.J. (1962) Interpretation of gas analyses from the Wairakei hydrothermal area. *N.Z.J.Sci.* **5**, 434-452.

Ellis A.J. (1970) Quantitative interpretation of chemical characteristics of hydrothermal systems. *Geothermics,* Spec. Issue **2**, 516-528.

Ellis A.J. (1971) Magnesium ion concentrations in the presence of magnesium chlorite, calcite, carbon dioxide, quartz. *Amer. J. Sci*. **271**, 481-489.

Ellis A.J. and Golding R.M. (1963) The solubility of carbon dioxide above 100°C in water and in sodium chloride solutions. *Amer. J. Sci.* **261**, 47-60.

Ellis A.J. and Mahon W.A.J. (1964) Natural hydrothermal systems and experimental hot water/rock interactions. *Geochim. Cosmochim. Acta* **28**, 1323-1357.

Ellis A.J. and Mahon W.A.J. (1967) Natural hydrothermal systems and experimental hot water/rock interactions (Part II). *Geochim. Cosmochim. Acta* **31**, 519-538.

Ellis A.J. and Mahon W.A.J. (1977) *Chemistry and Geothermal Systems*, Academic Press, 392 pp.

Ellis A.J. and Wilson S.H. (1960) The geochemistry of alkali metal ions in the Wairakei hydrothermal system. *N.Z.J. Geol. Geophys.* **3**, 593-617.

Faure G. (1986) *Principles of Isotope Geology*. 2nd Ed. Wiley, New York.

Fleming B.A. and Crerar D.A. (1982) Silicic acid ionization and calculation of silica solubility at elevated temperature and pH. Application to geothermal fluid processing and reinjection. *Geothermics* **11**, 15-29.

Fouillac C. and Michard G. (1981) Sodium/lithium ratios in water applied to geothermometry of geothermal reservoirs. *Geothermics* **10**, 55-70.

Fournier R.O. (1973) Silica in thermal waters: laboratory and field investigations. *Proc. Int.l Symp. Hydrogeochemistry and Biogeochemistry*, *Tokyo*, pp. 122-139.

Fournier R.O. (1979a) Geochemical and hydrological considerations and the use of enthalpy-chloride diagrams in the prediction of underground conditions in hot-spring systems. *J. Volcanol. Geotherm. Res*. **5**, 1-16.

Fournier R.O. (1979b) A revised equation for the Na/K geothermometer. *Geotherm. Res. Counc. Trans*. **5**,1-16.

Fournier R.O. (1985) The behavior of silica in hydrothermal solutions. In *Geology and Geochemistry of Epithermal Systems* (B.R. Berger and P.M. Bethke, Eds) *Rev. Econ. Geol.* **2**, 45-61.

Fournier R.O. (1991) Water geothermometers applied to geothermal energy. In *Application of Geochemistry in Geothermal Reservoir Development*. (F. D'Amore, co-ordinator), UNITAR, 37-69.

Fournier R.O. and Marshall W.L. (1983) Calculation of amorphous silica solubilities at 25° to 300°C and apparent cation hydration numbers in aqueous salt solutions using the concept of effective density of water. *Geochim. Cosmochim. Acta* **47**, 587-596.

Fournier R.O. and Potter R.W. (1979) Magnesium correction to the Na-K-Ca chemical geothermometer. *Geochim. Cosmochim. Acta* **43**, 1543-1550.

Fournier R.O. and Potter R.W.II (1982) A revised and expanded silica (quartz)geothermometer. *Geothermal Resources Council Bulletin* **11**, 3-12.

Fournier R.O. and Rowe J.J. (1977) The solubility of amorphous silica in water at high temperatures and high pressures. *Am. Min*. **62**, 1052-1056.

Fournier R.O. and Truesdell A.H. (1973) An empirical Na-K-Ca geothermometer for natural waters. *Geochim. Cosmochim. Acta* **37**, 1255-1275.
Fournier R.O., Rosenbauer R.J., Bischoff J.L. (1982) The solubility of quartz in aqueous sodium chloride solution at 350°C and 180 to 500 bars. *Geochim. Cosmochim. Acta* **46**, 1975-1978.
Friedman I. and O'Neil J.R. (1977) *Compilation of stable isotope fractionation factors of geochemical interest*. U.S. Geological Survey Professional Paper 440.44.
Fudali R.F. (1965) Oxygen fugacities of basaltic and andesitic magmas. *Geochim. Cosmochim. Acta* **29**, 1063-1075.
Gambardella B. (2001) *Concentrazione e rapporto isotopico dello zolfo dei fluidi fumarolici della Solfatara di Pozzuoli e di altre manifestazioni campane*. Unpublished report for Osservatorio Vesuviano – Istituto Nazionale di Geofisica e Vulcanologia, Sede di Napoli.
Ganeyev I.G. (1975) Solubility and crystallization of silica in chloride. *Doklady Akademia Nauk*. SSSR **224**, 248-250.
Geotermica Italiana (1983a) *Étude de préfaisibilité des ressources geothermiques. Zone du Hanlé-Gaggadé. Geochemistry.* Report for the Institut Supérieur d'Etudes et des Recherches Scientifiques et Techniques. République de Djibouti.
Geotermica Italiana (1983b) *Reconnaissance survey of the geothermal resources of Northern Thailand. Geochemistry.* Report TCD CON 32/83-THA/82/002
Gherardi F., Panichi C., Yock A., Gerardo-Abaya J. (2002) Geochemistry of the surface and deep fluids of the Miravalles volcano geothermal system (Costa Rica). *Geothermics* **31**, 91-128.
Giggenbach W.F. (1975a) A simple method for the collection and analysis of volcanic gas samples. *Bull. Volcanol.* **39**, 132-145.
Giggenbach W.F. (1975b) The chemistry of Crater Lake, Mt. Ruapehu (New Zealand) during and after the 1971 active period. *N.Z.J. Sci*. **17**, 33-45.
Giggenbach W.F. (1978) The isotopic composition of waters from the El Tatio geothermal field, northern Chile. *Geochim. Cosmochim. Acta* **42**, 979-988
Giggenbach W.F. (1980) Geothermal gas equilibria. *Geochim. Cosmochim. Acta* **44**, 2021-2032.
Giggenbach W.F. (1984) Mass transfer in hydrothermal alterations systems. *Geochim. Cosmochim. Acta* **48**, 2693-2711.
Giggenbach W.F. (1987) Redox processes governing the chemistry of fumarolic gas discharges from White Island, New Zeland. *Appl. Geochem.* **2**, 143-161.
Giggenbach W.F. (1988) Geothermal solute equilibria. Derivation of Na-K-Mg-Ca geoindicators. *Geochim. Cosmochim. Acta* **52**, 2749-2765.
Giggenbach W.F. (1991a) Chemical techniques in geothermal exploration. In *Application of Geochemistry in Geothermal Reservoir Development*. (F. D'Amore, co-ordinator), UNITAR, 119-144.
Giggenbach W.F. (1991b) Isotopic composition of geothermal water and steam discharges. In *Application of Geochemistry in Geothermal Reservoir Development*. (F. D'Amore, co-ordinator), UNITAR, 253-273.
Giggenbach WF (1992a) Isotopic shifts in waters from geothermal and volcanic systems along convergent plate boundaries and their origin. *Earth Planet. Sci. Lett.* **113**, 495-510
Giggenbach W.F. (1992b) The composition of gases in geothermal and volcanic systems as a function of tectonic setting. In *Proc. 7th Int. Symp. Water-Rock Interaction*, Park City, Utah, 873-878
Giggenbach W.F. (1993) Redox control of gas compositions in Philippine volcanic-hydrothermal systems. *Geothermics* **22**, 575-587.

Giggenbach W.F. (1996) Chemical composition of volcanic gases. In: *Monitoring and Mitigation of Volcano Hazards* (R. Scarpa and R.I. Tilling, Eds.) Springer, 221-256

Giggenbach W.F. (1997a) The origin and evolution of fluids in magmatic-hydrothermal systems. In: *Geochemistry of hydrothermal ore deposits, 3d Edition* (H. L. Barnes, Ed.), Wiley, 737-796.

Giggenbach W.F. (1997b) Relative importance of thermodynamic and kinetic processes in governing the chemical and isotopic composition of carbon gases in high-heatflow sedimentary basins. *Geochim. Cosmochim. Acta* **61**, 3763-3785.

Giggenbach W.F. and Stewart M.K. (1982) Processes controlling the isotopic composition of steam and water discharges from steam vents and steam-heated pools in geothermal areas. *Geothermics* **11**, 71-80.

Giggenbach W.F. and Goguel R.L. (1989) *Collection and analysis of geothermal and volcanic water and gas discharges*. Report No. CD 2401. Department of Scientific and Industrial Research. Chemistry Division. Petone, New Zealand.

Giggenbach W.F. and Corrales Soto R. (1992) The isotopic and chemical composition of water and steam discharges from volcanic-magmatic-hydrothermal systems of the Guanacaste Geothermal Province, Costa Rica. *Appl. Geochem*. **7**, 309-332.

Giggenbach W.F. and Matsuo S. (1991) Evaluation of results from second and third IAVCEI field workshop on volcanic gases, Mt Usu, Japan, and White Island, New Zealand. *Appl. Geochem*. **6**, 125-141

Giggenbach W.F. and Poreda R.J. (1993) Helium isotopic and chemical composition of gases from volcanic-hydrothermal systems in the Philippines. *Geothermics* **22**, 369-380.

Giggenbach W.F., Gonfiantini R., Jangi B.L., Truesdell A.H. (1983) Isotopic and chemical composition of Parbati Valley geothermal discharges, NW-Himalaya, India. *Geothermics* **12**, 199-222.

Giggenbach W.F., Sheppard D.S., Robinson B.W., Stewart M.K., Lyon G.L. (1994) Geochemical structure and position of the Waiotapu geothermal field, New Zealand. *Geothermics* **23**, 599-644

Glover R.B. (1970) Interpretation of gas compositions from the Wairakei field over 10 years. *Geothermics,* Spec. Issue **2**,1355-1366.

Goguel R.L. (1983) The rare alkalies in hydrothermal alteration at Wairakei and Broadlands geothermal fields, NZ. *Geochim. Cosmochim. Acta* **47**, 429-437.

Guidi M., Marini L., Principe C. (1990a). Hydrogeochemistry of Kizildere geothermal system and nearby region. *Geothermal Resorces Council Transactions*, 14-II, 901-908.

Guidi M., Marini L., Scandiffio G., Cioni R. (1990b). Chemical geothermometry in hydrothermal aqueous solutions: the influence of ion complexing. *Geothermics*, **19**, 415-441.

Heald P., Foley N.K., Hayba D.O. (1987) Comparative anatomy of volcanic-hosted epithermal deposits: acid-sulfate and adularia-sericite deposits. *Econ. Geol*. **82**, 1-26.

Hedenquist J.W. (1986) Geothermal systems in the Taupo volcanic zone; their characteristics and relation to volcanism and mineralisation. In: *Late Cenozoic volcanism in New Zealand* (I.E.M. Smith, Ed.) *Bulletin – Royal Society of New Zealand* **23**, 134-168.

Hedenquist J.W. (1987) Mineralisation associated with volcanic-related hydrothermal systems in the Circum-Pacific Basin. *Trans. 4th Circum-Pacific Energy and Mineral Resources Conference*, Singapore, 513-524.

Hedenquist J.W. and Lowenstern J.B. (1994) The role of magmas in the formation of hydrothermal ore deposits. *Nature* **370**, 519-526

Helgeson H.C. (1968) Evaluation of irreversible reactions in geochemical processes involving minerals and aqueous solutions: I. Thermodynamic relations. *Geochim. Cosmochim. Acta*, **32**, 853-877.

Helgeson H.C. (1979) Mass transfer among minerals and hydrothermal solutions. In: *Geochemistry of Hydrothermal Ore Deposits*, H.L. Barnes (ed), 2nd Ed, Wiley. New York, 568-610.

Helgeson H.C., Garrels R.M., Mackenzie F.T. (1969) Evaluation of irreversible reactions in geochemical processes involving minerals and aqueous solutions: II Applications. *Geochim. Cosmochim. Acta*, **33**, 455-481.

Helgeson H.C., Brown T.H., Nigrini A., Jones T.A. (1970) Calculation of mass transfer in geochemical processes involving aqueous solutions. *Geochim. Cosmochim. Acta*, **34**, 569-592.

Hemley J.J. (1967) Aqueous Na/K ratios in the system $K_2O$-$Na_2O$-$Al_2O_3$-$SiO_2$-$H_2O$. *Program, 1967 Ann. Meeting Geol. Soc. Amer. New Orleans*, 94-95.

Hemley J.J., Montoya M., Luce R.W. (1980) Equilibria in the system $Al_2O_3$-$SiO_2$-$H_2O$ and some general implications for alteration/mineralization processes. *Econ. Geol*. **75**, 210-228.

Henley, R.W. and Ellis, A.J. (1983) Geothermal systems, ancient and modern: a geochemical review. *Earth Science Review* **19**, 1-50.

Henley R.W., Truesdell A.H., Barton P.B.Jr, Whitney J.A. (1984) Fluid-mineral equilibria in hydrothermal systems. *Reviews in Economic Geology* **1**, 267 pp.

Horita J. and Wesolowski D.J. (1994) Liquid-vapor fractionation of oxygen and hydrogen isotopes of water from the freezing to the critical temperature. *Geochim. Cosmochim. Acta* **58**, 3425-3437.

Horita J., Cole D.R., Wesolowski D.J. (1995) The activity-composition relationship of oxygen and hydrogen isotopes in aqueous salt solutions: III. Vapor-liquid water equilibration of NaCl solutions to 350°C. *Geochim. Cosmochim. Acta* **59**, 1139-1151.

Hulston J.R. and McCabe W.J. (1962) Mass spectrometer measurements in the thermal areas of New Zealand. *Geochim. Cosmochim. Acta* **26**, 383-397.

Janik C.J., Truesdell A.H., Goff F., Shevenell L., Stallard M.L., Trujillo P.E. Jr., Counce D. (1991) A geochemical model of the Platanares geothermal system, Honduras. *J. Volcanol. Geotherm. Res*. **45**, 125-146.

Johnson J.W., Oelkers E.H., Helgeson H.C. (1992) SUPCRT 92: A software package for calculating the standard molal thermodynamic properties of minerals, gases, aqueous species, and reactions from 1 to 5000 bars and 0 to 1000°C. *Computers & Geosciences* **18**, 899-947.

Kavouridis T., Kuris D., Leonis C., Liberopoulou V., Leontiadis, J., Panichi C., La Ruffa G., Caprai A. (1999) Isotope and chemical studies for a geothermal assessment of the island of Nisyros (Greece). *Geothermics* **28**, 219-239.

Keenan J.H., Keyes F.G., Hill P.G., Moore J.G. (1969) Steam tables. Thermodynamic properties of water including vapor, liquid, and solid phases (international system of units-S.I.). Wiley, 162 pp.

Kempter K.A., Rowe G.L. (2000) Leakage of Active Crater lake brine through the north flank at Rincón de la Vieja volcano, northwest Costa Rica, and implications for crater collapse. In: J.C. Varekamp and G.L. Rowe Jr. (Editors), *Crater Lakes. J. Volcanol. Geotherm. Res*., **97**, 143-159.

Kennedy, V.C. and Zellweger, G.W. (1974) Filter pore-size effects on the analysis of Al, Fe, Mn, and Ti in water. *Water Resour. Res*. **10**, 785-790.

Kharaka Y.K. and Mariner R.H. (1989) Chemical geothermometers and their application to formation waters from sedimentary basins. In: *Thermal History of Sedimentary Basins* (N.D. Naeser and T.H. McCollon, Eds.), Springer, 99-117.

Kieffer S.W. (1982) Thermodynamics and lattice vibrations of minerals: 5. Applications to phase equilibria, isotopic fractionation, and high pressure thermodynamic properties. *Rev. Geophys. Space Phys.* **20**, 827-849.

Kita I., Nitta K., Nagao K., Taguchi S., Koga A. (1993) Difference in $N_2$/Ar ratio of magmatic gases from northeast and southwest Japan: New evidence for different states of plate subduction. *Geology* **21**, 391-394

Knight C.L. and Bodnar R.J. (1989) Synthetic fluid inclusions: IX. Critical properties of NaCl-$H_2O$ solutions. *Geochim. Cosmochim. Acta* **53**, 3-8.

Laxen, D.P.H. and Chandler, I.M. (1982) Comparison of filtration techniques for size distribution in freshwater. *Anal. Chem*. **54**, 1350-1355.

La Ruffa G., Panichi C., Kavouridis T., Liberopoulou V., Leontiadis J., Caprai A. (1999) Isotope and chemical assessment of geothermal potential of Kos Island, Greece. *Geothermics* **28**, 205-217.

Marini L. and Chiodini G. (1994). The role of carbon dioxide in the carbonate-evaporite geothermal systems of Tuscany and Latium (Italy). *Acta Vulcanologica* **5**, 95-104.

Marini L. and Cioni R. (1985). A chloride method for the determination of the enthalpy of steam/water mixtures discharged from geothermal wells. *Geothermics* **14**, 29-34

Marini L., Chiodini G., Cioni R. (1986). New geothermometers for carbonate-evaporite geothermal reservoirs. *Geothermics* **15**, 77-86.

Marini L., Agostini A., Cioni R., Guidi M., Leon O. (1991) Guagua Pichincha volcano, Ecuador: fluid geochemistry in volcanic surveillance. *J. Volcanol. Geotherm. Res.* **46**, 21-35.

Marini L., Cioni R., Guidi M. (1998). Water chemistry of San Marcos area, Guatemala. *Geothermics*, 27, 331-360.

Marini L., Bonaria V., Guidi M., Hunziker J.C., Ottonello G., Vetuschi Zuccolini M. (2000) Fluid geochemistry of the Acqui Terme-Visone geothermal area (Piemonte, Italy). *Appl. Geochem.* **15**, 917-935.

Marini L., Vetuschi Zuccolini M., Saldi G., (2003a) The bimodal pH distribution in volcanic lake waters. *J. Volcanol. Geotherm. Res*., **121**, 83-98.

Marini L., Yock Fung A., Sanchez E. (2003b) Use of reaction path modeling to identify the processes governing the generation of neutral Na-Cl and acidic Na-Cl-$SO_4$ deep geothermal liquids at Miravalles geothermal system, Costa Rica. *J. Volcanol. Geotherm. Res*., **128**, 363-387.

Marshall W.L. (1980) Amorphous silica solubilities - III. Activity coefficient relations and predictions of solubility behavior in salt solutions, 0-350°C. *Geochim. Cosmochim. Acta* **44**, 925-931.

Martinotti G., Marini L., Hunziker J.C., Perello P., Pastorelli S. (1999). Geochemical and geothermal study of springs in the Ossola-Simplon region. *Eclogae Geol. Helv.*, **92**, 295-305.

Marty B, Jambon A, Sano Y (1989) Helium isotopes and $CO_2$ in volcanic gases of Japan. *Geology* **76,** 25-40.

Matsuo S., Suzuki M., Mizutani Y. (1978) Nitrogen to agron ratio in volcanic gases. *Adv. Earth Planet. Sci.* **3**, 17-25

Michard G., Fouillac C., Grimaud D., Denis J. (1981) Une méthode globale d'estimation des températures des resérvoirs alimentant les sources thermales. Exemple du Massif Central Français. *Geochim. Cosmochim. Acta* **45**, 1199-1207.

Murray C. and Cubicciotti D. (1983) Thermodynamics of aqueous sulfur species to 300°C and potential-pH diagrams. *J. Electrochem. Soc*. **38**, 863-869.

Naumov G.B., Ryzhenko B.N., Khodakovsky I.L. (1974) *Handbook of thermodynamic data*. Report No. USGS-WRD-74-001. U.S. Geological Survey. Water Resources Division, Menlo Park, California.

Nehring N.L. and D'Amore F. (1984) Gas chemistry and thermometry of the Cerro Prieto, Mexico, geothermal field. *Geothermics* **13**, 75-89.

O'Neil J.R. (1986) Theoretical and experimental aspects of isotopic fractionation. In: *Stable isotopes in high temperature geological processes* (J.W. Valley, H.P. Taylor, Jr., J.R. O'Neil, Eds.) *Reviews in Mineralogy* **16**, 1-40.

Orville P.M. (1963) Alkali ion exchange between vapor and feldspar phases. *Amer. J. Sci.* **261**, 201-237

Paces T. (1975) A systematic deviation from Na-K-Ca geothermometer below 75°C and above $10^{-4}$ atm $P_{CO2}$. *Geochim. Cosmochim. Acta* **39**, 541-544.

Pang Z.-H. and Reed M. (1998) Theoretical chemical thermometry on geothermal waters: Problems and methods. *Geochim. Cosmochim. Acta* **62**, 1083-1091.

Pastorelli S., Marini L., Hunziker J.C. (1999). Water chemistry and isotope composition of the Acquarossa thermal system, Ticino, Switzerland. *Geothermics*, **28**, 75-93.

Pastorelli S., Marini L., Hunziker J.C. (2001). Chemistry, isotope values ($\delta D$, $\delta^{18}O$, $\delta^{34}S_{SO4}$) and temperatures of the water inflows in two Gotthard tunnels, Swiss Alps. *Applied Geochemistry*, **16**, 633-649.

Perello P., Marini L., Martinotti G., Hunziker J.C. (2001). The thermal circuits of the Argentera Massif (western Alps, Italy): an example of low-enthalpy geothermal resources controlled by Neogene alpine tectonics. *Eclogae Geol. Helv.*, **94**, 75-94.

Poorter R.P.E., Varekamp J.C., van Bergen M.J., Kreulen B., Siriwana T., Vrool P.Z., Wirakusumah A.D. (1989) The Sirung volcanic boiling spring: an extreme chloride-rich, acid brine on Pantar (Lesser Sunda Islands, Indonesia). *Chem. Geol*. **76**, 215-228.

Reed M.H. (1982) Calculation of multicomponent chemical equilibria and reaction processes in systems involving minerals, gases and an aqueous phase. *Geochim. Cosmochim. Acta* **46**, 513-528.

Reed M.H. (1997) Hydrothermal alteration and its relationship to ore fluid composition. In: G*eochemistry of hydrothermal ore deposits, 3d Edition* (H. L. Barnes, editor), Wiley, 517-611.

Reed M.H. and Spycher N.F. (1984) Calculation of pH and mineral equilibria in hydrothermal waters with application to geothermometry and studies of boiling and dilution. *Geochim. Cosmochim. Acta* **48**, 1479-1492.

Reyes A.G. (1990) Petrology of Philippine geothermal systems and the application of alteration mineralogy to their assessment. . *J. Volcanol. Geotherm. Res*. **43**, 279-309.

Reyes A.G. and Giggenbach W.F. (1992) Petrology and fluid chemistry of magmatic-hydrothermal systems in the Philippines. In: *Water-Rock Interaction* (Y.K. Kharaka and A.S. Maest, Eds.) A.A. Balkema, Rotterdam, 1341-1344.

Richet P. and Bottinga Y. (1976) L'energie de zero des molecules et le fractionnement des isotopes stables. *C. R. Acad. Sci. Paris*, B, 425-428.

Richet P., Bottinga Y., Javoy M. (1977) A review of H, C, N, O, S and Cl stable isotope fractionation among gaseous molecules. *Ann Rev. Earth Planet. Sci. Lett*. **5**, 65-110.

Rimstidt J.D. and Barnes H.L. (1980). The kinetics of silica-water reactions. *Geochim. Cosmochim. Acta* **44**, 1683-1699.

Rowe Jr G.L., Ohsawa S., Takano B., Brantley S.L., Fernandez J.F., Barquero J. (1992) Using crater lake chemistry to predict volcanic activity at Poas volcano, Costa Rica. *Bull. Volcanol*. **54**, 494-503.

Ryzhenko B.N. and Malinin S.D. (1971) The fugacity rule for the systems $CO_2$-$H_2O$, $CO_2$-$CH_4$, $CO_2$-$N_2$, and $CO_2$-$H_2$. *Geochem. Int.* 562-574.

Ryzhenko B.N. and Volkov V.P. (1971) Fugacity coefficients of some gases over a broad range of temperatures and pressures. *Geochem. Int.* 468-481.

Salonga N.D., Dacillo D.B., Siega F.L. (2004) Providing solutions to the rapid changes induced by stressed production in Mahanagdong geothermal field, Philippines. *Geothermics*, **33**, 181-212.

Sano Y. and Marty B. (1995) Origin of carbon in fumarolic gas from the island arcs. *Chem. Geol.* **119**, 265-274.

Seward T.M.S. (1974) Equilibrium and oxidation potential in geothermal waters at Broadlands, New Zealand. *Am. J. Sci.* **274**, 190-192.

Srinivasan P.T., Viraraghavan T., Subramanian K.S. (1999) Aluminium in drinking water: an overview. *Water SA*, **25**, 47-56 (available on website http://www.wrc.org.za).

Sriwana T., van Bergen M.J., Varekamp J.C., Sumarti S., Takano B., van Os B.J.H., Leng M.J. (2000) Geochemistry of the acid Kawah Putih lake, Patuha Volcano, West Java, Indonesia. In: J.C. Varekamp and G.L. Rowe Jr. (Editors), *Crater Lakes. J. Volcanol. Geotherm. Res*. **97**, 77-104.

Steiner A. (1977) The Wairakei geothermal area, North Island, New Zealand. *N. Z. Geol. Surv. Bull.*, **90**, 136 pp.

Stolper E.M. and Newman S. (1994) The role of water in the petrogenesis of Mariana Trough magmas. *Earth Planet. Sci. Lett.* **121**, 293-325.

Stull D.R., Westrum E.F., Sinke G.G. (1969) *The chemical thermodynamics of organic compounds*. Wiley.

Sugiaman F., Sunio E., Molling P., Stimac J. (2004) Geochemical response to production of the Tiwi geothermal field, Philippines. *Geothermics*, **33**, 57-86.

Sussman D., Javellana S.P., Benavidez P.J. (1993) Geothermal energy development in the Philippines: an overview. *Geothermics* **22**, 353-367.

Takano B. and Watanuki K. (1990) Monitoring of volcanic eruptions at Yugama crater lake by aqueous sulfur oxyanions. *J. Volcanol. Geotherm. Res*. **40**, 71-87.

Tonani F. (1970) Geochemical methods of exploration for geothermal energy. *Geothermics,* Spec. Issue **2**, 492-515.

Tonani F. (1973) Equilibria that control the hydrogen content of geothermal gases. *Unpublished Phillips Petroleum Co. report*.

Tonani F. (1980) Some remarks on the application of geochemical techniques in geothermal exploration. *Proc. Adv. Eur. Geoth. Res., 2nd Symp*, Strasbourg, 428-443.

Truesdell A.H. (1975) Geochemical techniques in exploration. *Proc. 2nd UN Symp. Development and Use of Geothermal Resources* **1**, 53-86.

Truesdell A.H. (1991a) Origins of acid fluids in geothermal reservoirs. *Geotherm. Res. Counc. Trans*. **15**, 289-296.

Truesdell A.H. (1991b) Effects of physical processes on geothermal fluids. In *Application of Geochemistry in Geothermal Reservoir Development*. (F. D'Amore, co-ordinator), UNITAR, 71-92.

Truesdell A.H. and Fournier R.O. (1977) Procedure for estimating the temperature of a hot-water component in a mixed water by using a plot of dissolved silica versus enthalpy. *U.S. Geol. Surv. J. Res*. **5**, 49-52.

Truesdell A.H. and Hulston J.R. (1980) Isotopic evidence on environments of geothermal systems. In: *Handbook of Environmental Isotope Geochemistry* (P. Fritz and J.Ch. Fontes, Eds) The Terrestrial Environment, A, Elsevier **1**, 179-226

Truesdell A.H., Nathenson M., Rye R.O. (1977) The effects of subsurface boiling and dilution on the isotopic compositions of Yellowstone thermal waters. *J. Geophys. Res.* **82**, 3694-3703

Varekamp JC, Kreulen R, Poorter RPE, Van Bergen MJ (1992) Carbon sources in arc volcanism, with implications for the carbon cycle. *Terra Nova* **4**, 363-373.

Varekamp J.C., Pasternack G.B., Rowe G.L. Jr. (2000) Volcanic lake systematics II. Chemical constraints. In: J.C. Varekamp and G.L. Rowe Jr. (Editors), Crater Lakes. *J. Volcanol. Geotherm. Res*., **97**, 161-179.

Varekamp J.C., Ouimette A.P., Herman S.W., Bermúdez A., Delpino D. (2001) Hydrothermal element fluxes from Copahue, Argentina: A "beehive" volcano in turmoil. *Geology*, **29**, 1059-1062.

White D.E. (1957) Magmatic, connate, and metamorphic waters. *Geol. Soc. Amer. Bull.* **69**, 1659-1682.

White D.E. (1965) Saline waters of sedimentary rocks. In *Fluids in Subsurface Environments.* Symp. Amer. Assoc. Petroleum Geologists, 342-366.

White N.C. and Hedenquist J.W. (1990) Epithermal environments and styles of mineralisation: variations and their causes, and guidelines for exploration. *J. Geochem. Explor.* **36**, 445-474.

Wilhelm E., Battino R., Wilcock R.J. (1977) Low-pressure solubility of gases in liquid water. *Chemical Reviews* **77**, 219-262.

Wolery T.J. (1979) *Calculation of chemical equilibrium between aqueous solutions and minerals: the EQ3/6 software package*. Report UCRL-52658, Lawrence Livermore National Laboratory. Livermore.

Wolery T.J. (1992) *EQ3NR, A computer program for geochemical aqueous speciation-solubility calculations: Theoretical manual, user's guide and related documentation (version 7.0).* Report UCRL-MA-110662 PT III. Lawrence Livermore National Laboratory, Livermore.

Wolery T.J., Daveler S.A. (1992) *EQ6, A computer program for reaction path modeling of aqueous geochemical systems: Theoretical manual, user's guide, and related documentation (version 7.0).* Report UCRL-MA-110662 PT IV. Lawrence Livermore National Laboratory, Livermore.